Acoustical wave propagation in buried water filled pipes

by

Antonios Kondis

B.E., M.Eng. Civil Engineering
National Technical University of Athens (July 2003)

Submitted to the Department of Civil and Environmental Engineering
in partial fulfillment of the requirements for the degree of

Master of Science in Civil and Environmental Engineering

at the

Massachusetts Institute of Technology

February 2005

Signature of Author: _____
Department of Civil and Environmental Engineering
January 14, 2005

Certified by: _____
Eduardo Kausel
Professor of Civil and Environmental Engineering
Thesis Supervisor

Accepted by: _____
Andrew Whittle
Professor of Civil and Environmental Engineering
Chairman, Departmental Committee on Graduate Students

Acoustical wave propagation in buried water filled pipes

by

Antonios Kondis

Submitted to the Department of Civil and Environmental Engineering
on January 14, 2005 in partial fulfillment of the requirements for the degree of
Master of Science in Civil and Environmental Engineering

Abstract

This thesis presents a comprehensive way of dealing with the problem of acoustical wave propagation in cylindrically layered media with a specific application in water-filled underground pipes. The problem is studied in two stages: First the pipe is considered to be very stiff in relation to the contained fluid and then the stiffness of the pipe and the soil are taken into account. In both cases the solution process can take into account signals of any form, generated in any point inside the pipe. The simplified method provides the basic understanding on wave propagation and noise generation in the pipe in relation to pipe radius and frequency of excitation. Following the simplified analysis, the beam forming method is discussed and applied in order to reduce the noise in the pipe. Moving on to the complete analysis of the pipe, the stiffness matrix method is used to take into account the properties of the system. The solution time is proven to be much higher in this case, but the results vary from the simplified case in many real value problems. The results of the two methods are compared in more detail and then a decision making process for the choice of method is developed. This decision process is based on the frequency of the excitation, the properties of the materials and the dimensions of the system.

Thesis Supervisor: Eduardo Kausel
Title: Professor of Civil and Environmental Engineering

Acknowledgements

Above all, I would like to thank my advisor Prof. Eduardo Kausel for his intellectual guidance and comments on my work. He made my thesis a learning experience above civil engineering principles, teaching me how to develop my research and communication skills. Many thanks go also to George Kokosalakis for his helpful comments and bibliography suggestions, which helped the validation of the computer codes.

Moreover, I would like to thank my family and friends in Cambridge and Athens, who provided me with their support during the busy days of MIT.

Cambridge, Massachusetts
January 2005

Table of Contents

1. Introduction

1.1 Objectives

The purpose of this thesis is to investigate with numerical models the transmission of acoustic signals in water filled pipes that are buried in the ground, and by extension, to explore the transmission of waves in an arbitrarily layered cylindrically system consisting of solid and/or fluid media. This problem constitutes an essential first step when deciding if acoustic information can indeed be transmitted through pipes over significant distances, and if so, to determine the configuration and placement of sensors needed to collect the acoustic data. Although the application of acoustic signal transmission within cylindrical media is widespread and includes boreholes and oil pipelines, this thesis is focused solely on wave propagation in water mains.

1.2 Thesis layout

After reviewing the available literature on acoustic propagation in water-filled pipes as well summarizing the essential mathematical tools, we shall begin our investigation of this problem by means of a simplified model. For this purpose, the pipe will be considered to be much stiffer than the water it contains, in which case the fluid is surrounded by a cylindrical boundary that allows no motions in the radial direction. After presenting the analytical details of this model, we shall use it, in combination with realistic values for the various physical parameters, for a preliminary assessment of the characteristics of acoustic transmission in an actual pipe.

It is well known that when waves are transmitted through a waveguide such as a pipe, the signal suffers dispersion, that is, the component frequencies in the signal travel at different speed, and as a result the signal distorts and spreads out. Thus, the information is altered in its path from the source to the receiver. After analyzing the problem of transmission, this thesis will also consider briefly the problem of de-reverberation at the receiving point. This will be accomplished by what is referred to as *beam forming*, which consists in transmitting

the same signal, with appropriate delays, from neighboring points in the medium, or alternatively, measuring the response by means of an array of receivers and manipulating the recorded signals to extract the information at the source.

In the final part of this thesis, a more advanced and general analytical framework for ways of dealing with the problem of waves in radially layered media will be provided, which takes into account the flexibility of the pipe as well as of the surrounding soil. Comparisons will then be made between the predictions obtained by means of this rigorous model and the initial simplified method. It must be mentioned that the level of computational effort required for in this more accurate method is substantially higher than that of the simplified model. Nevertheless, in this modern age of fast personal computers, the time required for the computation is found to be manageable, with the advantage that the rigorous method is much more general and can be used for any kind of layered medium, regardless of the material characteristics of the layers (i.e. fluid or solid), their thicknesses and/or their rigidity (or lack thereof).

2. Literature review

2.1 Introduction

The literature on the subject of acoustic wave propagation is rather extensive and covers wide-ranging aspects of structure and fluid borne sound, which includes also fluid–structure interaction. Thus, it is not possible to provide herein a compact review of the entire field. Instead, we shall focus solely on acoustic wave propagation and fluid-structure interaction in fluid-filled, cylindrical pipes embedded in an elastic medium. Even here, however, the literature in this specific area is rich, due in part to the many different approaches available to deal with this subject. Indeed, the motivation for studying pipe acoustics arose from the need to provide practical solutions to a broad range of problems in engineering acoustics, physics and geophysics, such as understanding musical wind instruments, monitoring and inspection of petroleum pipelines, locating pipe defects in water mains, borehole logging, and many, many more.

2.2 Early research (up to 1990)

The first research on pipe acoustics may have been done on musical instruments. One of the very first books on sound in a pipe is due to Mersenne (1636), but in the ensuing centuries many more followed (e.g. Broadhouse, 1926, Olson, 1952). A great number of books on general theory of sound propagation appeared in the second half of the 19th century and in the early 20th century, among which the most notable were the ones those by Tyndall (1867), Lord Rayleigh (1877), Stone (1879) and Lamb (1910), and others listed in the bibliography section. While these early works on structure-borne sound provide for the most part only general, simplified solutions to an extensive area of acoustic problems, they do offer considerable insight into this difficult problem.

Among the more modern and detailed researches on pipe acoustics one must cite the works of Biot (1952), Lin & Morgan (1956), Gazis (1959), and Tyler & Sofrin (1962). From these

works one learns that there exist three kinds of waves that propagate in a hollow, fluid-filled, elastic cylinder:

- Longitudinal waves
- Helical (torsional) waves
- Flexural waves

Silk and Bainton (1979) denoted these different modes of propagation as L, T, F (m, n) respectively, in which the integers m, n are modal indices.

In these formulations, it was found that the dispersion equations for guided waves in a pipe system were characterized by so-called cut-off frequencies that relate to resonances within the pipe, and each propagation mode had different such frequencies. One of the most important features is that the cut-off frequency defines the frequency below which a wave cannot propagate; instead, the wave field for that mode decays exponentially with distance to the source. These waves are said to be evanescent, and are only important in the vicinity of an acoustic source. Furthermore, at any given frequency there exist only a finite number of modes that can propagate. The lower the frequency, the less the number of propagating modes, and for very low frequencies, there exists only one mode, the fundamental mode, which is found to be non-dispersive.

In the modern treatment of wave propagation in pipes, especially in works after the 1980's, both the elasto-dynamic characteristics of the cylindrical container as well as the flow properties of the contained medium were taken into account. As a result, a variety of ad-hoc theories and models were developed for thin-walled shells, for stiff pipes, or for viscous and non-viscous fluids, in most cases surrounded by either a vacuum or air.

Other influential papers of this research era were:

- Fuller (1983), who used analysis in the complex wavenumber domain and the theorem of the residues to analytically calculate the pressures in a thin cell that contains fluid.

- James (1982), who studied the vibration of a fluid-filled pipe from a point force excitation and also gave numerical results for a steel pipe containing water and surrounded by air.
- Merkulov et al (1978), Fuller and Fahy (1982) and Möser (1986), who investigated fluid-filled cells, where the acoustic propagation is very different in relation to pipes filled with fluid, due to the difference in stiffness of the containing mediums. At the same time they set the fundamentals for calculating the dispersion laws for the coupled system of the fluid-cell.

2.3 Recent research (after 1990)

During the last two decades, the research on acoustic wave propagation became more focused on the underlying scientific and application areas, so it is only necessary to review those researches that are relevant to the immediate goals of this thesis. A major contribution to buried, water-filled pipes was done by M.J.S. Lowe and P. Cawley from Imperial College, who published together a number of papers on the subject, both theoretical and experimental. This research resulted in a software package called "Disperse" (1997), which can calculate the dispersion curves of any cylindrically or planar layered system. Together with other researchers, such as R. Long, they have studied the dispersion characteristics of metal, water-filled pipes in vacuum or in soil. Among the principal finding are the following:

- The existence of the outer soil layer allows energy leakage from the system and makes the first axisymmetric longitudinal L (0,1) along with the first flexural F (1,1) mode of the pipe to suffer the most dispersion. The axisymmetric longitudinal mode of the water (α mode as defined by Aristegui, 1999) is the one that propagates less dispersively. These results were accompanied by experimental data, which showed that only the α mode was found after the wave had traveled for a great distance.
- On account of leak noise detection, the authors and R. Long (2002) found out that disregarding energy losses led to serious errors in locating the leak position. So, they concluded that it is imperative to calculate the dispersion characteristics of the system.

Other researchers that have contributed to today's understanding of acoustic propagation and especially dispersion are V.N. Rama Rao and J. K. Vandiver (1999), who investigated borehole acoustics of pipes immersed in a fluid surrounded by hard and soft soil formations. Their results for the different modes agree with those of Imperial College. X.M. Zhang et al (2001) developed a simple analytical way to study the fluid-structure interaction between pipe and water (with no surrounding soil) and compared his results to FEM and BEM analyses results, presenting the reader with a good understanding of the relative displacements and general oscillation patterns for the coupled system. Hegeon Kwun et al (1999) dealt with the problem of signal noise due to the existence of the higher modes in the pipe, noting that when the frequency of the signal (inverse of signal length in time) is higher than the interval between the cut-off frequencies, the excitation response has trailing pulses that follow the leading signal.

The previously cited works dealt for the most part with sources of low and medium frequency content. Inasmuch as the goal in this thesis is to use a fluid-filled pipe as a medium for the transmission of signals, the problem at hand must consider also high frequencies, since the rate of information transmission is known to grow in proportion to the frequency of the carrier frequency. Consequently, there is a need to investigate many more than the first two or three modes than can be excited in the system, a task that will be accomplished in the ensuing sections. On the other hand, it is also recognized that the higher the excitation frequency, the more modes propagate and the stronger the dispersion characteristics become, so the difficulty in de-reverberating and deciphering the signal at the receiving end grows in tandem with the frequency.

3. Mathematical preliminaries

3.1 Introduction

This chapter will introduce some fundamental mathematical concepts that are relevant to our analysis.

3.2 Laplacian in cylindrical coordinates

The Laplacian in Cartesian coordinates has the form of:

$$\nabla^2 f = \frac{\partial^2 f}{\partial x^2} + \frac{\partial^2 f}{\partial y^2} + \frac{\partial^2 f}{\partial z^2}$$

Knowing that the cylindrical coordinates come from the one-to-one transformation

$$\begin{Bmatrix} x = r\cos\theta \\ y = r\sin\theta \\ z = z \end{Bmatrix} \Leftrightarrow \begin{Bmatrix} r = \sqrt{x^2 + y^2} \\ \theta = \tan^{-1}\left(\frac{y}{x}\right) \\ z = z \end{Bmatrix}$$

the Laplacian in cylindrical coordinates will then be:

$$\nabla^2 f = \frac{1}{r}\frac{\partial}{\partial r}\left(r\frac{\partial f}{\partial r}\right) + \frac{1}{r^2}\frac{\partial^2 f}{\partial \theta^2} + \frac{\partial^2 f}{\partial z^2} = \frac{\partial^2 f}{\partial r^2} + \frac{1}{r}\frac{\partial f}{\partial r} + \frac{1}{r^2}\frac{\partial^2 f}{\partial \theta^2} + \frac{\partial^2 f}{\partial z^2}$$

The Laplacian will be used in the wave equation and the Helmholtz equation.

3.2 Bessel functions

The Bessel equation's solutions are called Bessel functions:

$$y''(x) + \frac{1}{x}y'(x) + \left(1 - \frac{m^2}{x^2}\right)y(x) = 0$$

Bessel functions graphs

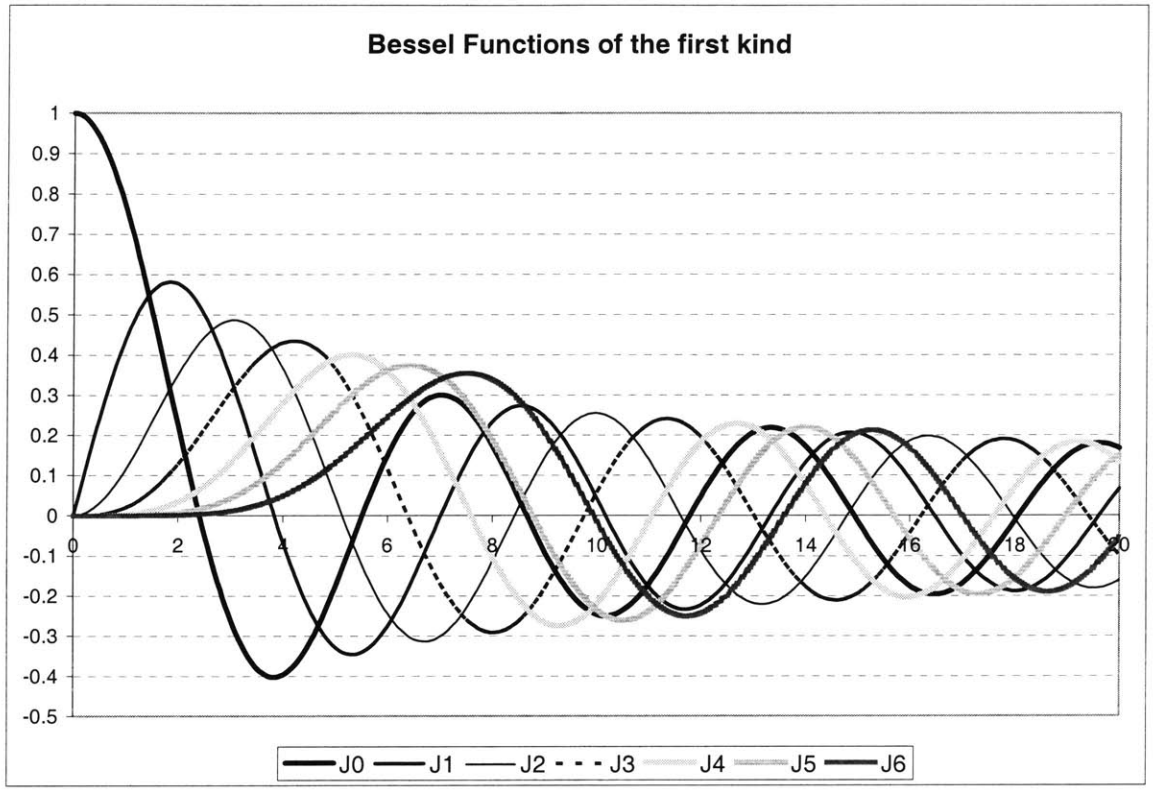

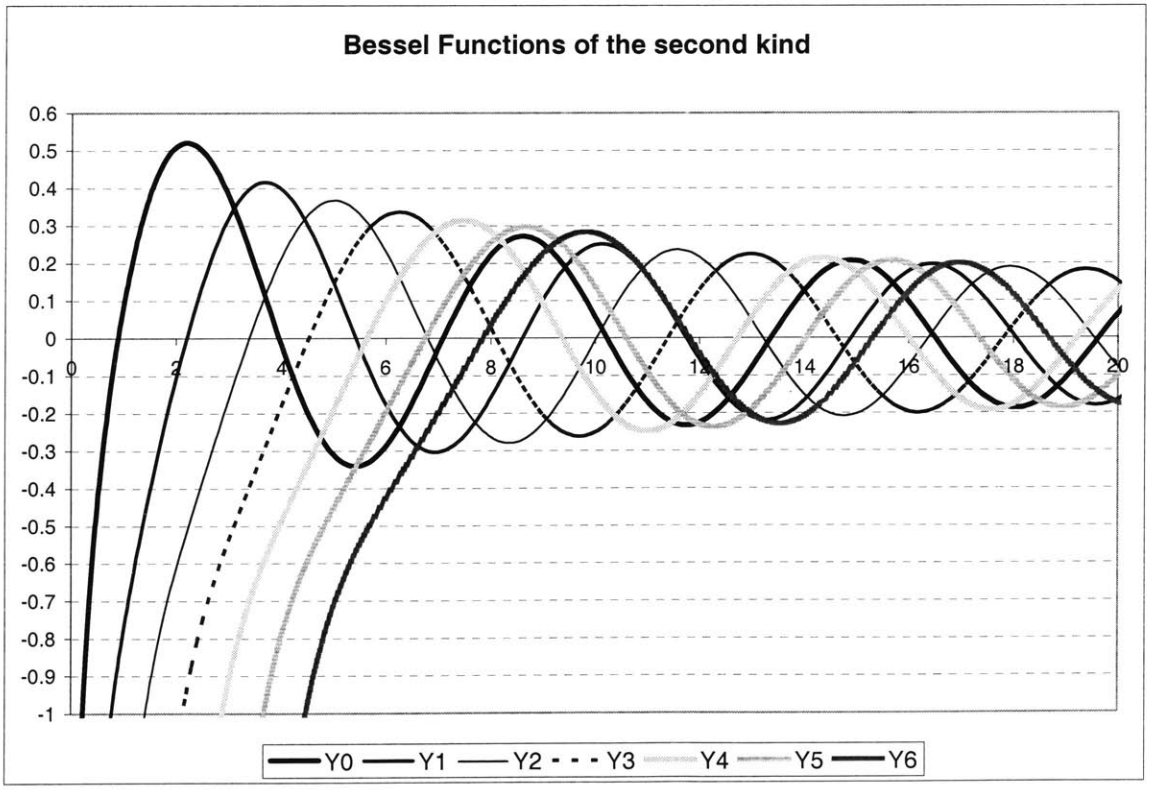

The functions that will be used in the next chapters are Bessel of the first kind (J), second kind (Y), and the Hankel functions of Bessel function of the third kind, namely

$$H_n^1(x) = J_n(x) + i \cdot Y_n(x)$$
$$H_n^2(x) = J_n(x) - i \cdot Y_n(x)$$

Orthogonality of the Bessel Functions

Bessel functions of the first kind satisfy the following integrals and orthogonality conditions:

$$\int_0^R J_n(\alpha r)\, J_n(\beta r)\, r\, dr = \frac{R\left[J_n(\alpha R)\, J_n'(\beta R) - J_n'(\alpha R)\, J_n(\beta R)\right]}{\alpha^2 - \beta^2} \quad \alpha \neq \beta$$

$$\int_0^R J_n^2(\alpha r)\, r\, dr = \frac{R^2}{2}\left\{\left(\frac{1}{\alpha}\frac{dJ_n(\alpha r)}{dr}\right)^2\Bigg|_{r=R} + \left[1 - \left(\frac{n}{\alpha R}\right)^2\right] J_n^2(\alpha R)\right\}$$

First orthogonality condition:

$$\int_0^R J_n(k_{ni} r)\, J_n(k_{nj} r)\, r\, dr = \tfrac{1}{2} R^2 \left[\tfrac{d}{dx} J_n(x)\Big|_{x=k_{nj}R}\right]^2 \delta_{ij}$$

Second orthogonality condition:

$$\int_0^R J_n(k'_{ni} r)\, J_n(k'_{nj} r)\, r\, dr = \tfrac{1}{2} R^2 J_n^2(k'_{ni} R)\left[1 - \left(\frac{n}{k'_{ni} R}\right)^2\right] \delta_{ij}$$

4. Simplified analysis of water filled pipe

4.1 Introduction

As mentioned earlier in the introduction, the rigorous formulation of sound propagation in cylindrical coordinates is a rather difficult problem if the waves can travel through more than one medium, and especially if there is interaction between the solid and the fluid phases. So, before considering the problem with an elaborate formulation, a very simple physical model will be presented first. This has the advantage that some of the salient mechanisms of the acoustic wave propagation will become apparent, which simplifies considerably our task of studying the transmission of acoustic signals in fluid-filled pipes.

This simple method of analysis is based on the assumption that the pipe's material is much stiffer than the water that it contains, so the pipe can be considered to be infinitely rigid. This means that the fluid boundary at the pipe wall cannot undergo radial displacements. The following chapter will present the equations in full detail, and provide a discussion of the trade-offs between the simplification and the realism with which it can (or not) model the actual, more complex system.

4.2 Simplified model

As mentioned earlier, the simplified analysis is based on the observation that the pipe's material (concrete or steel) is at least one order of magnitude stiffer than water. To a first approximation, the bulk modulus of steel and concrete is 160 GPa and 25 GPa respectively, while that of water is only 2.2 GPa.

Inasmuch as sound waves generate only small displacements, the materials will interact without causing separation or voids, which means that the radial displacements and pressure at the interfaces must be compatible and in equilibrium. It is also known that when two materials are arranged in series, the softer one will deform proportionally more than the stiffer under the same load. Hence, in the case of a large stiffness contrast, the stiffer

material will undergo little deformation, and can thus to a fist approximation be considered infinitely stiff, in which case the radial displacement (or velocity) of the fluid must vanish at the external stiff boundary. The advantage is that this simplified model admits and exact solution.

Assuming a pipe with a uniform flow, the acoustical velocity potential equation can be written as:

$$\nabla^2\phi = \frac{1}{c^2}\frac{\partial^2\phi}{\partial t^2}$$

As noted in Chapter 3, the Laplacian in cylindrical coordinates equals:

$$\nabla^2\phi = \frac{\partial^2\phi}{\partial r^2}+\frac{1}{r}\frac{\partial\phi}{\partial r}+\frac{1}{r^2}\frac{\partial^2\phi}{\partial\theta^2}+\frac{\partial^2\phi}{\partial z^2}$$

$$\frac{\partial^2\phi}{\partial r^2}+\frac{1}{r}\frac{\partial\phi}{\partial r}+\frac{1}{r^2}\frac{\partial^2\phi}{\partial\theta^2}+\frac{\partial^2\phi}{\partial z^2}-\frac{1}{c^2}\frac{\partial^2\phi}{\partial t^2}=0$$

The solution of this differential equation, as shown by Kausel [Compendium of Fundamental Solutions in Elastodynamics, Cambridge University Press, in print], is of the form:

$$\phi(r,\theta,z)=\left(c_1\cos(n\theta)+c_2\sin(n\theta)\right)\cdot\left(c_3J_n(k_a r)+c_4Y_n(k_a r)\right)\cdot\left(c_5e^{ik_z z}+c_6e^{-ik_z z}\right) \text{ with}$$

$$k_a=\sqrt{k_p^2-k_z^2}$$

In the problem discussed here the waves move outwards from the source and have a finite strength close to the source, so ϕ can be written as:

$$\phi(r,\theta,z)=\left(c_1\cos(n\theta)+c_2\sin(n\theta)\right)\cdot J_n(k_a r)\cdot e^{-ik_z z}$$

The boundary condition of the simplified case can be written as:

$u_r=\phi_{,r}=0$ at r=R for every θ and z.

This can be translated into:

$$J_n'(k_{nj}R) = 0 \Leftrightarrow k_{nj}R = z'_{nj} \Leftrightarrow k_{nj} = \frac{z'_{nj}}{R}$$

Let $S(r,\theta,k_z,\omega)$ be the strength of a source with arbitrary spatial distribution in r, θ and harmonic distribution in z, t. This source is expanded in a Fourier-Bessel series of the form

$$S(r,\theta,k_z,\omega) = \sum_{n=0}^{\infty}\sum_{j=1}^{\infty} S_{nj} = \sum_{n=0}^{\infty}\sum_{j=1}^{\infty}\left(a_{nj}\cos n\theta + b_{nj}\sin n\theta\right) J_n(k_{nj}r)$$

in which the wavenumbers k_{nj} are the roots of $J_n'(k_{nj}R) = 0$, and the coefficients are to be determined. Thus, each term in the series satisfies the homogeneous Helmholtz equation in cylindrical coordinates with boundary condition $J_n'(k_{nj}R) = 0$. To obtain the coefficients a_{nj}, b_{nj}, one needs to multiply by an appropriate factor, integrate over the area of the circle, and use the orthogonality conditions, after which it is obtained that:

$$a_{nj} = \frac{\int_0^R \int_0^{2\pi} S(r,\theta,\omega)\cos m\theta\, J_m(k_{mi}r)\, r\, dr\, d\theta}{\frac{\pi}{2}\left(1+\delta_{0n}\right)R^2 J_n^2(k_{nj}R)\left[1-\left(\frac{n}{k_{nj}R}\right)^2\right]} \quad \text{for } n = 0,\ 1,\ 2,\ \ldots$$

$$b_{nj} = \frac{\int_0^R \int_0^{2\pi} S(r,\theta,k_z,\omega)\sin m\theta\, J_m(k_{mi}r)\, r\, dr\, d\theta}{\frac{\pi}{2}R^2 J_n^2(k_{nj}R)\left[1-\left(\frac{n}{k_{nj}R}\right)^2\right]} \quad \text{for } n > 0$$

The differential equation, as noted before adding the load term, for waves in the pipe is then:

$$\nabla^2\phi + k^2\phi = \sum_{n=0}^{\infty}\sum_{j=1}^{\infty}\left(a_{nj}\cos n\theta + b_{nj}\sin n\theta\right) J_n(k_{nj}r)$$

in which $k^2 = k_0^2 - k_z^2$ and $k_0 = \omega / c$. To solve this equation, ϕ is expressed in terms of a Fourier-Bessel series analogous to the expansion used for the source, namely

$$\phi(r,\theta,k_z,\omega) = \sum_{n=0}^{\infty}\sum_{j=1}^{\infty}\phi_{nj} = \sum_{n=0}^{\infty}\sum_{j=1}^{\infty}\left(A_{nj}\cos n\theta + B_{nj}\sin n\theta\right)J_n(k_{nj}r)$$

Substitution into the differential equation yields

$$\sum_{n=0}^{\infty}\sum_{j=1}^{\infty}\left(\nabla^2 + k^2\right)\left(A_{nj}\cos n\theta + B_{nj}\sin n\theta\right)J_n(k_{nj}r) = \sum_{n=0}^{\infty}\sum_{j=1}^{\infty}\left(a_{nj}\cos n\theta + b_{nj}\sin n\theta\right)J_n(k_{nj}r)$$

Clearly, if each term of the two series is equal, so are also the sums. Hence,

$$\left(\nabla^2 + k^2\right)\left(A_{nj}\cos n\theta + B_{nj}\sin n\theta\right)J_n(k_{nj}r) = \left(a_{nj}\cos n\theta + b_{nj}\sin n\theta\right)J_n(k_{nj}r)$$

This implies

$$\left\{\left[\left(J_n'' + \tfrac{1}{r}J_n' + \left(k_{nj}^2 - \left(\tfrac{n}{r}\right)^2\right)J_n\right)\right] + \left(k^2 - k_{nj}^2\right)J_n\right\}\left(A_{nj}\cos n\theta + B_{nj}\sin n\theta\right) = \left(a_{nj}\cos n\theta + b_{nj}\sin n\theta\right)J_n$$

The term in square brackets is zero, because it is the differential equation for $J_n(k_{nj}r)$. Considering that $k^2 - k_{nj}^2 = k_0^2 - k_{nj}^2 - k_z^2$, then

$$A_{nj} = \frac{a_{nj}}{k_0^2 - k_{nj}^2 - k_z^2} \text{ and } B_{nj} = \frac{b_{nj}}{k_0^2 - k_{nj}^2 - k_z^2}$$

which can be written as

$$A_{nj} = \frac{-a_{nj}}{\left(k_z - \sqrt{k_0^2 - k_{nj}^2}\right)\left(k_z + \sqrt{k_0^2 - k_{nj}^2}\right)} \text{ and } B_{nj} = \frac{-b_{nj}}{\left(k_z - \sqrt{k_0^2 - k_{nj}^2}\right)\left(k_z + \sqrt{k_0^2 - k_{nj}^2}\right)}$$

These are the only terms in the solution for ϕ that contain the axial wavenumber k_z. Hence, for a concentrated load $\delta(z)$, the inverse Fourier transform back into the spatial domain will involve the integral

$$I_j = \frac{1}{2\pi}\int_{-\infty}^{+\infty} \frac{e^{-\mathrm{i}k_z z}\, dk_z}{\left(k_z - \sqrt{k_0^2 - k_{nj}^2}\right)\left(k_z + \sqrt{k_0^2 - k_{nj}^2}\right)}$$

which can be evaluated by contour integration. This requires determining the proper location of the poles. Adding a small amount of damping, then k_0 has a small negative imaginary part, and it can be seen that the two square roots $\pm\sqrt{k_0^2 - k_{nj}^2}$ lie in the second and fourth quadrants, respectively. Now, for $z>0$, the exponential term in the integrand is bounded in the lower half-plane, which contains only one pole, namely $\sqrt{k_0^2 - k_{nj}^2}$. Hence, a contour integration must be carried out in that plane in clockwise direction, which in turn introduces a negative sign. The result is

$$I_j = -2\pi\mathrm{i}\frac{1}{2\pi}\frac{e^{-\mathrm{i}z\sqrt{k_0^2 - k_{nj}^2}}}{2\sqrt{k_0^2 - k_{nj}^2}} = -\frac{\mathrm{i}e^{-\mathrm{i}z\sqrt{k_0^2 - k_{nj}^2}}}{2\sqrt{k_0^2 - k_{nj}^2}}$$

Finally, the solution in the frequency-space domain is

$$\phi(r,\theta,z,\omega) = \frac{\mathrm{i}}{2}\sum_{n=0}^{\infty}\sum_{j=1}^{\infty}\frac{e^{-\mathrm{i}z\sqrt{k_0^2 - k_{nj}^2}}}{\sqrt{k_0^2 - k_{nj}^2}}\left(a_{nj}\cos n\theta + b_{nj}\sin n\theta\right)J_n(k_{nj}r)$$

For the generalized case of an off-center point source the above equations are shaped as follows:

$$S(r,\theta,z,\omega)=\tfrac{1}{r}\delta(r-a)\delta(\theta)\delta(z)f(\omega)$$

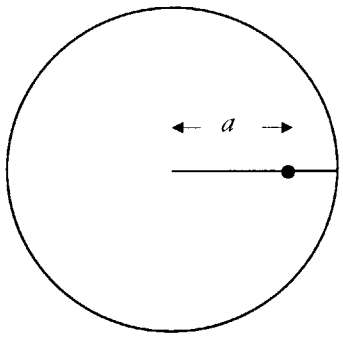

which satisfies

$$\int_0^R\int_0^{2\pi} S\left(r,\theta,k_z,\omega\right)r\,dr\,d\theta=\delta(z)\,f\left(\omega\right)$$

In this case,

$$a_{nj}=\frac{J_n(k_{nj}a)}{\frac{\pi}{2}\left(1+\delta_{0n}\right)R^2J_n^2(k_{nj}R)\left[1-\left(\frac{n}{k_{nj}R}\right)^2\right]},\ b_{nj}=0$$

and consequently

$$\phi(r,\theta,z,\omega)=\frac{\mathrm{i}}{\pi R^2}f(\omega)\,e^{\mathrm{i}\omega t}\sum_{n=0}^{\infty}\sum_{j=1}^{\infty}\frac{e^{-\mathrm{i}z\sqrt{k_0^2-k_{nj}^2}}}{\sqrt{k_0^2-k_{nj}^2}}\frac{\cos n\theta\ J_n(k_{nj}a)\ J_n(k_{nj}r)}{\left(1+\delta_{0n}\right)J_n^2(k_{nj}R)\left[1-\left(\frac{n}{k_{nj}R}\right)^2\right]}$$

From the last equation it is easy to see that the calculation of ϕ or any other component of the response (pressure, displacement etc) will require a double summation for a substantial range of n and j, which is computationally expensive. To investigate the axisymmetric case (excitation on the axis of the pipe) only n=0 is required and therefore the calculations are much less expensive than the generalized case. In particular, for a centered source a=0:

$$S(r,\theta,z,\omega)=\tfrac{1}{r}\delta(r)\delta(\theta)\delta(z)f(\omega)$$

which satisfies

$$a_{0j}=\frac{1}{\pi R^2J_0^2(k_{0j}R)},\ a_{n>0,j}=0,\ b_{nj}=0$$

so that

$$\phi(r,\theta,z,\omega)=\frac{\mathrm{i}}{2\pi R^2}f(\omega)e^{\mathrm{i}\omega t}\sum_{j=1}^{\infty}\frac{e^{-\mathrm{i}z\sqrt{k_0^2-k_{0j}^2}}}{\sqrt{k_0^2-k_{0j}^2}}\frac{J_0(k_{0j}r)}{J_0^2(k_{0j}R)}$$

and

$$p(r,\theta,z,\omega)=\frac{\rho}{cR^2}\omega f(\omega)e^{\mathrm{i}\omega t}\sum_{j=1}^{\infty}\frac{e^{-\mathrm{i}z\sqrt{k_0^2-k_{0j}^2}}}{\sqrt{k_0^2-k_{0j}^2}}\frac{J_0(k_{0j}r)}{J_0^2(k_{0j}R)}$$

Observe that the normal modes of the pipe are given by $k_{0j}=\omega_{0j}/c=z_{0j}/R$, i.e.

$$\omega_{nj}=z_{nj}\frac{c}{R}\rightarrow k_{nj}r=z_{nj}\frac{r}{R},k_{nj}a=z_{nj}\frac{a}{R}\text{ with }J_n'(z_{nj})=0$$

Given the above equation one can calculate the time response of the pipe pressures (or any other attribute) for any kind of excitation. In order to do that, the excitation signal must be analyzed with a Fourier transform to break it down to different frequencies. This transformation will change the forcing function from time to frequency domain for a given range of frequencies. The response of the system for this range of frequencies can be then calculated from the transfer function for a substantially high number of *j*. The inverse Fourier transform of the resulting response function (product of transfer function and FFT of force) in the frequency domain will give the response of the pipe in the time domain.

Notice here that the aforementioned forward and inverse Fourier transforms are discrete and not analytical, since the Fourier transform (from time to frequency domain) of the excitation force cannot always be analytically expressed. Therefore, a Fast Fourier transformation (FFT) is the best way to calculate it, according to Frigo and Johnson (1998). However, to perform the FFT the time (and frequency) domain will need to be discretized considerably to allow for a good numerical simulation. At the same time, it is known that, when the FFT of a non-periodic signal is computed, the frequency distribution suffers from leakage. This results in the smearing out of the energy of the excitation over a wide frequency range in the FFT when it should be in a narrow frequency range. Since the forcing function is not going to be periodic in general, in order to prevent the leakage one

must apply a window to the forcing function. Many types of windows exist in the literature and in the leading signal processing software packages, but the most appropriate for an impact loading, like the one under consideration, is the exponential window. The exponential window method (EWM) was developed specifically for the modal analysis of an impact hammer excitation. One of the main benefits of the exponential window method is that it forces the response to zero at the end of the "period" and, therefore, lessens the effect of all the other sources in the pipe (contamination of response).

As explained in detail by Kausel and Roësset (1992) the exponential window method is applied as follows:

Given a displacement (or any other variable) of the form:

$u(t) = \frac{1}{2\pi}\int_{-\infty}^{\infty} F(\omega)\mathrm{H}(\omega)e^{i\omega t}d\omega$, if one adds an artificial damping to the frequency, this integral can be evaluated by contour integration as:

$$u(t) = \frac{1}{2\pi}\int_{-\infty}^{\infty} F(\omega - i\eta)\mathrm{H}(\omega - i\eta)e^{i(\omega - i\eta)t}d\omega =$$

$$= \frac{1}{2\pi}e^{\eta t}\int_{-\infty}^{\infty} F(\omega - i\eta)\mathrm{H}(\omega - i\eta)e^{i\omega t}d\omega = e^{\eta t}\bar{u}(t)$$

with

$$F(\omega - i\eta) = \int_0^{t_0}\left(e^{-\eta t}f(t)\right)e^{-i\omega t}dt = \int_0^{t_0}\bar{f}(t)e^{-i\omega t}dt$$

It is generally agreed that the artificial damping ratio must be of the order of $d\omega/2$, with $d\omega$ the increment of frequency in the discretization in the FFT calculations. This level of artificial damping ratio forces the waves traveling from the adjacent sources to have a minimal effect on the solution.

Consequently, the EWM for the acoustic propagation problem requires the following steps:

- Calculate the FFT of the forcing function
- Multiply it by a falling exponential window
- Calculate the transfer function for the complex frequency
- Multiply the FFT of the forcing function and the transfer function to get the response function
- Do the inverse FFT
- Multiply the resulting displacement by a rising exponential window with the same parameter η to get the actual response

After these brief notes on the EWM application the layout of the numerical code that calculates the response to an impact excitation will be:

1. Defining the forcing function
2. Choosing the distance for which the response is calculated
3. Choosing the timeframe under which the system is studied
4. Deciding on the number of discretization points
5. Calculating the Nyquist frequency for the FFT
6. Discretizing the frequency domain
7. Calculating the forcing function strength at all the discretization points
8. Calculating the FFT of forcing function
9. Choosing a value of damping for the EWM
10. Calculating the EW function
11. Multiplying the EW with the FFT of the forcing function
12. Choosing the appropriate number of modes (value of n) and of terms of the Bessel-Fourier series (value of j)
13. Calculating the response for all the frequencies (transfer function)
14. Multiplying the transfer function with the FFT of the forcing function
15. Executing an IFFT to calculate the response of the system in time
16. Multiplying the response with the inverse EW
17. Doing the above analysis for a range of distances

Note the following:

1) Practically, only a few number of the discrete time points will give a non-zero forcing function value, since the excitation under consideration is an impact, but the trailing zeros are necessary to execute the FFT.
2) In order to calculate the response for all the terms of the Bessel-Fourier series, the roots of the first derivative of the Bessel function are needed. These roots can be found tabulated, but in the current case a separate code for calculation of the roots was used. The code was based on the bisection method and made use of the fact that the solutions of the derivative of the Bessel function lie around the terms of a linear series based on the order of the Bessel function and the number of the root.

One can use this procedure get insight into the wave propagation in the pipe especially around main frequency of impact and noise levels in the pipe. This is the reason why only one axial wavenumber is enough to get very useful results, which will be used later on in the detailed three-dimensional analysis of the complete pipe system.

Before going into the analyses with real data, one must consider the effect of the FFT sampling rate. The following criteria must be satisfied in order to have a fairly accurate analysis:

- Nyquist criterion: The maximum frequency of the FFT analysis must be at least 2 times higher than the main frequency of the forcing function
- The force in the time domain must discretized using at least 6 points, in order to express the forcing function relatively accurately.

4.3 Practical uses

In this chapter the developed EWM code will be used to calculate the pressures in the pipe in response to various kinds of excitations. The only variable in the analyses will be the duration of the force applied, since a specific forcing function type will be used.

In order to see the effect of frequency of excitation and propagation in the pipe, the radius of the pipe will be taken equal to R=1m for normalization reasons. This way the normal modal frequencies will be calculated as $\omega_{nj} = z_{nj}\frac{c}{R} = z_{nj}c$ with $J_n'(z_{nj}) = 0$. The following analyses (and all the analyses in this thesis) assume that the compressional wave speed of water is 1500m/s. Given that the pipe is considered to be very stiff, the properties of the pipe material and the surrounding soil are not needed for the analyses of this chapter.

At this point, it is useful to note down the cut-off frequencies for the pipe, since the frequency of the excitation will play a very important role in the response of the pipe. In the following table one can find the z_{nj} up till n=20, the associated cut-off frequencies and the period of the excitation having this frequency. Nevertheless, the table is only indicative, since the analyses presented here go beyond the first 20 modes.

n	z_{n0} (1/m)	f_n (KHz)	ω_n (rad/msec)	T_n (msec)
0	0	0	0	∞
1	3.832	0.915	5.75	1.093
2	7.016	1.675	10.52	0.597
3	10.17	2.429	15.26	0.412
4	13.32	3.181	19.99	0.314
5	16.47	3.932	24.71	0.254
6	19.62	4.683	29.42	0.214
7	22.76	5.434	34.14	0.184
8	25.90	6.184	38.86	0.162
9	29.05	6.934	43.57	0.144
10	32.19	7.685	48.28	0.130
11	35.33	8.435	53.00	0.119
12	38.47	9.185	57.71	0.109
13	41.62	9.935	62.43	0.101
14	44.76	10.69	67.14	0.094
15	47.90	11.44	71.85	0.087
16	51.04	12.19	76.57	0.082
17	54.19	12.94	81.28	0.077
18	57.33	13.69	85.99	0.073
19	60.47	14.44	90.70	0.069
20	63.61	15.19	95.42	0.066

Table 4.1: Axisymmetric modes and related frequencies

From the above table one can see that the number of different modes that can propagate in a rigid pipe increases superlinearly in relation to the frequency of excitation. Consequently, in order to transmit information twice as fast, the energy of the excitation will be distributed to more than twice the amount of modes. In the following analysis the forcing

function is not periodic, but the characteristic "period" of the signal will be assumed equal to the total time of excitation.

Before going into the analyses, it must be made clear that the sampling rate of the FFT is very crucial to the accuracy of the transformation. According to the Nyquist criterion "the sampling rate must be at least two times the highest frequency of interest". However, since this frequency is more of an estimate than a given number, the analysis must go well beyond that rate. For every analysis the Fourier spectrum of the excitation will be shown, so that it is more apparent where the maximum frequency is adequate to capture the response of the system. At the same time this chapter will be used to draw conclusions on the required highest frequency for the more detailed analysis that is to follow.

As it will be discussed in chapter 6 in detail, the major frequency content of a squared sinusoidal wavelet goes up to 3 times the inverse of its period, so given table 4.1, one should expect to have only the first mode for periods higher than 3ms. To show the behavior of the stiff pipe under low frequency excitations an initial 5ms pulse will be used, followed by higher frequency excitations of 2,1 and 0.5ms. In all the following analyses the pipe will have a radius of 1m and the compressional wave velocity of the water will be 1.5Km/s.

Low frequency excitation (5ms pulse)

This excitation can only produce the "zero" axisymmetric mode in the pipe and so the initial pulse gets transmitted without any noise. However, since this pulse is made up from sinusoidal forms of higher frequencies as well, which attenuate faster, it gets dispersed while traveling in the pipe and it seems to extend in duration, as it can be shown by the next graphs. The graphs show the response function (product of the transfer function and the force FFT), the normalized pressure response in space and time and the pressure response at selected points in the pipe (at approximately 0, 18m, 38m and 75m from source).

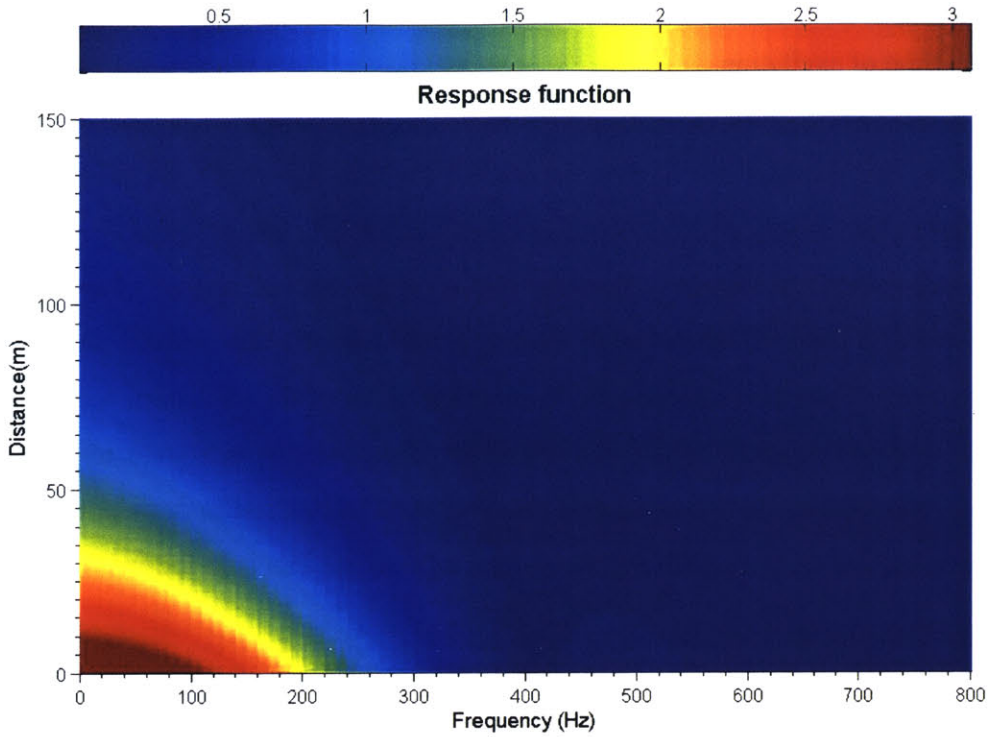

Figure 4.1: Response function (5ms pulse)

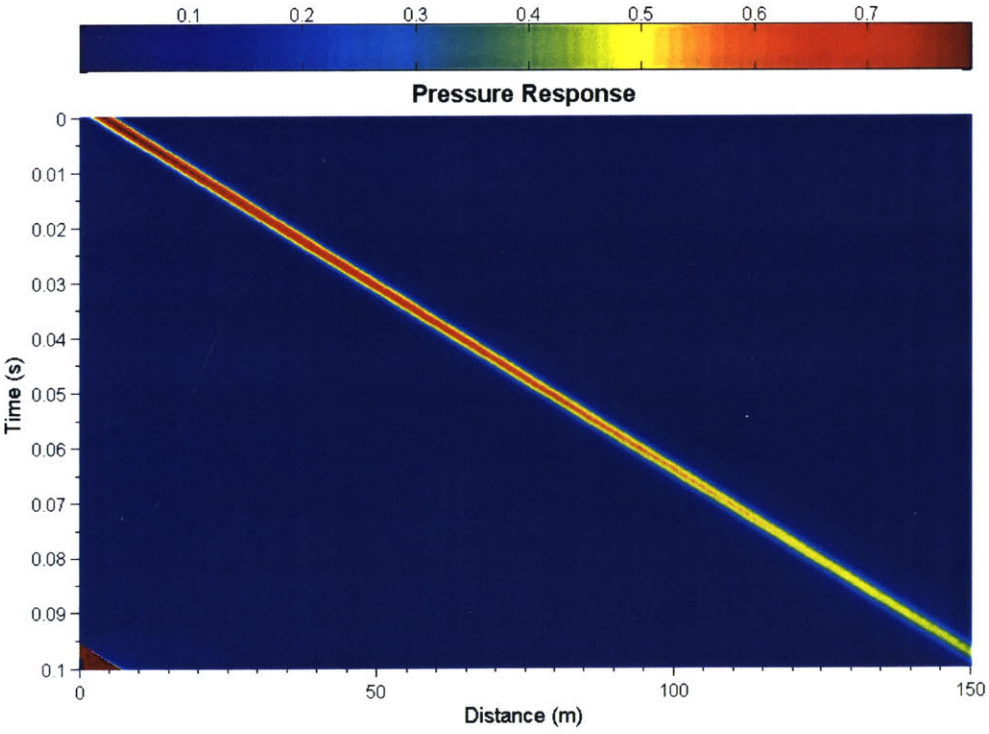

Figure 4.2: Pressure response (5ms pulse)

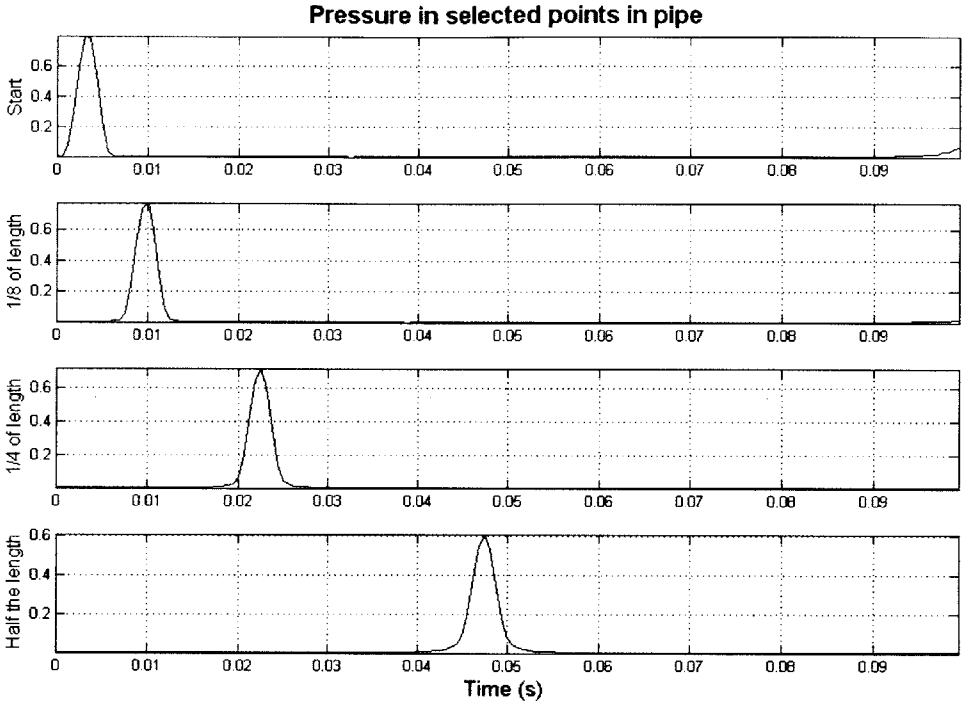

Figure 4.3: Pressure response in selected points in pipe (5ms pulse)

The above graphs show that the theoretically expected behavior is well reproduced. Figure 4.2 shows that the wave travels with a speed of 1.5Km/s (the speed of sound in water) and that only the "zero" mode is excited in the pulse. At the same time, in figure 4.3 (but also in figure 4.2) one can notice the slight dispersion of the wave's higher frequencies that result in the extension of the initial pulse and the smoothening out of the pulse's starting and ending regions. Although the initial pulse has a duration of 5ms, after 75m of propagation it lengthens up to 15ms, as it can be seen in the last part of figure 4.3.

High frequency excitations (0.2,0.5,1,2 ms pulses)

The following graphs show the response function (product of the transfer function and the force FFT), the response in space and time and the normalized pressure response at selected points in the pipe (at approximately 0, 18m, 38m and 75m from source).

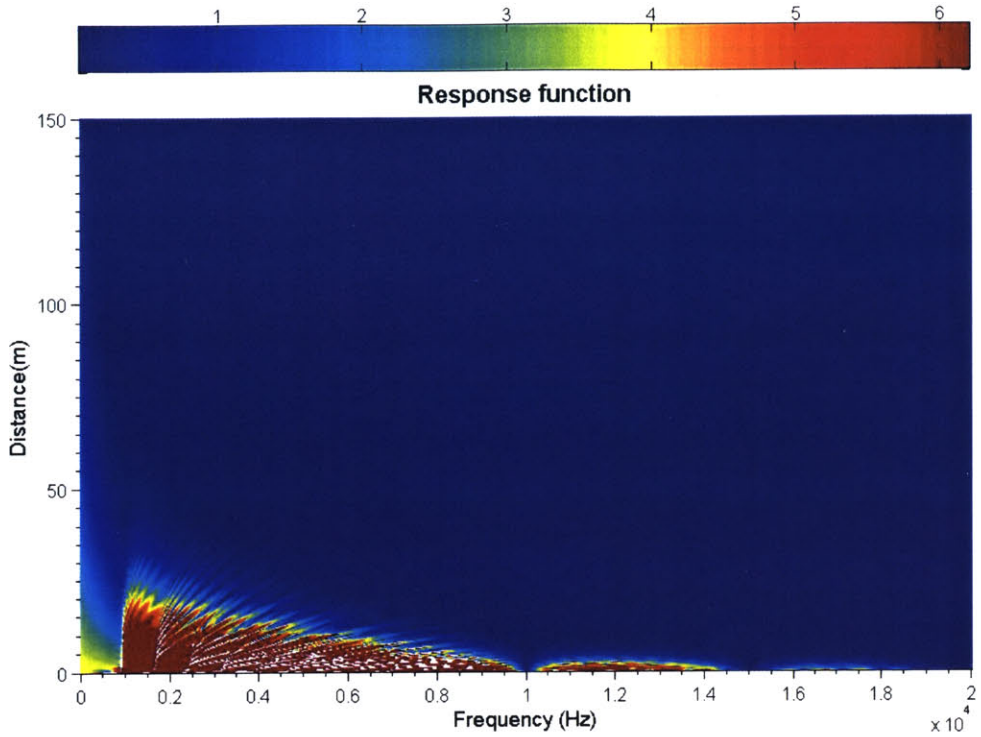

Figure 4.4: Response function (0.2ms pulse)

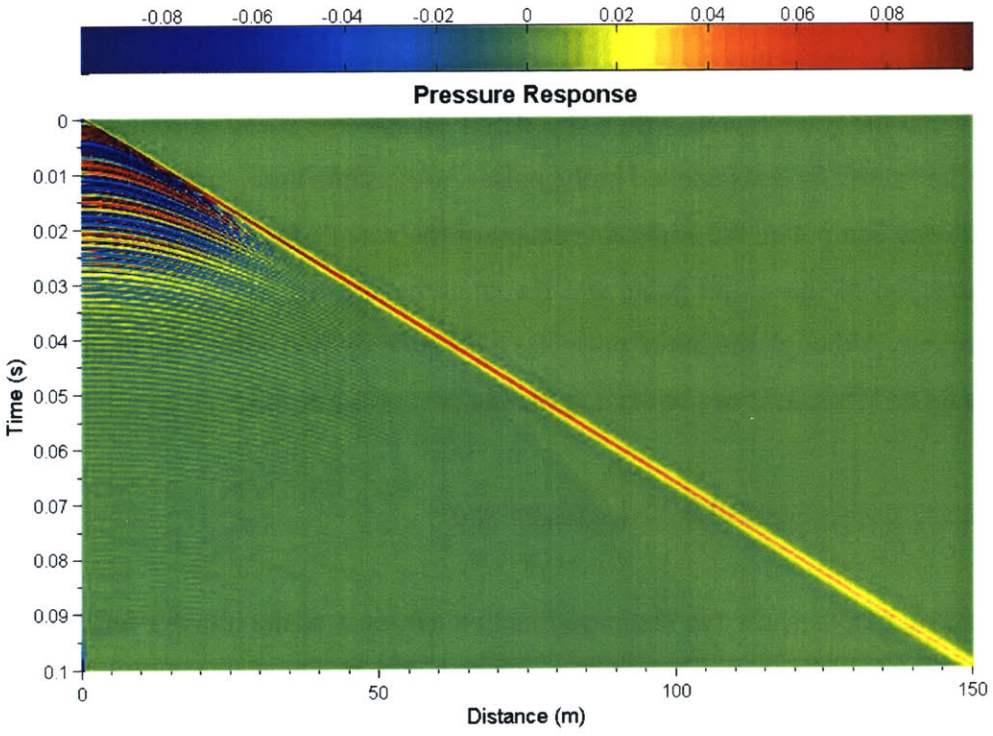

Figure 4.5: Pressure response (0.2ms pulse)

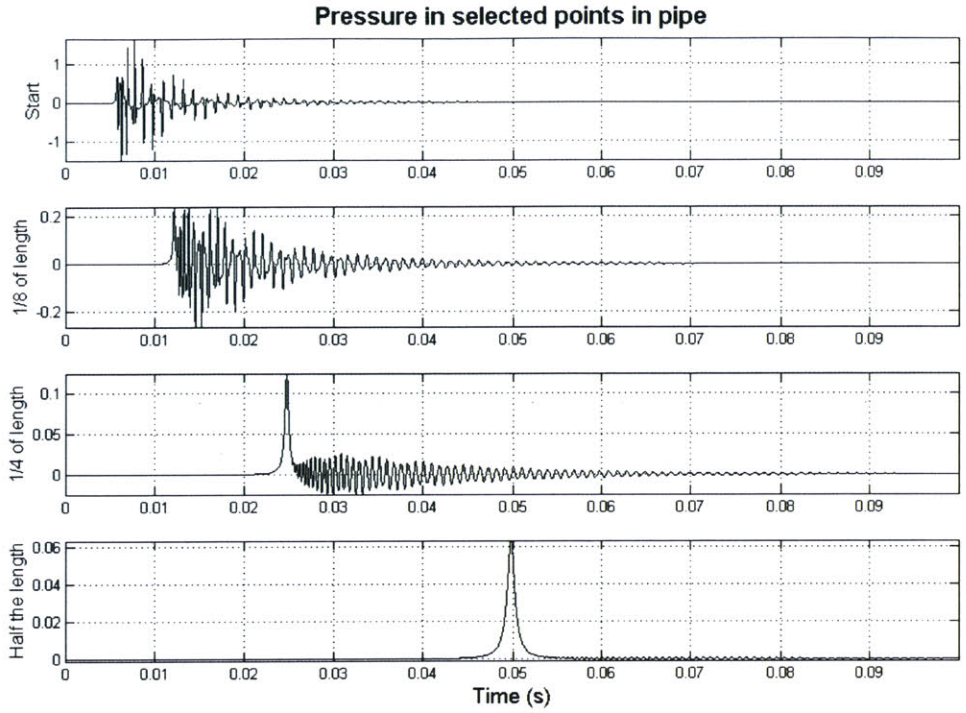

Figure 4.6: Pressure response in selected points in pipe (0.2ms pulse)

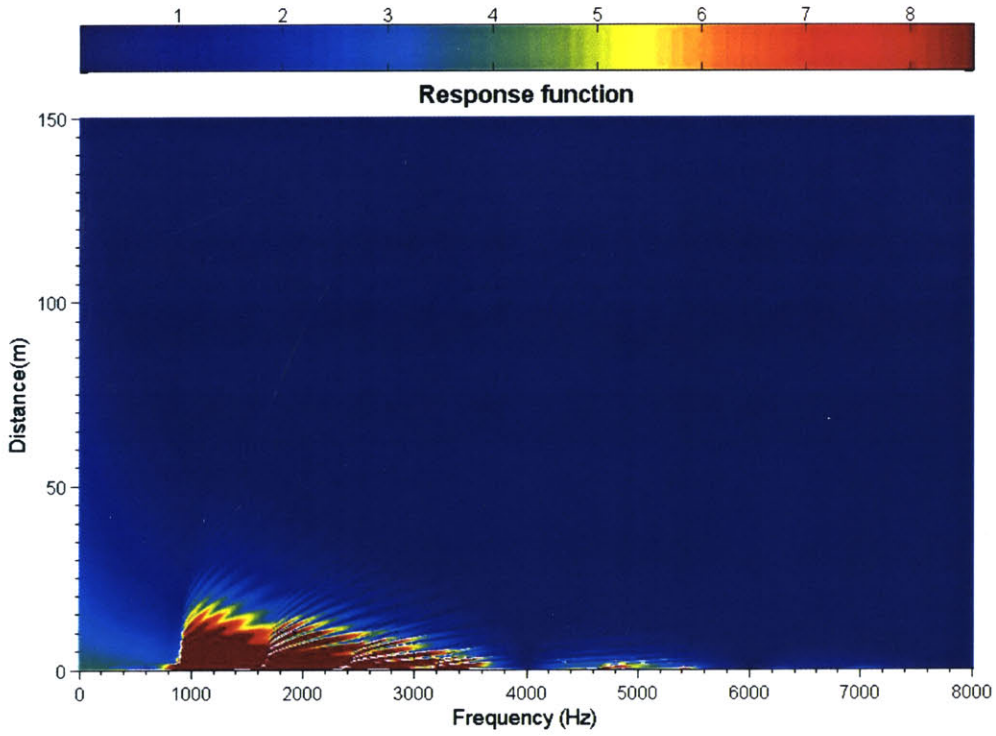

Figure 4.7: Response function (0.5ms pulse)

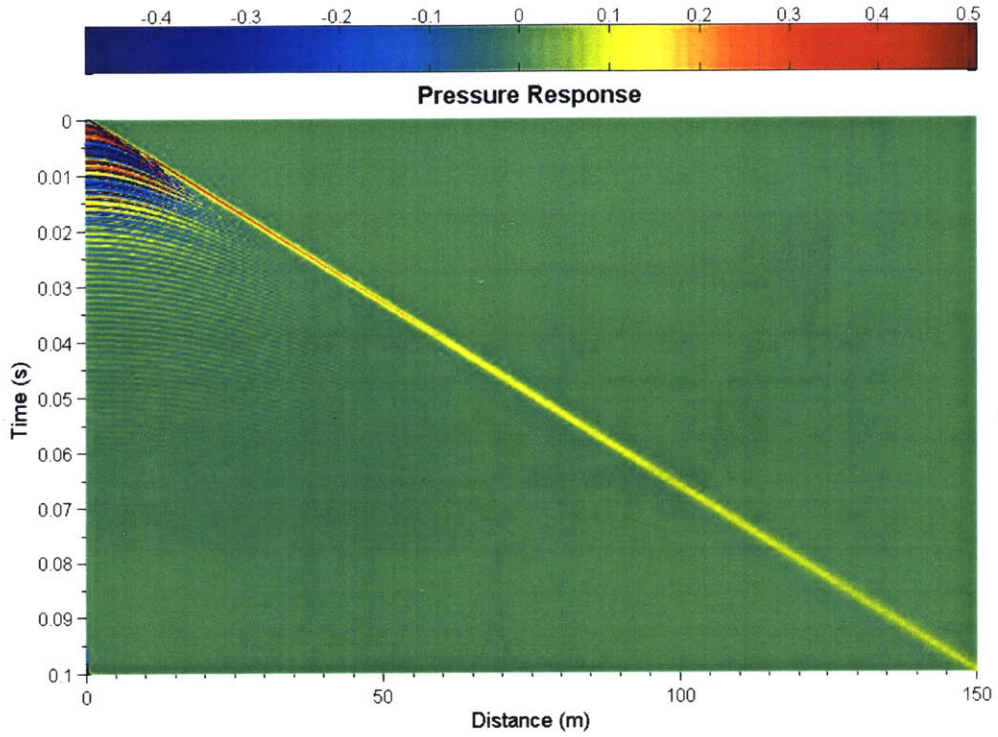

Figure 4.7: Pressure response (0.5ms pulse)

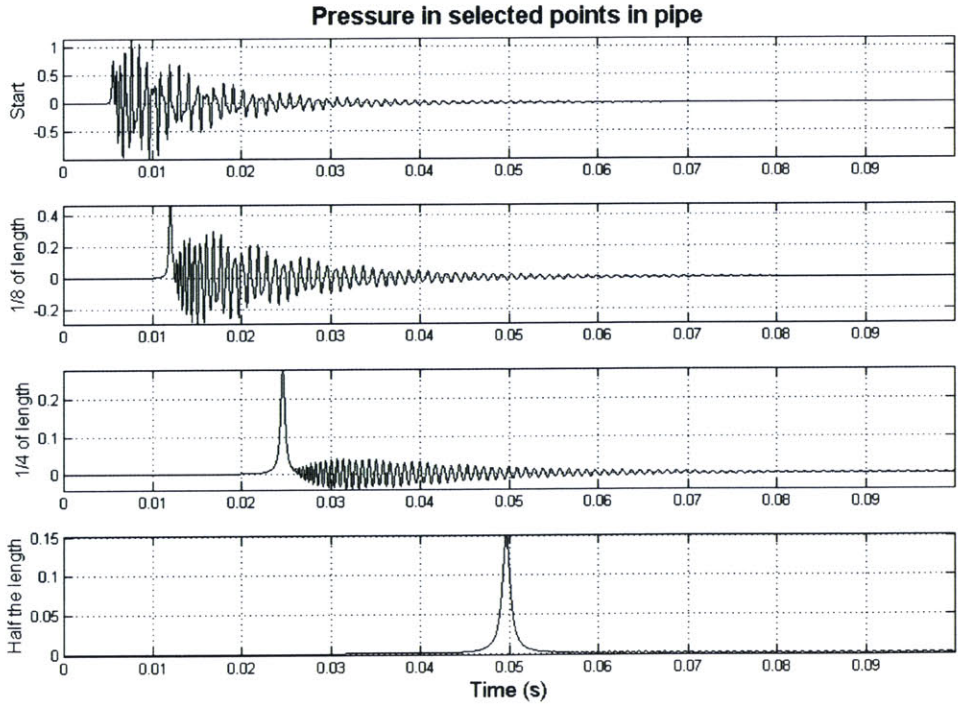

Figure 4.9: Pressure response in selected points in pipe (0.5ms pulse)

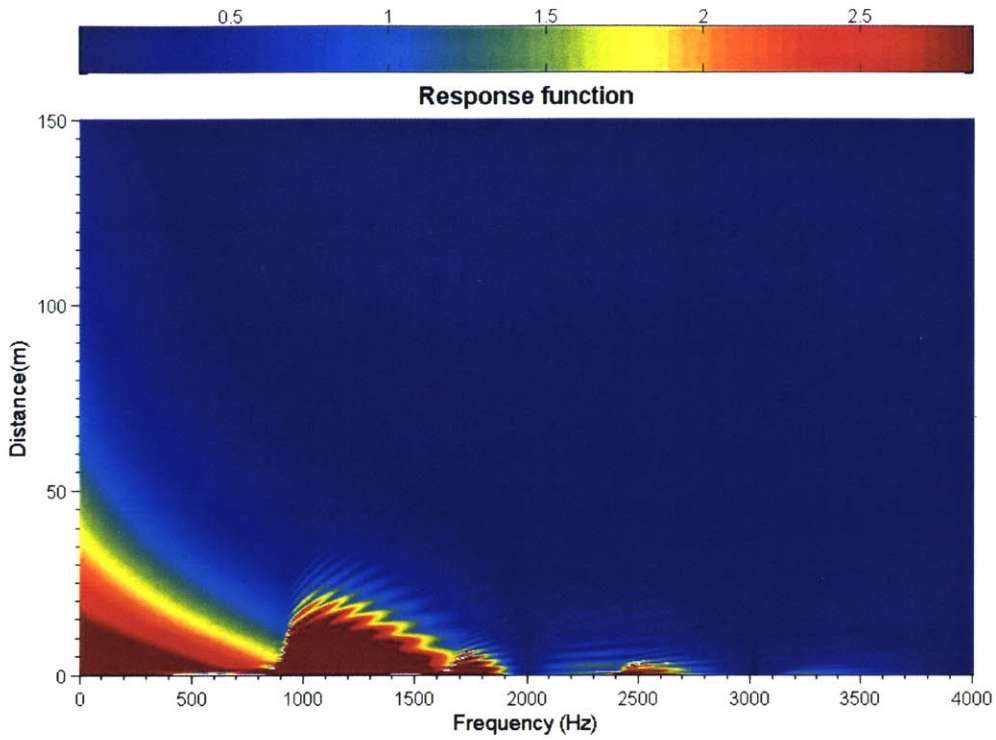

4.10: Response function (1ms pulse)

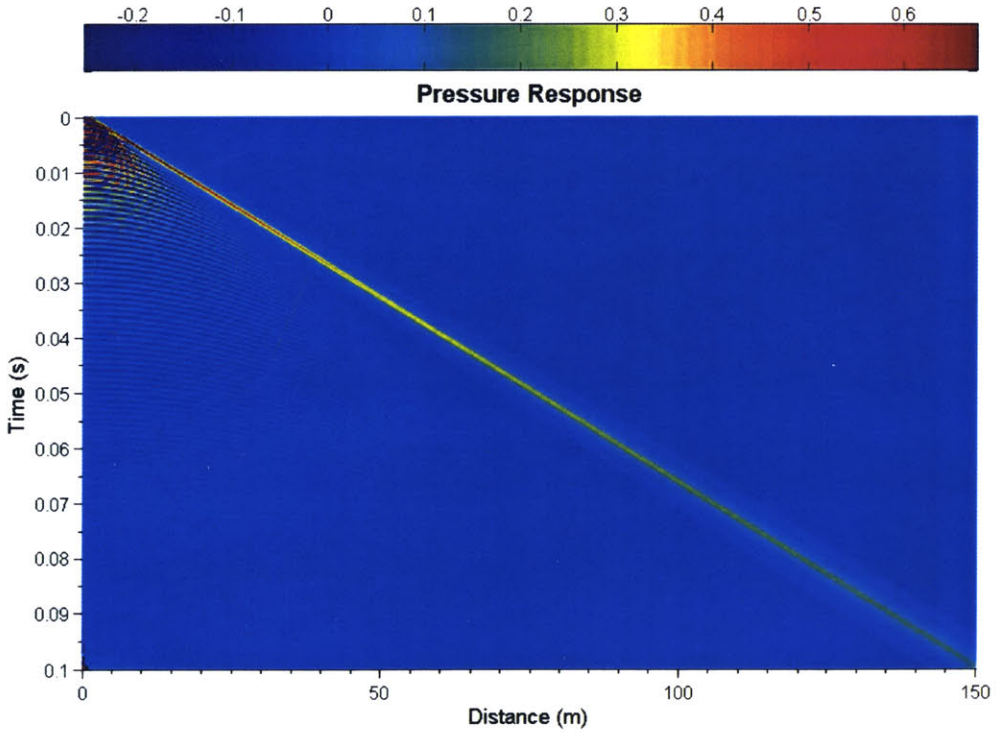

Figure 4.11: Pressure response (1ms pulse)

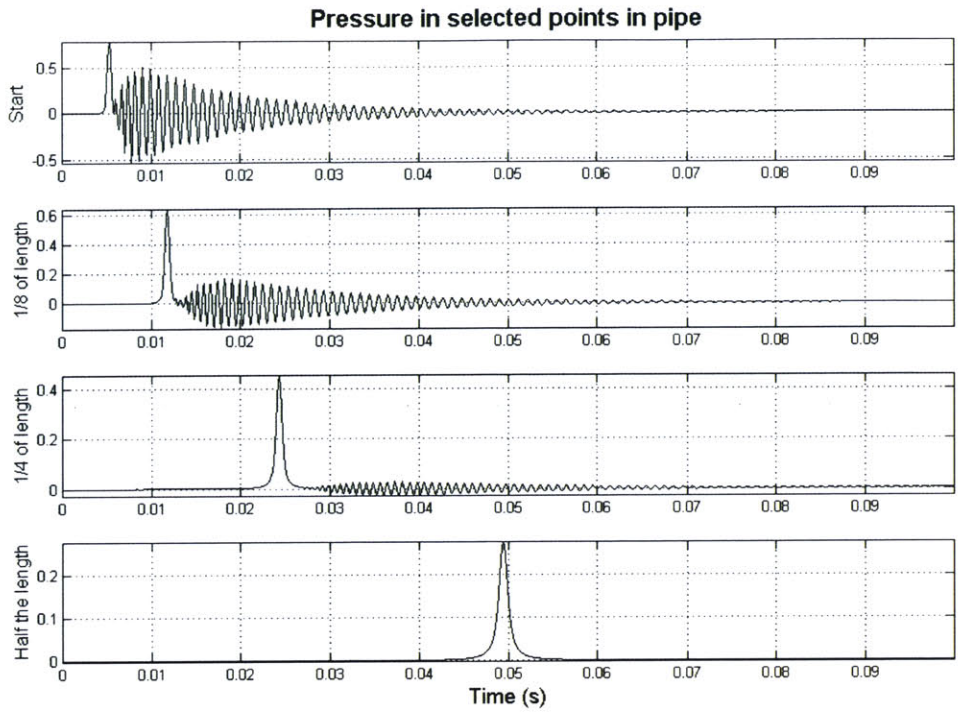

Figure 4.12: Pressure response in selected points in pipe (1ms pulse)

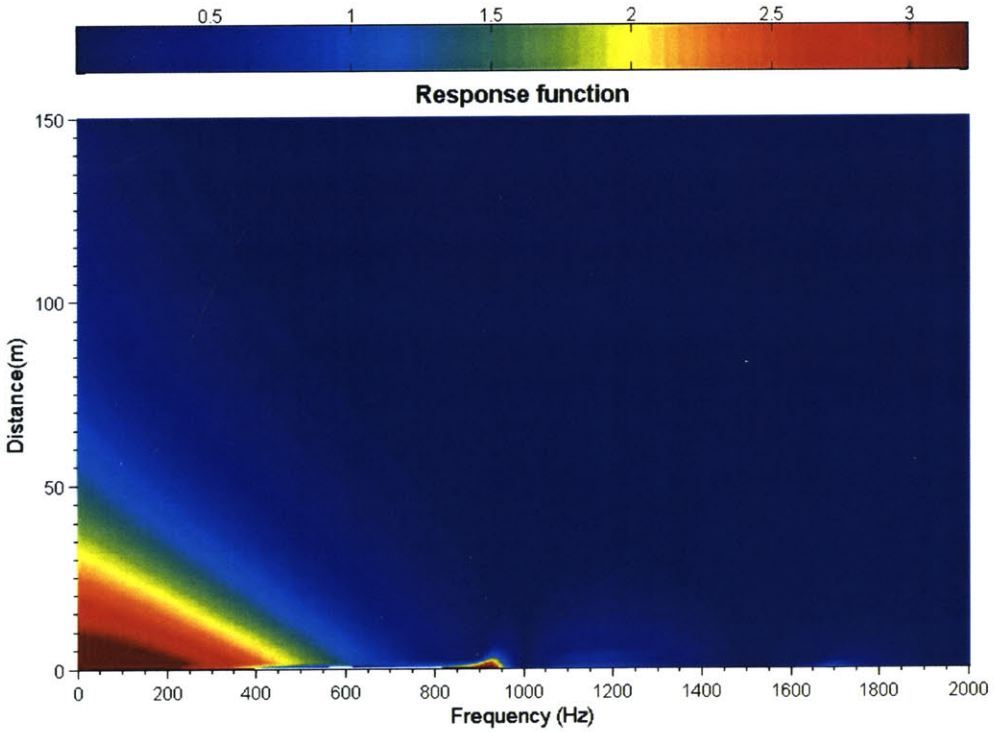

4.13: Response function (2ms pulse)

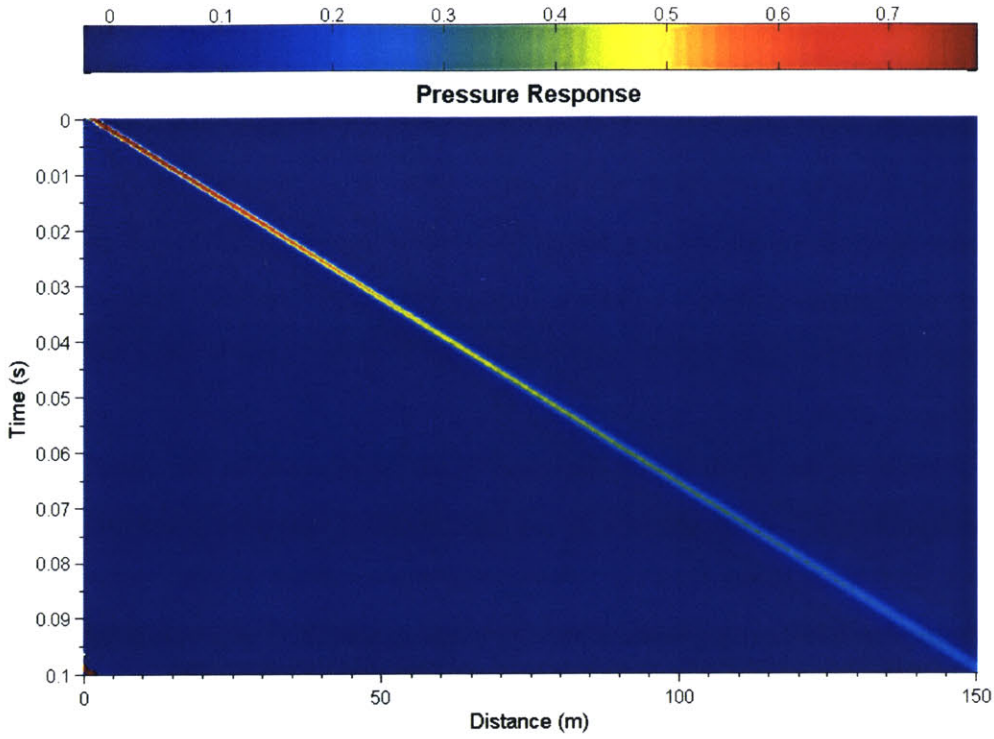

Figure 4.14: Pressure response (2ms pulse)

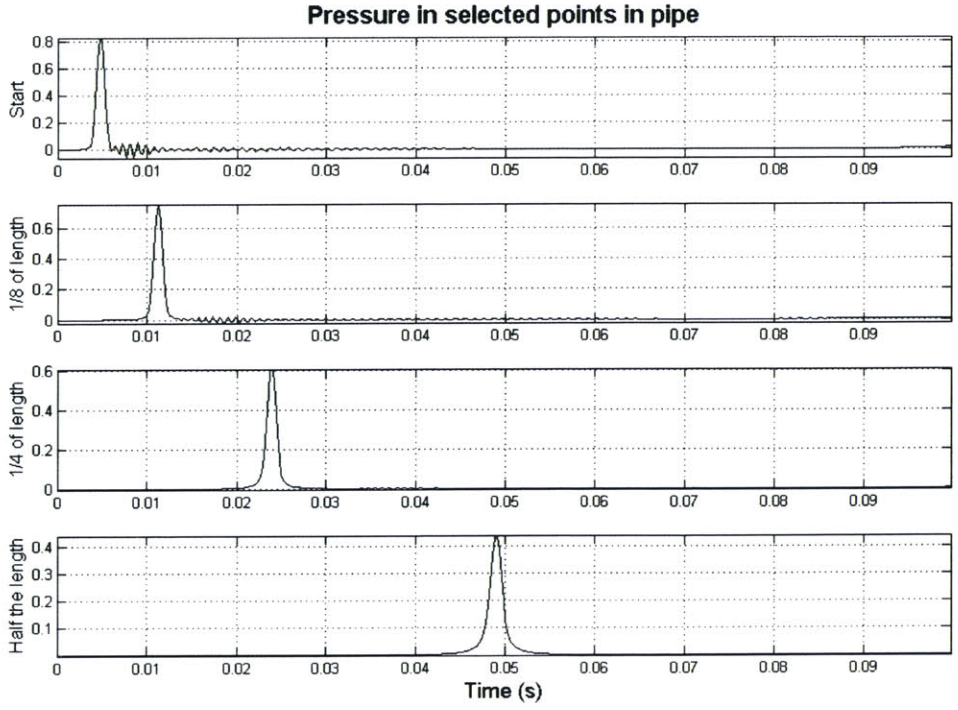

Figure 4.15: Pressure response in selected points in pipe (2ms pulse)

In the above graphs one can see the following major properties of high frequency wave propagation in the rigid pipe:

- The noise level increases with the increase of the frequency, but decreases very fast with the distance the wave has traveled from the source. One can notice that, although the reverberations caused by pulses shorter than 1ms are very strong (sometimes stronger than the actual signal), at a distance of 75m the noise level is well below the main signal strength.
- The strength of the main signal decreases with an increase in the signal frequency, since significant part of the energy of the signal is carried by the higher modes. However, as already noted, these modes attenuate much faster and so the final signal remaining has a lesser amplitude when the frequency of the excitation is higher.
- Initially, the noise seems to travel at a very high speed and later on, as it approaches the main signal, it shifts to the expected speed. This happens because, at start, it travels as a spherical wave, reaching the boundary of the pipe at close distances very fast. However, when the wave dominates all the cross-sectional area of the pipe it travels as a wave front with the acoustic wave velocity of the water.
- As in the low frequency case, the signal's duration seems to extend and the signal smoothens out due to the attenuation of the higher modes.

In general, after a certain propagation distance, one expects to find no or very low noise and a signal with an extended duration which resembles the original one, having a lesser strength due to the attenuation of the "zero" mode, but mainly due to the loss of energy to the higher modes, which will have died out by that point. Consequently, at large enough distances the signal will come out clear, but one must be prepared to receive a fainter pulse than the one sent. A possible solution to long distance communication in the pipe would then be to use a very strong pulse, which will be cleared out and still have high enough amplitude.

4.4 Conclusions

In chapter 4 a simplified analysis of the pipe was carried out to show the expected response of the system when the pipe has a much higher stiffness than the water it contains. The modes and characteristic frequencies were computed from the analytical solution and conclusions were drawn on the modes propagating in the pipe under a given frequency of excitation. The noise level was also associated with the frequency content of the excitation and the pressure-time relationship was calculated in many points inside the pipe. Moreover, it was concluded that, even for very high frequencies, the noise dies out after propagating a relatively small distance (75m maximum) compared to the propagation distance of the main signal. As a final remark, due to the high frequency content of the noise, the signal was proven to sustain its strength much more than the noise following it, so any receiver placed downstream or upstream at an adequate distance will be certain to receive a clear signal, although weaker than the one transmitted.

5. Beam Forming

5.1 Introduction

As proven analytically and shown in Chapter 4.3, it is impossible to emit a sound signal of high enough frequency without having it spread in time and losing its strength due to its propagation. Nonetheless, high frequencies enable information transmission much faster and the success of the method of transmission lies upon this fact. So, it is easily understood that a noise reduction method is very valuable in this case. Although a lot of sophisticated filters from the branch of signal processing do exist, there is a much easier and cheaper method of noise filtering that is called "beam forming".

"Beam forming" is the alignment of sound signals in space and time so that the random noise in the conjoined received signal cancels out, while the coherent part is strengthened. In this chapter the analytical background for beam forming will be discussed and at the same time some practical uses of beam forming will be modeled. After these analyses it will be proven that the use of beam forming against noise reduction will allow for higher frequencies to be emitted and so for much more information to be channeled in the same amount of time.

5.2 Analytical considerations

In this chapter it will be shown that the analytical manipulation of the transfer function that describes the pressures in the pipe (or any attribute of the response for that matter) in the time and space domain is of no practical use and therefore there is no way to analytically calculate the joint response of the two sources. However, after understanding the noise problem in the pipe, it is relatively straightforward to position the sources' excitation in space and time to achieve the required noise reduction.

The analytical calculation of the beam forming response, based on the response of a single source, is not trivial. This is due to the inverse Fourier transformation, which the data must go under, and the summation of the different terms of the series as follows:
If the second source is spaced z_0 away from the first one and "fires" at t_0 after the first one the transfer function of the pressures inside the pipe will have the form of:

$$p'(r,\theta,z,\omega) = \frac{\rho}{2\pi R^2}\omega f(\omega) e^{i\omega(t-\Delta t_0)} \sum_{j=1}^{\infty} \frac{e^{-i(z-z_0)\sqrt{k_0^2-k_{0j}^2}}}{\sqrt{k_0^2-k_{0j}^2}} \frac{1}{J_0^2(k_{0j}R)}$$ (given that the pressure is

calculated at the center of the pipe, r=0)

It is easy to see that the exponential term of $e^{-iz_0\sqrt{k_0^2-k_{0j}^2}}$ has a different value for each term and therefore cannot be factorized and used outside the Fourier integral. At the same time the $e^{-i\omega\Delta t_0}$ term, although equal for all j, cannot be factorized out of the Fourier integral, because it contains the integration variable ω. Consequently, there is not easy to derive formula that simulates the response of the system under the beam forming loading.

However, knowing the response function of the system and observing its maximum value region, one can get a fairly good estimation of a relationship between the delay and the spacing of the second source. Given that these must be linked through a wave speed of approximately 1.5 Km/s, one can then calculate the required z_0 and Δt_0. The following chapter will show how this can be done, given the dimension of the pipe and the signal properties.

5.3 Practical uses

Assuming a pipe of 1m radius under different kinds of excitation, this chapter will demonstrate how to space apart the second source and the delay required for a substantial noise reduction. The excitations used will be of high frequency content, so that they can generate enough noise. The term "intermediate noise level" is used to signify noise that has maximum amplitude equal to the initial signal strength, while the "high noise level" refers to noise that can exceed the initial signal in amplitude. The results will show the difference

between the response of the system to a single source loading and a beam forming with 2 sources.

1ms pulse (intermediate noise level)

This pulse will have a response function (for the single source) as shown in the next graph:

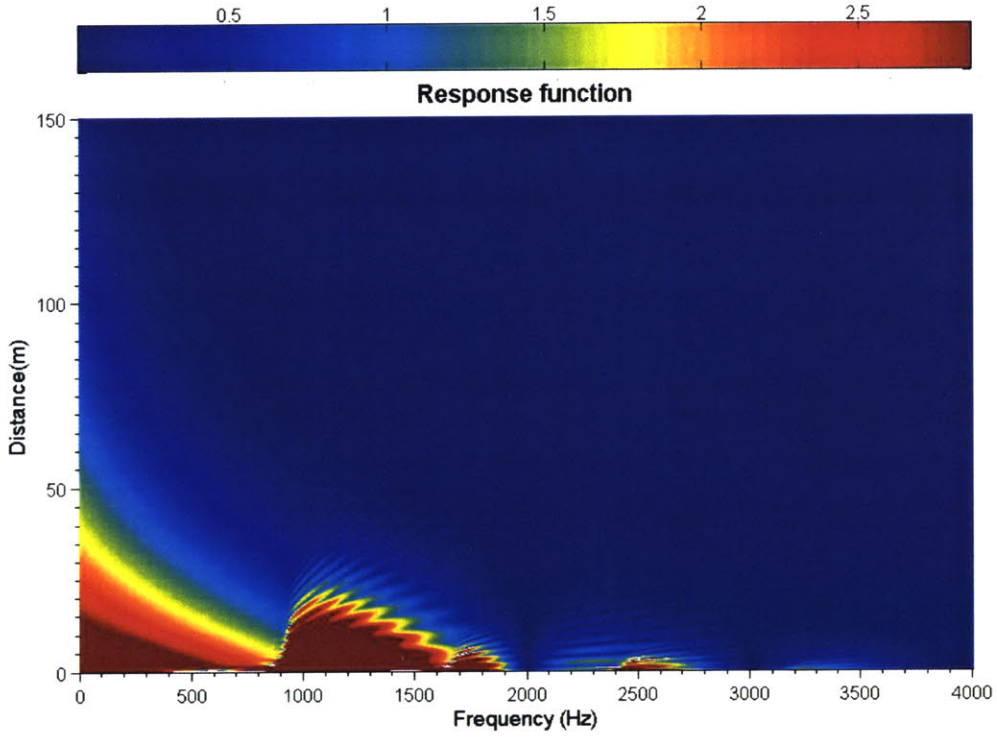

Figure 5.1: Response function of a single 1ms pulse

Assuming that only the "zero", first and second mode can propagate, given that the graph has substantial values for $z \geq 5m$ only for the first three frequencies, then the equation of the pressure caused by two sources can be written as:

$$\sum p(r,\theta,z,\omega) = \frac{A(z,\omega)}{2} \cdot \left(e^{-i\omega\Delta t_0} \sum_{j=1}^{3} \frac{e^{-i(z-z_0)\sqrt{\left(\frac{\omega}{c}\right)^2 - k_{0j}^2}}}{\sqrt{k_0^2 - k_{0j}^2}} \frac{1}{J_0^2(k_{0j})} + \sum_{j=1}^{3} \frac{e^{-iz\sqrt{\left(\frac{\omega}{c}\right)^2 - k_{0j}^2}}}{\sqrt{k_0^2 - k_{0j}^2}} \frac{1}{J_0^2(k_{0j})} \right)$$

This equation assumes that each source generates half the pressure it would generate if it were a single source, so that the result is comparable to the pressure caused by a single source.

For each mode, except the "zero" one, only the frequencies below its cut-off frequency will give a propagating wave, while all other frequencies will result in waves that die out exponentially with time and do not affect the pressure distribution at distances higher than ; R=1m. Consequently, the first mode (j=2) doesn't have any high response function values below its cut-off frequency $(;\ 1.68\ \text{KHz})$ and for $z \geq 5m$. On the contrary, the second mode (j=3) has very high response function values below its cut-off frequency $(;\ 0.92\ \text{KHz})$, around the first mode cut-off frequency $(;\ 1.68\ \text{KHz})$.

Given the above observations, the analytical problem shrinks down to:

$$\sum p(r,\theta,z,\omega) = \frac{A(z,\omega)}{2} \cdot \left(e^{i\left(z_0 \sqrt{\left(\frac{\omega}{c}\right)^2 - k_{02}^2} - \omega \Delta t_0 \right)} + 1 \right)$$

So, in order to eliminate the noise pressure the exponential term must be equal to -1 or equivalently:

$$z_0 \sqrt{\left(\frac{\omega}{c}\right)^2 - k_{02}^2} - \omega \Delta t_0 = \pi$$

The physical interpretation of the previous equation is that the noise generated by the second mode will have a phase shift of π for the two signals. In this way this noise will cancel out. However, this equation cannot provide a set of unique solutions for z_0 and t_0.

Given that the response function has the highest values around frequencies that give the lowest wavenumbers $\left(k_z = \sqrt{\left(\frac{\omega}{c}\right)^2 - k_{0j}^2} \right)$, the equivalent wavelengths will be very high. However, waves with length above R cannot propagate without heavy attenuation and so the maximum wavelengths can be in the order of R. Consequently, one can expect that the waves with lengths around 1m will be the ones with the highest strength. According to this note, in order to magnify the main signal, one has to space the two sources about 1m apart.

For two sources spaced 1m apart, the time difference would be about 0.86ms. Since these values were calculated assuming that only three modes can propagate, one can expect that these values are not optimal, but a good starting approximation. After changing the numbers around these values it was found that the optimal values are:

$\Delta t_0 = 0.795\ ms$
$z_0 = 0.9\ m$

These values are a solution of the above equation and at the same time make the noise from the other modes die out faster as it can be seen in the following graphs. The graphs, as in chapter 4, show the pressures in space and time in a three dimensional graph and the pressures time history close to the source and at distances equal to 9.38, 18.75 and 37.5m.

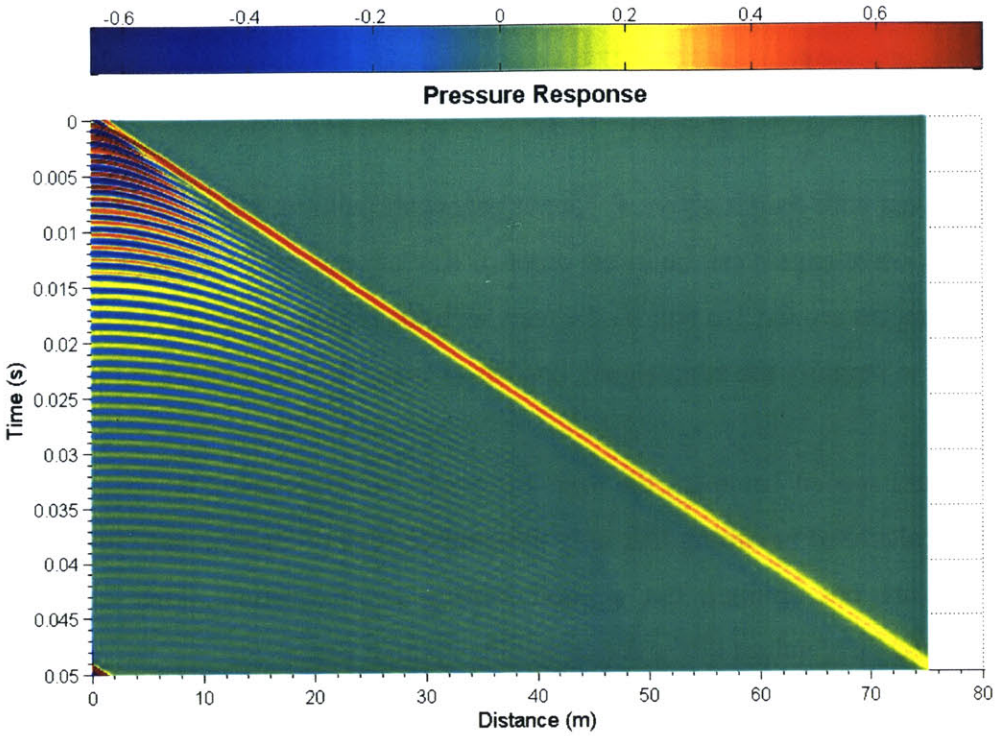

Figure 5.2: Pressures generated by single source (1ms pulse)

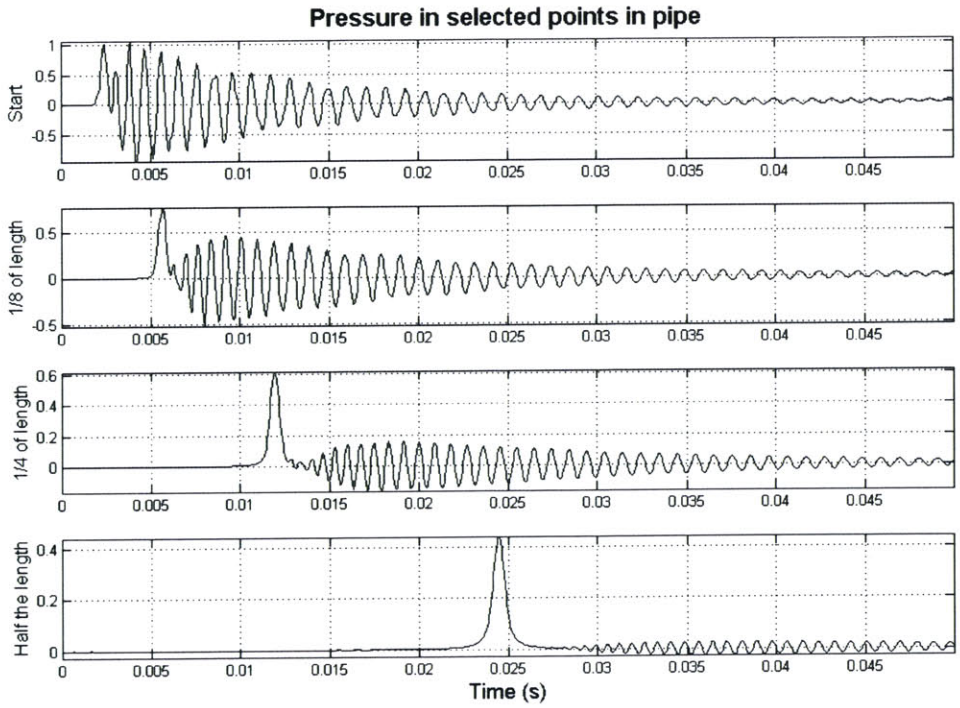

Figure 5.3: Pressures in selected points in pipe (1ms single pulse)

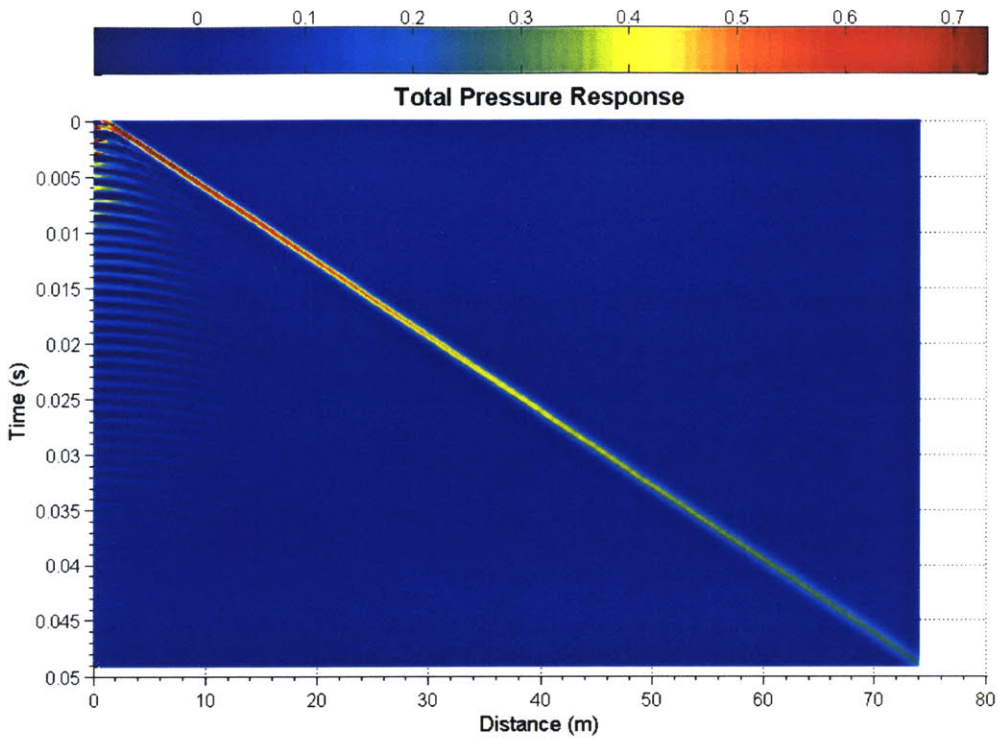

Figure 5.4: Pressures generated by beam forming (1ms pulse)

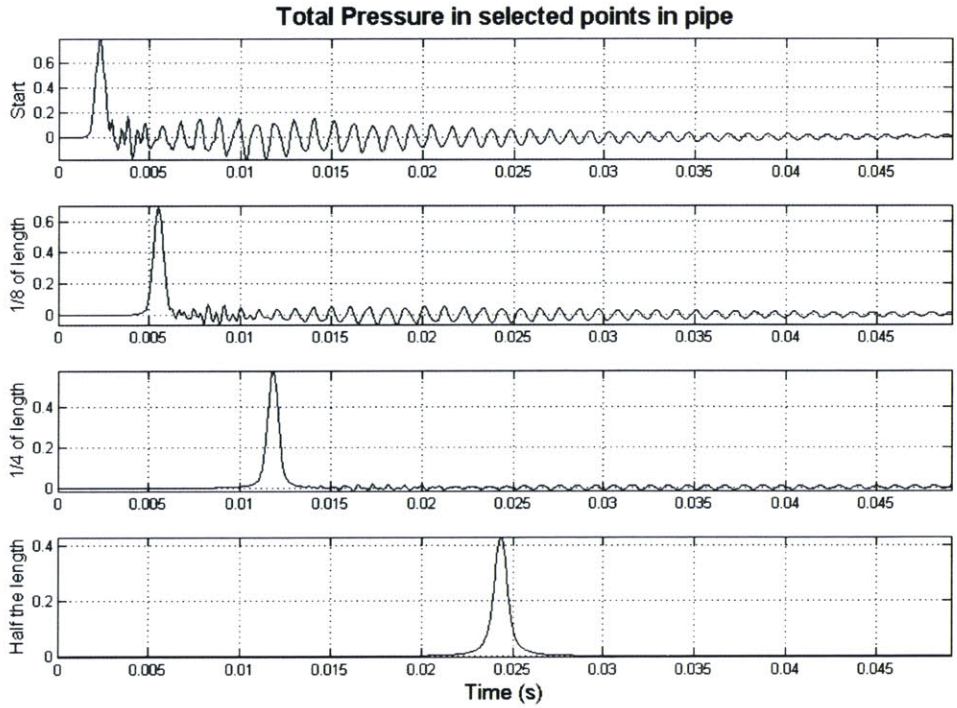

Figure 5.5: Pressures in selected points in pipe (1ms pulse of beam forming)

In the above graphs one should notice the reduction of the noise level in every point in the pipe, but furthermore that the signal is fairly clear after the first 10m of propagation.

0.5ms pulse (high noise level)

Following the same procedure as with the 1ms pulse, the analytical solution for a spacing of 0.5m is 0.45ms. Changing the numbers again to achieve the optimal noise reduction, the final answer is:

$\Delta t_0 = 0.48\ ms$
$z_0 = 0.49\ m$

These numbers will give the following response:

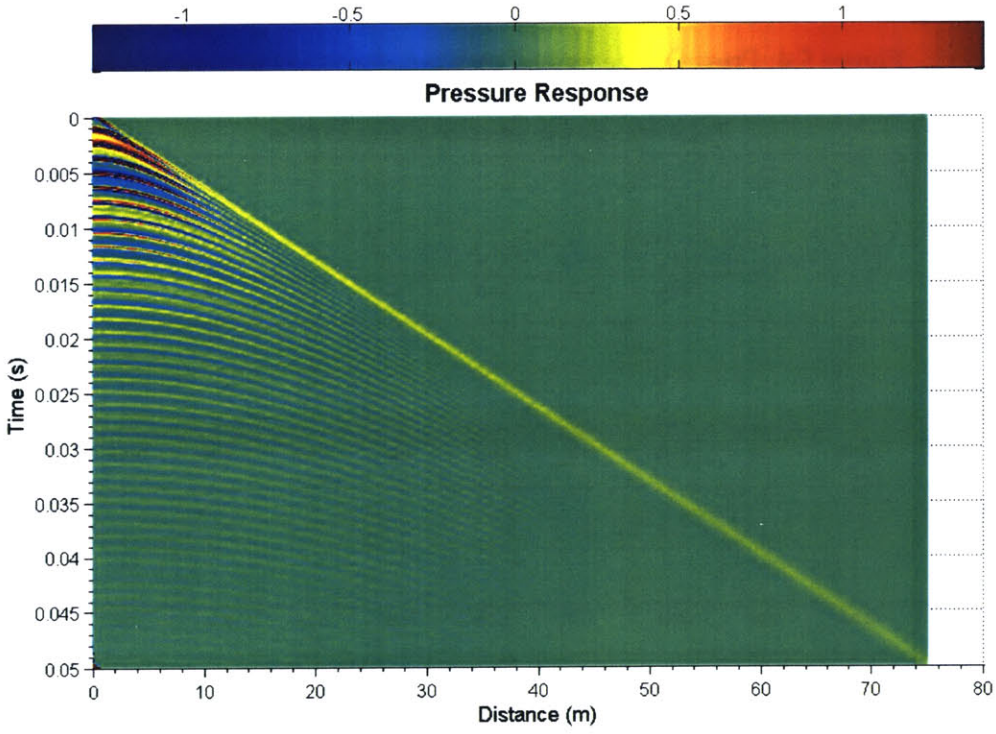

Figure 5.6: Pressures generated by single source (0.5ms pulse)

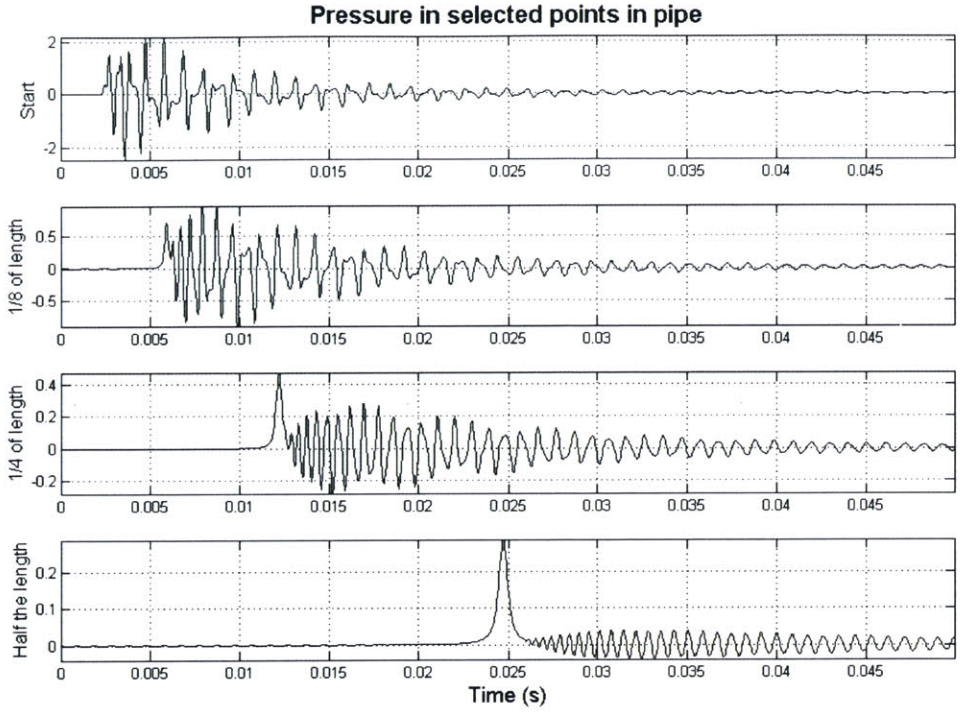

Figure 5.7: Pressures in selected points in pipe (0.5ms single pulse)

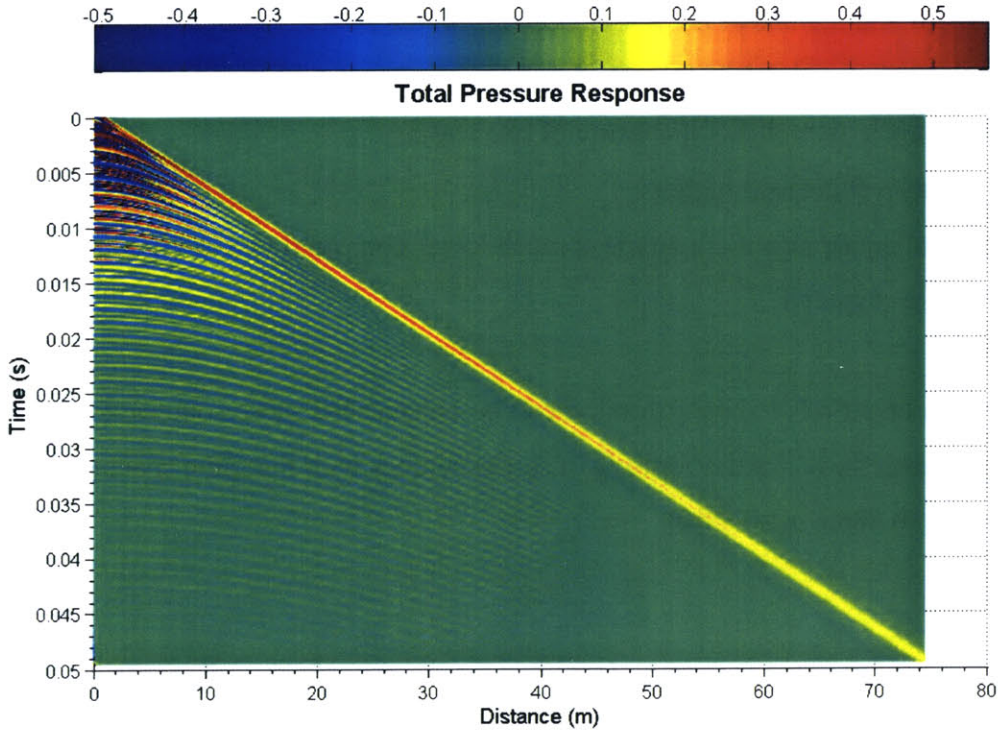

Figure 5.8: Pressures generated by beam forming (0.5ms pulse)

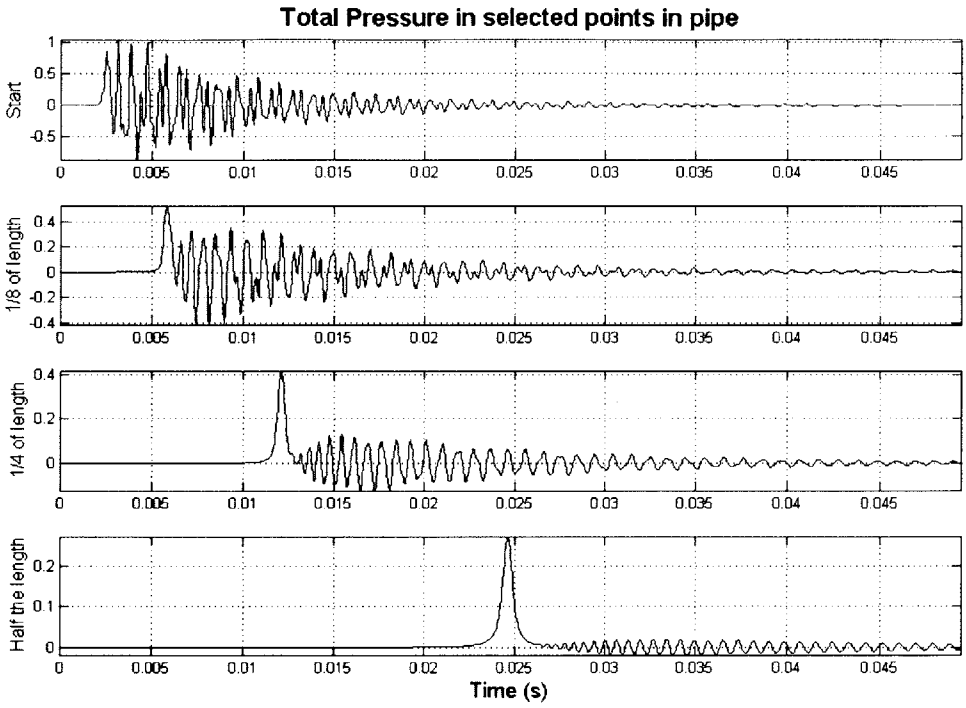

Figure 5.9: Pressures in selected points in pipe (0.5ms pulse of beam forming)

As Figures 5.8 and 5.9 show, the noise reduction in the system is not adequate, even with the optimal spacing and delay. One must notice here that the noise reduction in the 0.5ms pulse case is much more difficult because of two reasons:

- The noise level is much higher
- The "zero" mode signal amplitude is much lower compared to a low frequency signal, as noted in chapter 4

However, the effect of the beam forming can be enhanced if more sources are used. The following graphs show a beam forming of threes sources with the same spacing and delay as before (Δt_0=0.48ms, z_0=0.49m).

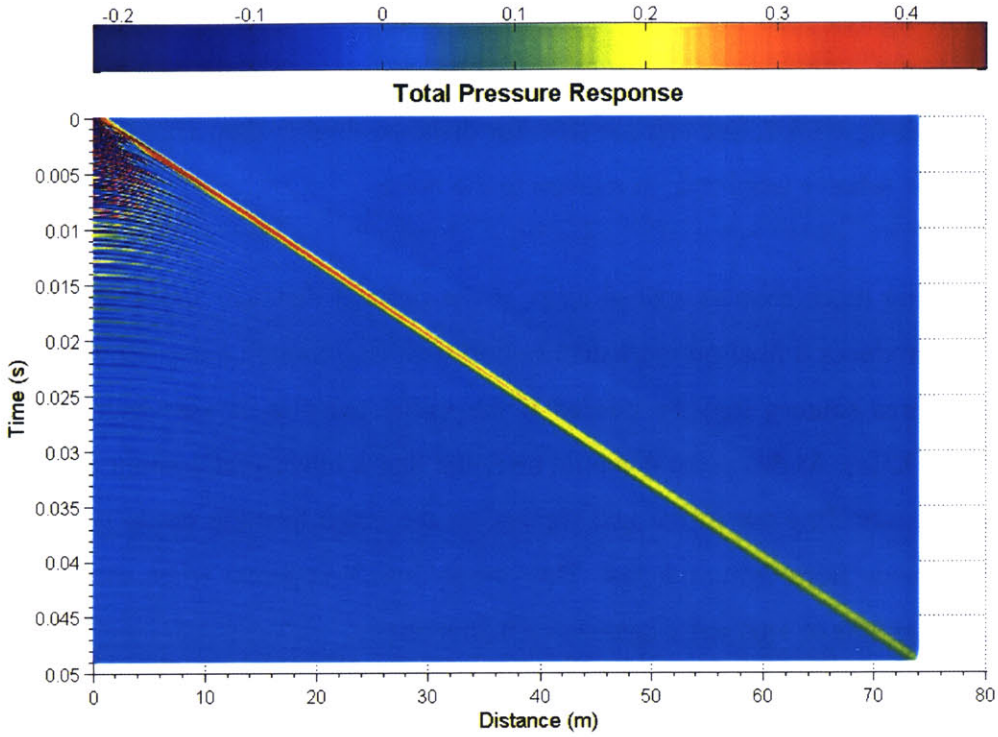

Figure 5.10: Pressures generated by triple beam forming (0.5ms pulse)

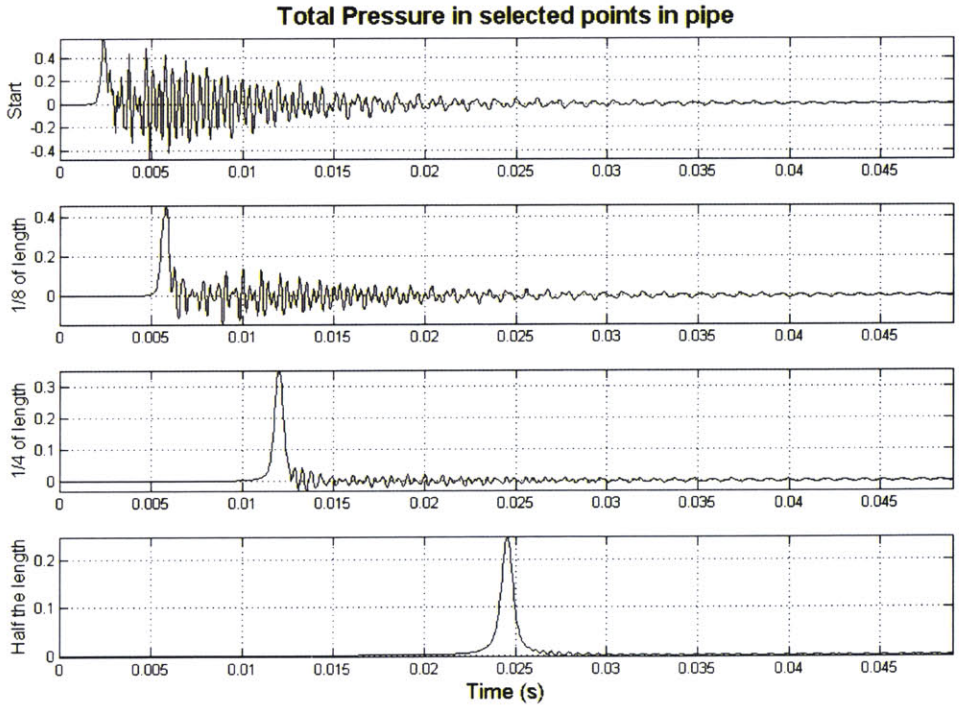

Figure 5.11: Pressures in selected points in pipe (0.5ms pulse of triple beam forming)

As shown in figures 5.10 and 5.11, using three sources resulted in very strong noise reduction, which is of the same level as the one of the 1ms beam forming pulse. Comparing figure 5.11 with figure 5.5, one can see that, for distances higher than 10m, the signal has almost the same relative amplitude in relation to the noise.

In general, using more sources spaced apart at the optimal distance and delayed for the optimal time produces a final pressure distribution with low enough noise. However, more than two or three sources may be needed if the initial pulse is of very high frequency (higher than 1 KHz). At this point it should be noted that a substantial amount of energy is lost due to the canceling out of the two signals, so the beam forming doesn't prevent the signal's zero mode from dying out fast. This energy loss is apparent when comparing the beam forming graphs of 1ms pulse against the 0.5ms ones.

5.4 Conclusions

As shown in chapter 4, any signal of high frequency content is bound to have some noise associated with it up till a certain propagation distance. If the receivers must be placed close to each other, or if the signal strength is very important for the analysis, there is no way to make the signal clear by using only one source of excitation. The beam forming method analyzed in this chapter solves the problem of the noise generated close to the source by placing two or more transmitters at a certain distance and delaying their firing time. This form of pressure generation, which applied the same total pressure in the pipe, forces the noise reverberations of the different sources to cancel out. This chapter gave a simple analytical way of calculating the time delay and spacing of the sources to achieve the maximum noise reduction. The level of noise reduction was shown to be adequate, even for high frequency excitations, given that most of the noise dies out within the first 10-15m of propagation, making the initial signal easy to discern even in close range.

6. Analysis of cylindrically layered system

6.1 Introduction

After presenting the simplified solution for wave propagation inside a rigid water-filled pipe in chapter 4, one can scale up the problem to take into account the stiffness of the pipe and the surrounding medium (or media). At the same time, since the formulation of the stiffness matrix of the problem can be generalized to describe any possible cylindrically layered medium arrangement, one can use the proposed method to analyze the wave propagation in any kind of layout. The stiffness matrix will be calculated in cylindrical coordinates depending on axial wavenumber, frequency of excitation and azimuthial number. However, for the sake of computational brevity, the analysis will be done assuming that the source and the receiver both lie on the axis of the cylindrically layered system, so that only axisymmetric waves exist. In this specific case the azimuthial number will be considered equal to zero. Even on this simplified case, however, a double Fourier transformation is required to calculate the pressures in the pipe depending on time and distance from the source.

6.2 Formulation of cylindrically layered system stiffness matrix

Consider a system of N_l-1 concentric cylindrical layers of arbitrary thickness each, whose N_l interfaces we number from the inside to the outside. Optionally, an unboundedly large exterior region can surround these layers. The material properties in each layer will be assumed independent of the azimuth θ and homogeneous within each cylindrical layer.

As shown by Kausel [Compendium of Fundamental Solutions in Elastodynamics, Cambridge University Press, in print], for given axial wavenumber k_z and frequency ω, a particular solution to the elastic wave equation for the displacement vector at a point in the interior of an individual cylindrical layer is of the form:

$$\bar{\mathbf{u}}(r,\theta,z,\omega) = \begin{bmatrix} \bar{u}_r & \bar{u}_\theta & -\mathrm{i}\,\bar{u}_z \end{bmatrix}^T = \mathbf{T}_n \left(\mathbf{J}\,\mathbf{c}_1 + \mathbf{Y}\,\mathbf{c}_2 \right) e^{-\mathrm{i}k_z z} \equiv \mathbf{T}_n\, u\, e^{-\mathrm{i}k_z z}$$

$$u = u(r) = \left[\tilde{u}_r \quad \tilde{u}_\theta \quad -\mathrm{i}\,\tilde{u}_z\right]^T = \mathbf{J}\,\mathbf{c}_1 + \mathbf{Y}\,\mathbf{c}_2$$

in which $\mathbf{c}_1$, $\mathbf{c}_2$ are arbitrary constants, and the matrices $\mathbf{T}_n$, $\mathbf{J}$, $\mathbf{Y}$ are as listed in Table 2. The superscript bar is a reminder that this is a solution in the frequency-wavenumber domain, while the tildes indicate that the variations with z and θ have been separated. Also, the stresses in cylindrical surfaces are

$$\left[\bar{\sigma}_r \quad \bar{\sigma}_{r\theta} \quad -\mathrm{i}\,\bar{\sigma}_{rz}\right]^T = \mathbf{T}_n\left(\mathbf{Q}\,\mathbf{c}_1 + \mathbf{R}\,\mathbf{c}_2\right)e^{-\mathrm{i}k_z z} = \mathbf{T}_n\,\sigma\,e^{-\mathrm{i}k_z z}$$

$$\sigma = \sigma(r) = \left[\tilde{\sigma}_r \quad \tilde{\sigma}_{r\theta} \quad -\mathrm{i}\,\tilde{\sigma}_{rz}\right]^T = \mathbf{F}^{(1)}\,\mathbf{c}_1 + \mathbf{F}^{(2)}\,\mathbf{c}_2$$

in which $\mathbf{F}^{(1)}$, $\mathbf{F}^{(2)}$ are given in Table 3 and are constructed with Bessel functions of the first and second kind, respectively, as indicated by the superscript.

a) Single layer

The outermost layer is considered an isolated, free layer whose bounding outer and inner surfaces have radii r_1, r_2, respectively. Evaluating the displacements and stresses at these two surfaces, defining the tractions *per radian* as the product of the stresses and the interface radius, and writing both together in matrix form, one obtains:

$$\begin{Bmatrix} u_1 \\ u_2 \end{Bmatrix} = \begin{Bmatrix} \mathbf{J}_1 & \mathbf{Y}_1 \\ \mathbf{J}_2 & \mathbf{Y}_2 \end{Bmatrix}\begin{Bmatrix} \mathbf{c}_1 \\ \mathbf{c}_2 \end{Bmatrix}, \begin{Bmatrix} p_1 \\ p_2 \end{Bmatrix} = \begin{Bmatrix} r_1\,\sigma_1 \\ -r_2\,\sigma_2 \end{Bmatrix} = \begin{Bmatrix} r_1\,\mathbf{F}_1^{(1)} & r_1\,\mathbf{F}_1^{(2)} \\ -r_2\,\mathbf{F}_2^{(1)} & -r_2\,\mathbf{F}_2^{(2)} \end{Bmatrix}\begin{Bmatrix} \mathbf{c}_1 \\ \mathbf{c}_2 \end{Bmatrix}$$

in which subscripts indicate the location (i.e. radius) at which the matrices are being evaluated, and superscripts indicate the kind of Bessel functions used. The negative sign in the second row comes from the fact that external tractions are opposite in direction to the internal stresses at the inner surface. Eliminating the constants $\mathbf{c}_1$, $\mathbf{c}_2$ between these two matrices, one obtains:

$$\begin{Bmatrix} p_1 \\ p_2 \end{Bmatrix} = \begin{Bmatrix} r_1 \mathbf{F}_1^{(1)} & r_1 \mathbf{F}_1^{(2)} \\ -r_2 \mathbf{F}_2^{(1)} & -r_2 \mathbf{F}_2^{(2)} \end{Bmatrix} \begin{Bmatrix} \mathbf{J}_1 & \mathbf{Y}_1 \\ \mathbf{J}_2 & \mathbf{Y}_2 \end{Bmatrix}^{-1} \begin{Bmatrix} u_1 \\ u_2 \end{Bmatrix}$$
$$= \begin{Bmatrix} \mathbf{K}_{11} & \mathbf{K}_{12} \\ \mathbf{K}_{21} & \mathbf{K}_{22} \end{Bmatrix} \begin{Bmatrix} u_1 \\ u_2 \end{Bmatrix}$$

in which:

$$\mathbf{K} = \begin{Bmatrix} \mathbf{K}_{11} & \mathbf{K}_{12} \\ \mathbf{K}_{21} & \mathbf{K}_{22} \end{Bmatrix} = \begin{Bmatrix} r_1 \mathbf{F}_1^{(1)} & r_1 \mathbf{F}_1^{(2)} \\ -r_2 \mathbf{F}_2^{(1)} & -r_2 \mathbf{F}_2^{(2)} \end{Bmatrix} \begin{Bmatrix} \mathbf{J}_1 & \mathbf{Y}_1 \\ \mathbf{J}_2 & \mathbf{Y}_2 \end{Bmatrix}^{-1}$$

is the *symmetric* stiffness (or impedance) matrix of the cylindrical layer.

b) Unbounded external region:

In the case of a cylindrical cavity within an unbounded homogeneous space, the external region can be regarded as a layer whose external radius is infinitely large. In this case $\mathbf{c}_2$ must be set equal to zero (to satisfy the radiation and boundedness conditions at infinity) and use second Hankel functions instead of Bessel functions in our matrices. Hence, the 3×3 impedance matrix of the exterior region is

$$\mathbf{K}_{ext} = -r\mathbf{F}\mathbf{H}^{-1}$$

which is assembled with the matrices **H** and **F** in tables 2, 3, both of which must be constructed using second Hankel functions evaluated at the radius r of the external region.

c) Layered system:

Finally, consider a layered system, which may optionally be surrounded by an unbounded exterior region. To construct the global (system) stiffness matrix, it suffices to overlap the

layer matrices for each layer as appropriate, beginning with the impedance matrix of the exterior region. The result is a system of equations of the block-tridiagonal form

$$\begin{Bmatrix} p_1 \\ p_2 \\ \vdots \\ p_N \end{Bmatrix} = \begin{bmatrix} \mathbf{K}_{11} & \mathbf{K}_{12} & \mathbf{0} & \mathbf{0} \\ \mathbf{K}_{21} & \mathbf{K}_{22} & \mathbf{K}_{23} & \mathbf{0} \\ \mathbf{0} & \mathbf{K}_{32} & \ddots & \vdots \\ \mathbf{0} & \mathbf{0} & \mathbf{K}_{N,N-1} & \mathbf{K}_{NN} \end{bmatrix} \begin{Bmatrix} u_1 \\ u_2 \\ \vdots \\ u_N \end{Bmatrix}$$

or more compactly

$$p = \mathrm{K} \times u$$

in which p is the vector of external sources in the frequency-wavenumber domain, which act as external tractions at the layer interfaces.

After calculating the stiffness matrices of the various layers one must join them in their relative degrees of freedom by adding the stiffness components of these degrees. However, it should be understood that there is no relationship between the degrees of freedom in the axial and azimuthial direction in a solid-fluid interface. So, the degrees of freedom in this interface are three and the only joining of stiffness must happen in the radial dimension. Apart from that, the construction of the complete stiffness matrix for the whole system follows the standard stiffness matrix rules for joining terms of the same stiffness.

Note on numerical implementation

In order to calculate the relationship between the pressure matrix p and the displacement matrix u in the general form of $p = \mathrm{K} \times u$, one needs to inverse the Bessel function matrix, which relates the displacements to the arbitrary constants matrix **c**. The determinant of Hankel function matrix depends on axial wavenumber, frequency of excitation and the properties of the system. For a given system, the determinant of this matrix can be proven

to have alternate signs for different frequencies and axial wavenumbers. So, a pair of frequency and axial wavenumber that makes the determinant equal to zero exists.

When the determinant of the matrix is zero it means that some of the columns or rows of it are linearly dependent. So the rank of the matrix and its singular values are less than its dimension. Consequently, to solve the system of equations in this case one needs to decompose the Bessel function matrix using singular value decomposition (SVD) with a limited amount of singular values. So, one can decompose the matrix and then recompose it using as many singular values as prescribed by the rank of the matrix, achieving in this way the closest rank k approximation to the original matrix. The matrix to be decomposed is complex, so the generalized singular value decomposition will take the form of:

$SVD(A) = [U, D, V] \Rightarrow A = U^H D V^T$ where,

A is the matrix to be decomposed,

U and V are matrices with orthogonal columns,

U^H the conjugate transpose of U and

D is a diagonal $k \times k$ matrix.

After various analyses (in the range of millions) it was found that a k of five describes the Bessel function matrix good enough, so that there is no obvious change in behavior around the set of frequency and axial wavenumber in the response. Most of the times in which the determinant is zero, there is only one singular value substantially greater than zero to be considered an important one. Consequently, just one singular value can describe the matrix through SVD with a very good approximation in most cases, so five singular values are more than enough.

It must be noted here that the aforementioned analysis will be done only when the determinant of the Bessel function matrix is equal to zero. In all other cases one can easily inverse the matrix and left multiply it by the **F** matrix to get the stiffness matrix of the system.

6.3 Calculation of stresses and displacements inside the system for any kind of excitation

The scope of the thesis is to calculate the response of the system to any kind of excitation inside the core layer of the system, but the analysis presented here can be used to calculate the response to any load on any point inside the system. The generalized system presented in figure 6.1 will have the following stiffness matrix:

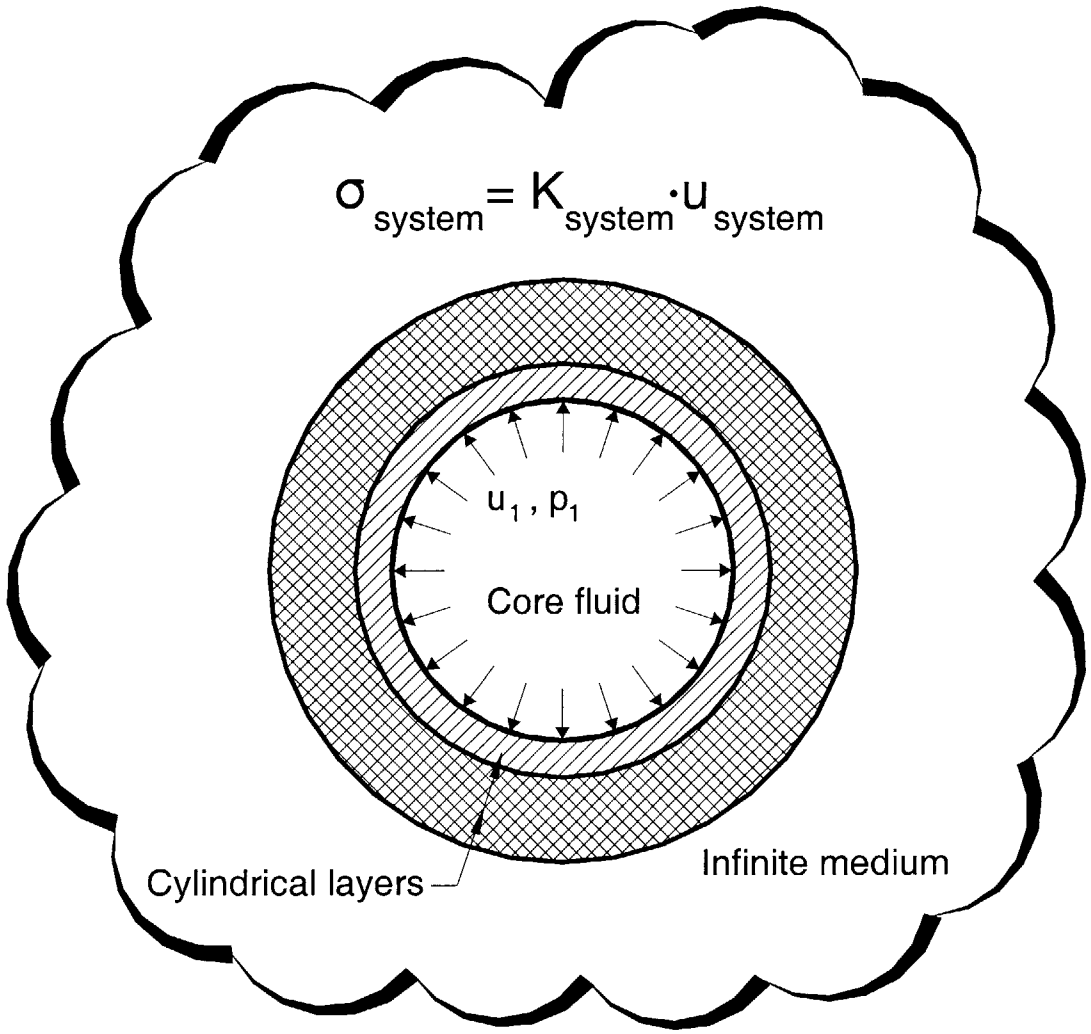

Figure 6.1: Cylindrically Layered System with fluid core

$$\begin{bmatrix} p_1 \\ p_2 \end{bmatrix} = \begin{bmatrix} K_{11} & K_{12} \\ K_{21} & K_{22} \end{bmatrix} \cdot \begin{bmatrix} u_1 \\ u_2 \end{bmatrix}, \text{ where}$$

p_1: the pressures acting on the fluid-solid interface (in the radial direction)

p_2: the pressure acting in any other degree of freedom

u_1: the displacement of the fluid-solid interface (in the radial direction)

u_2: the displacements of all the other degrees of freedom

K_{ii}: the sub-matrices of the total stiffness matrix connecting the pressures of the fluid-solid interface and all the remaining degrees of freedom to their respective displacements

K_{ij}: the sub-matrices of the total stiffness matrix expressing the pressures of the fluid-solid interface and all the remaining degrees of freedom to their unrelated displacements

The system's stiffness matrix will be used to solve for the p_1 pressure, given the solution for the infinitely extending fluid, as follows:

The infinite fluid medium will be divided in two parts: one fluid core and one infinitely extending fluid. Their separating interface will have a radius equal to the internal radius of the pipe, as shown in the following figure:

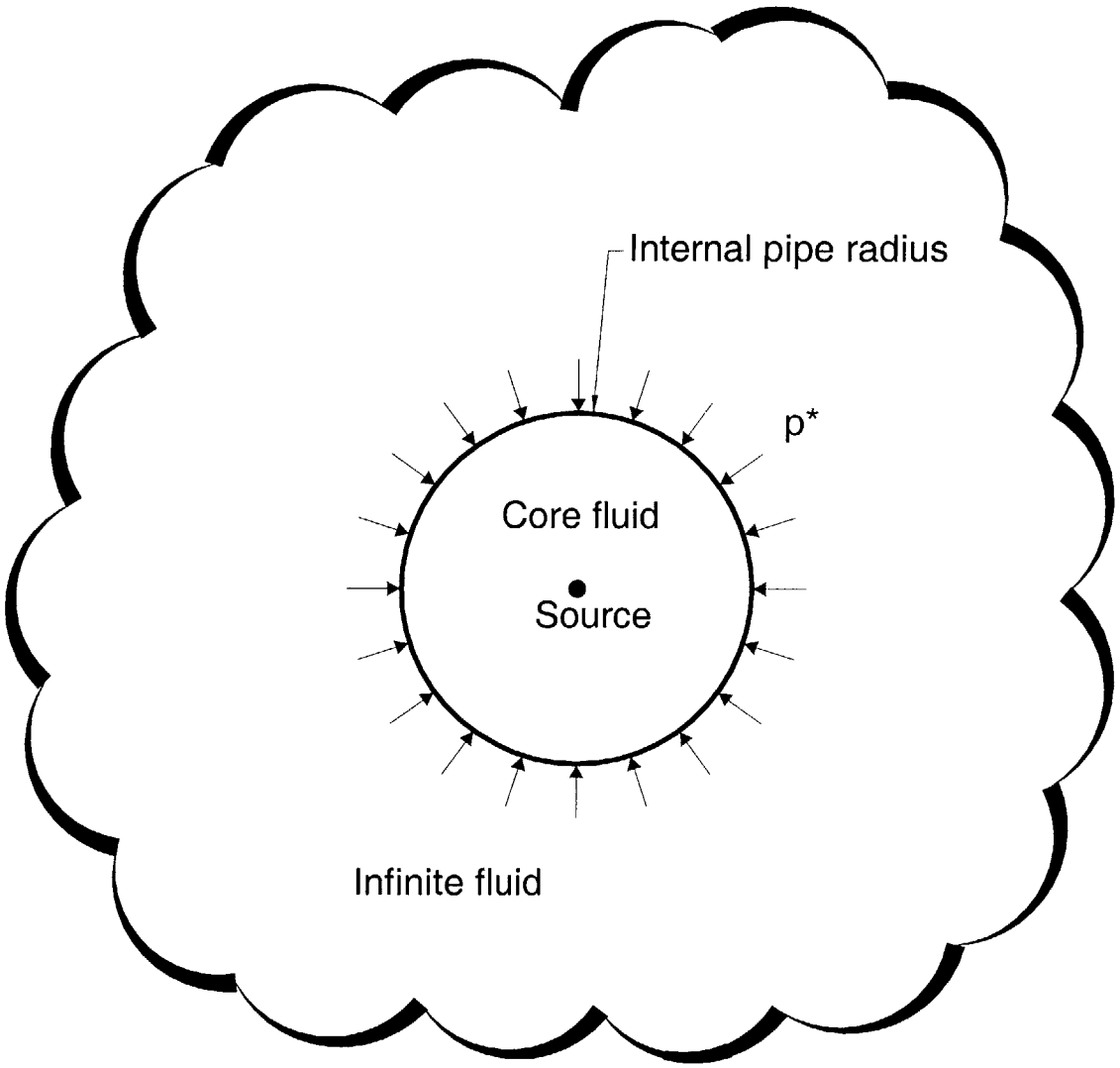

Figure 6.2: Pressures coming from the source in core fluid

The source in the fluid results in pressures, which are noted p^*, and act on the interface of the two fluid layers. Focusing on the external, infinite layer one can write the equation of displacement of the interface as:

$p^* = -K_{fe} \cdot u_r^*$, where

p^*: The pressure acting on the interface (due to the source in the fluid core)

u_r^*: The outward displacement of the interface

K_{fe}: The stiffness of the external layer of fluid

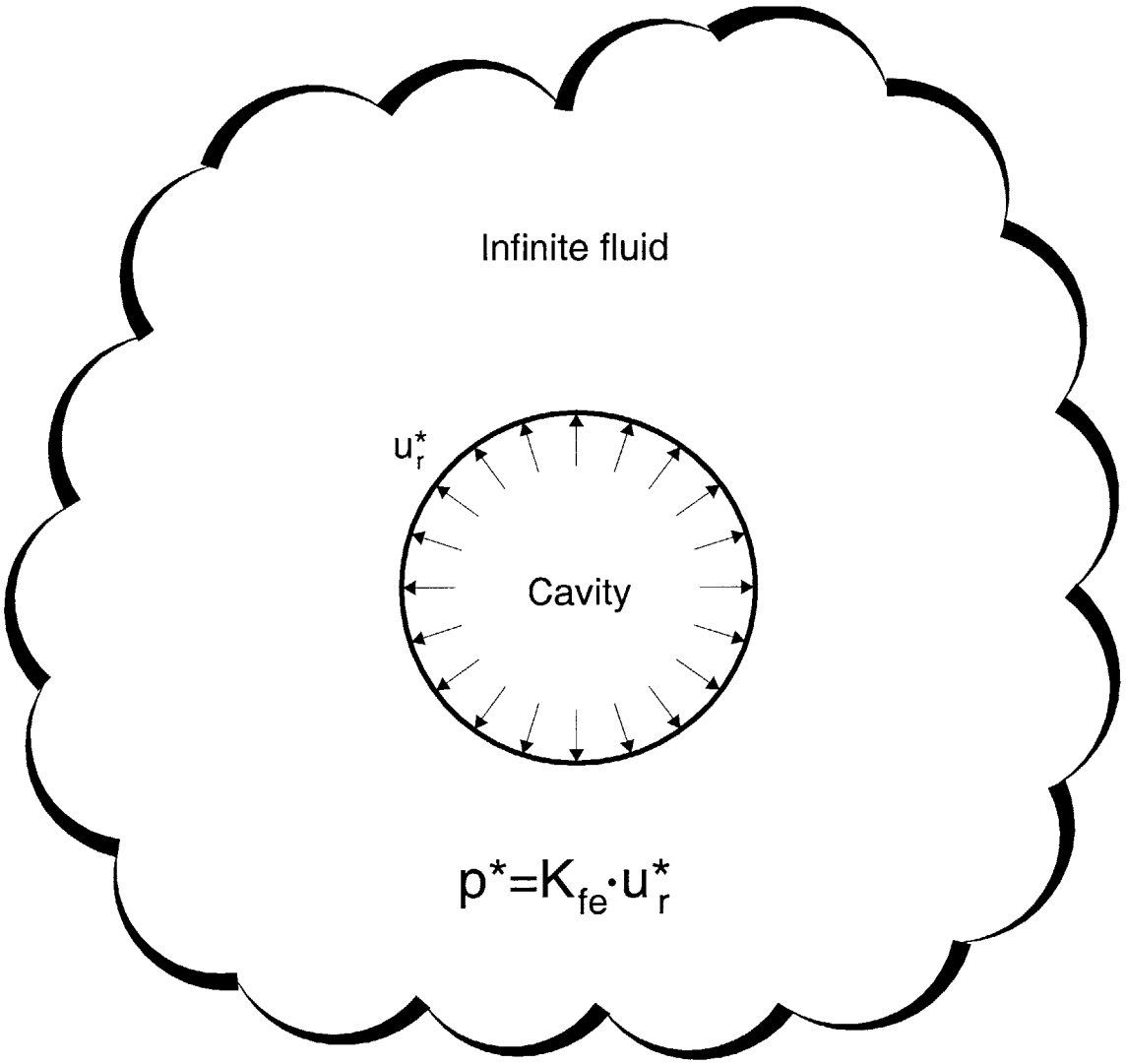

Figure 6.3: External fluid layer displacements and stresses

In the actual cylindrical layout the external layer is not an infinite fluid, but a complex cylindrically layered system. Assuming that a source in the fluid layer causes a stress equal to σ_{1r} on the interface between the core fluid and the external system, the resulting set of equations for the displacements of the system is:

$$\begin{bmatrix} \sigma_{1r} \\ [\sigma_2] \end{bmatrix} = \begin{bmatrix} K_{11} & K_{12} \\ K_{21} & K_{22} \end{bmatrix} \cdot \begin{bmatrix} u_{1r} \\ [u_2] \end{bmatrix}$$

Given the above set of equations, one can see that the application of a stress equal to σ_{1r} on the interface gave a displacement of u_{1r}.

Given that the stiffness of the internal fluid has not changed the difference in its displacement between the infinite fluid and the complete system model is only due to the difference in applied pressure. This relationship between the displacements and the stresses in the infinite fluid and the complete system model will then be (as shown in the graph):

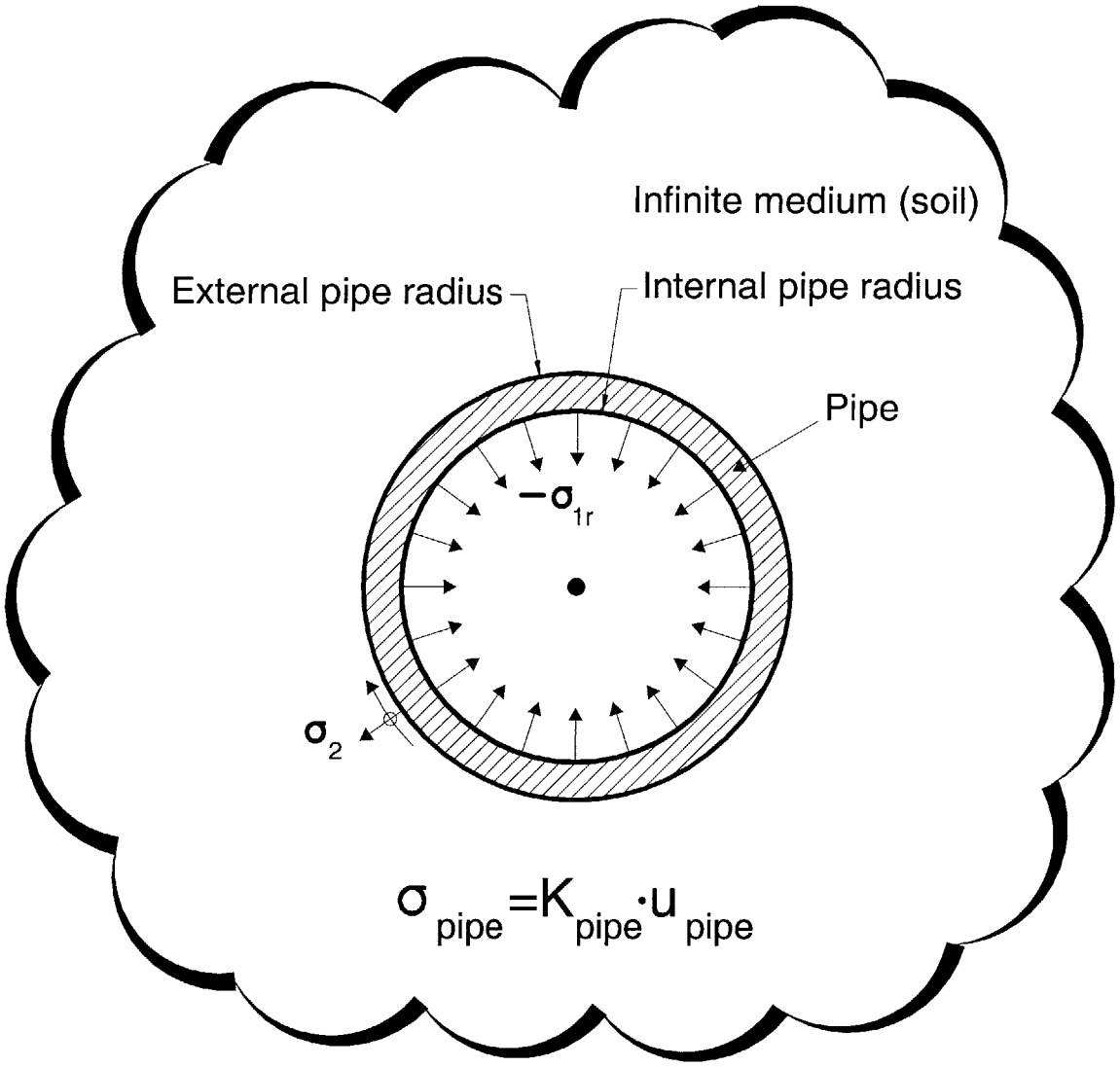

$$\Delta p = K_{fi}\cdot\Delta u \Leftrightarrow p^{*}-\left(-\sigma_{1r}\right)=K_{fi}\cdot\left(u_r{}^{*}-u_{1r}\right)\Leftrightarrow \sigma_{1r}=-p^{*}+K_{fi}u_r{}^{*}-K_{fi}u_{r1}=$$
$$=\left(K_{fe}+K_{fi}\right)u_r{}^{*}-K_{fi}u_{r1}$$

If no other stress is applied on the system, the equations of the complete model can now be written in a matrix form as:

$$\begin{bmatrix} \left(K_{fe}+K_{fi}\right)u_r^* \\ [0] \end{bmatrix} = \begin{bmatrix} K_{11}+K_{fi} & K_{12} \\ K_{21} & K_{22} \end{bmatrix} \cdot \begin{bmatrix} u_{1r} \\ [u_2] \end{bmatrix}$$

The above stiffness matrix is the stiffness matrix of the system containing the fluid, which is calculated, as mentioned before, by joining the various degrees of freedom together. This set of equation can be solved for the radial displacement of the interface as:

$u_{1r} = K_{cons}^{-1} \cdot \left(\left(K_{fe}+K_{fi}\right)u_r^*\right)$, where K_{cons} is the consolidated matrix of the system along the degree of freedom, which is related to the radial displacement of the interface as:

$K_{cons} = K_{11} - K_{12}K_{22}^{-1}K_{21}$

The pressure on the interface will then be:

$$\sigma_{1r} = \left(K_{fe}+K_{fi}\right)u_r^* - K_{fi}K_{cons}^{-1} \cdot \left(K_{fe}+K_{fi}\right)u_r^* = \left(1-K_{fi}K_{cons}^{-1}\right)\cdot\left(K_{fe}+K_{fi}\right)u_r^*$$

Until this point there was no constraint on the positioning of the source inside the fluid. However, in order to simplify the analysis, the source will be considered to lie on the axis of the pipe, so that there is no variation of stresses or displacements along the azimuth θ. In this case all calculations will be done for the axisymmetric mode of n=0, since this is the only mode generated in the pipe.

In order to find the pressure at the fluid-solid interface the only term missing is the displacement u_r* of an interface that has the same radius but lies in an infinitely extending fluid. This can be calculated from solving the Helmholtz equation in cylindrical coordinates for an infinitely extending medium. This solution will be of the form:

$\phi = A H_0^{(2)}(kr)e^{-k_z z}e^{-i\omega t}$ with $k = \sqrt{k_0^2 - k_z^2}$ and so the radial displacement will be equal to:

$\bar{u}_r(r,z,t) = -\frac{S(\omega)\cdot k}{4\omega} H_1^{(2)}(kr)e^{-k_z z}e^{-i\omega t}$ for given axial wavenumber and frequency of excitation, following the procedure for calculating the coefficient A, which was presented earlier. At this artificial "interface" (since the materials joint are of the same kind) of radius R_c the displacement will be equal to: $\bar{u}_r(z,t) = -\frac{S(\omega)\cdot k}{4\omega} H_1^{(2)}(kR_c)e^{-k_z z}e^{-i\omega t}$.

It must be noted here that the above analytical method of calculating the pressures is not limited to the interface between the two materials. If another layer is introduced in the fluid, one can calculate, using the exact same method the pressures in the fluid for any radial distance from the source.

After this analysis, the stresses and displacements inside the system can be calculated for a given axial wavenumber and frequency of excitation. Knowing that, the simplified method presented in chapter 3 can be used in a two dimensional FFT context. The transformation will now be, not only in the time-frequency domain, but also in the space-axial wavenumber domain to describe the full response in space and time. At the same time the transfer function must be calculated for all combinations of axial wavenumbers and frequencies under consideration. It is easy to understand at this point that the calculation of the response for all the different wavenumbers and frequencies scales up the time of execution significantly. From a practical point of view the time needed for a single calculation of the response taking into account the total stiffness components of the system is much more than the one needed for the simplified analysis. Moreover, the time needed for the two dimensional analysis scales up the total calculation time a lot. This fact, coupled with the need for a FFT in two dimensions and the IFFT needed for the calculation of the final response, makes the total time for a simple analysis extremely high.

In order to cut down the time needed to complete the task, one needs to understand how the FFT will work in two dimensions, the properties of the FFT for the forcing function and

how the system behaves under the excitation. After understanding the above, the time can be cut down using the properties of the transformation and the properties of the system. The following chapter will illustrate these properties and the ways to reduce the required calculations.

6.4 Reducing calculation time and memory usage

As shown in the previous chapter, the numerical considerations around time for the two dimensional analysis led to the fact that the calculations need to be reduced, so that more detailed analysis can be run. At the same time, the memory usage for large complex matrixes can surpass the capacity of many modern computers (1GB of memory) and in order to stay away from using disk space which will further reduce the speed of calculations, one must reduce the dimensions of the matrices. In the first part of this chapter the properties of the transforms are studied and used in order to reduce the dimensions of the matrices. In the second part the properties of the system and of the forcing function will be used to reduce the amount of FFT transforms and of frequency-axial wavenumber pairs, without reducing the accuracy of the result. This last fact will result in reducing the size of the matrices and the time needed to calculate the response function.

a) General Fourier and Fast Fourier transform properties

When any signal is transformed using the FFT the resulting DFT has some very interesting properties:

- As can be easily understood, the FFT of a zero signal is a zero function
- The FFT of any real series of N numbers (let this be denoted f_n), which represent the discretization of a signal, is a series of N numbers (denoted F_n) where F_1 and $F_{N/2}$ are real numbers and all the rest are complex sets with $F_{N-j}=\text{conj}(F_{2+j})$ with $j=0,1,\ldots\frac{N}{2}-2$, for N an even number. If N in odd then there is no $F_{N/2}$.
- The FFT is faster for lower N and for N that are powers of two. If N is broken down in prime factors, the lower these factors are the faster the transform.

- The FFT of a real and even function is a real and even function

It must be noted here that any kind of Fourier transform has many more properties than the ones presented here. The ones presented are those that will be useful for the following analysis.

b) FFT properties specific to the proposed analysis

The initial forcing function will be a squared sinusoidal wavelet in space and time, discretized by an odd number of points as: $(space, time) = (2 \cdot n_k + 1, 2 \cdot n_f + 1)$. The odd number of points was chosen in order to replicate the periodic signal in space and time around zero and around the end of each period, pinpointing the axis of symmetry exactly on the start and the end of the period, as shown in the next graph (The reason behind the choice of the forcing function will be analyzed later on):

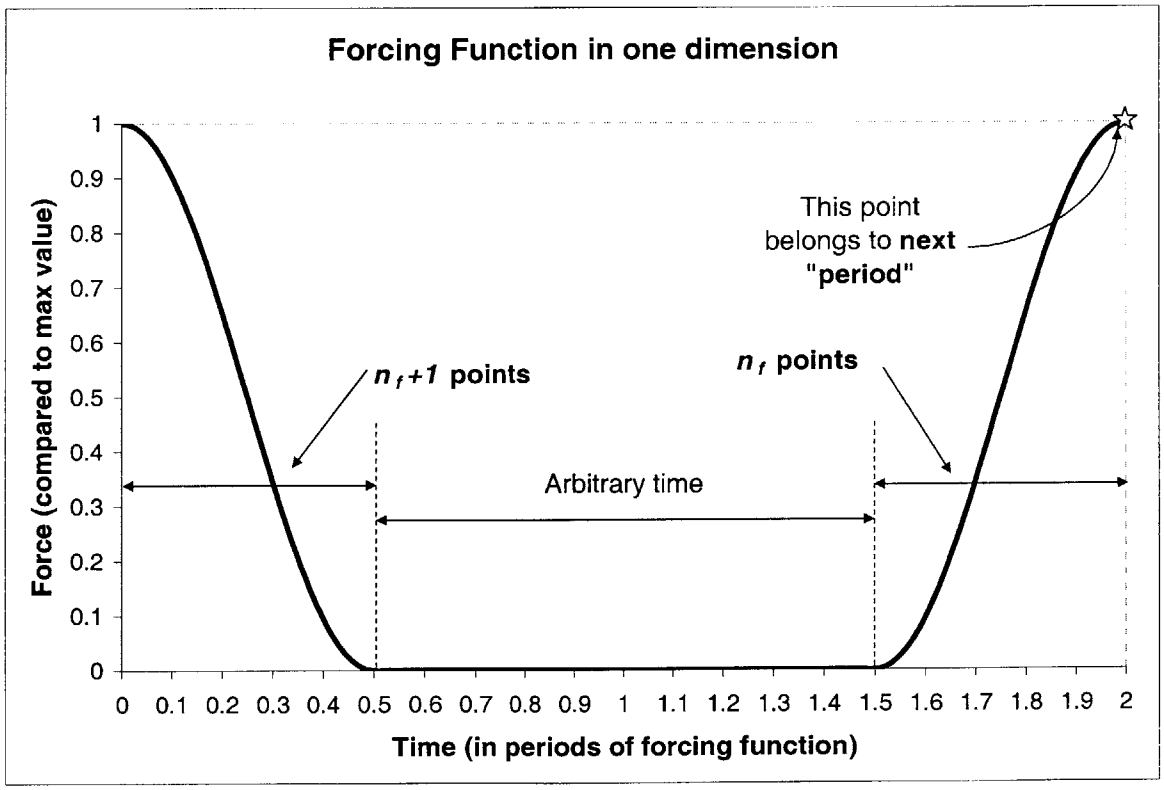

Figure 6.4: Force symmetry and matrix layout

General notes for the following matrices:

- The arrows in the matrices signify the original sequence of elements and the way it is inversed in other parts of each matrix.
- $n_m = (N-1)/2$ where N the even number of total discretization points

This forcing function will have the following discretized form (assuming the same total discretization points in space and time):

	Element	1	$2\ldots n_f$	n_f+1	n_f+2…N-n_f-1	N-n_f	N-n_f+1…N
Element	Points	1	n_f-1	1	N-2n_f-1	1	n_f-1
1	1	*peak*	$real_2 \rightarrow$	0	0	0	$\leftarrow real_2$*
$2\ldots n_k$	n_k-1	$real_1$ ↓	$real_3$ ↘				$real_3$* ↙
n_k+1	1	0				0	
n_k+2…N-n_k-1	N-2n_k-1	0					
N-n_k	1	0		0	0	0	0
N-n_k+1…N	n_k-1	↑ $real_1$*	↗ $real_3$*				↖ $real_3$**

Notes:

peak: The maximum value of the force, at $(space, time) = (0,0)$ (single value)

$real_1$: The force value for *space*=0 (column)

$real_2$: The force value for *time*=0 (row)

$real_3$: The force value at any other point in space and time (matrix)

The different columns signify different times (discretization of the total timeframe under consideration) and the different rows different distances from the start of the pipe (discretization of the total distance under consideration). After the zero element area in the middle of the matrix, column $real_1$ is up-down flipped, row $real_2$ is left-right flipped and

matrix $real_3$ is up-down and left-right flipped. The stars in the matrix denote the appropriate flipping of the matrix. To illustrate the FFT in two dimensions the transform will be done first in constant time for different distances and then the other way around, so first in columns and then in rows.

One can easily understand that the zero columns will yield a zero FFT, so they do not need to be operated. The total number of FFTs required is n_f and the maximum matrix needed to be stored is a matrix $n_k \times n_f$ before and a column of N elements for each FFT, which will be deleted after the operation. At the same time, in order to make the code run faster, after each column of the forcing function is used, it is deleted, so that by the end of the FFTs the forcing function matrix is completely deleted. The FFT transform will change the $f(x,t)$ to $f(k,t)$, which is discretized as the following matrix shows (FFT_1):

	Elements	1	$2\ldots n_f$	$n_f{+}1\ldots N{-}n_f$	$N{-}n_f{+}1\ldots N$
Elements	Points	1	$n_f{-}1$	$N{-}2n_f{+}1$	$n_f{-}1$
1	1	$REAL_1$	$REAL_2 \rightarrow$		$\leftarrow REAL_2{*}$
$2..n_m{+}1$	n_m	$REAL_3$ $\downarrow$	$REAL_4$ $\searrow$	0	$REAL_4{*}$ $\swarrow$
$n_m{+}2\ldots N$	n_m	$\uparrow$ $REAL_3{*}$	$\nearrow$ $REAL_4{*}$		$\nwarrow$ $REAL_4{**}$

Notes:

$REAL_1$: $f(k,t)$ for $k,t{=}0$ (single value)

$REAL_2$: $f(0,t)$ (row)

$REAL_2$: $f(k,0)$ (column)

$REAL_4$: $f(k,t)$ for $k,t \neq 0$ (matrix)

As in the forcing function matrix, the stars here denote the flipping of the matrices, to account for the symmetry. At this point the required matrices are a stored $(n_m+1)\times n_f$ matrix and a temporary column of N elements for each FFT in the time-frequency domain. The aforementioned method of deleting the elements that are not needed after each FFT is used again and the final result will be a discretized $f(k,\omega)$ as the following matrix shows (FFT_2)

	Elements	1	$2\ldots n_m+1$	$n_m+2\ldots N$
Elements	Points	1	n_m	n_m
1	1	**REAL$_1$**	**REAL$_2$** $\rightarrow$	$\leftarrow$ **REAL$_2$***
$2..\ n_m+1$	n_m	**REAL$_3$** $\downarrow$	**REAL$_4$** $\searrow$	**REAL$_4$*** $\swarrow$
$n_m+2\ldots N$	n_m	$\uparrow$ **REAL$_3$***	**REAL$_4$*** $\nearrow$	**REAL$_4$**** $\nwarrow$

Notes:

REAL$_1$: $F(k,\omega)$ for k,ω=0 (single value)

REAL$_2$: $F(0,\omega)$ (row)

REAL$_2$: $F(k,0)$ (column)

REAL$_4$: $F(k,\omega)$ for $k,\omega \neq 0$ (matrix)

All the previous notes on the storage reduction hold, but even in this case, the result needs a $(n_m+1)\times(n_m+1)$ matrix to be stored completely. At this point it is easily understood that the storage space for a matrix of that size is going to be substantial. However, there is room for more improvement, given the properties of the forcing function.

c) Properties of the FFT of the forcing function

After calculating the double FFT of the forcing function, the properties of the transform can be used to reduce the calculation time even more. The forcing function that is going to be used in the excitation of the pipe will be a squared cosine function in both directions (space and time).

After analyzing the forcing function of duration equal to $[t_0, A_0]$ in two dimensions one obtains the following three-dimensional graph (the "durations" used were 1ms and 1m):

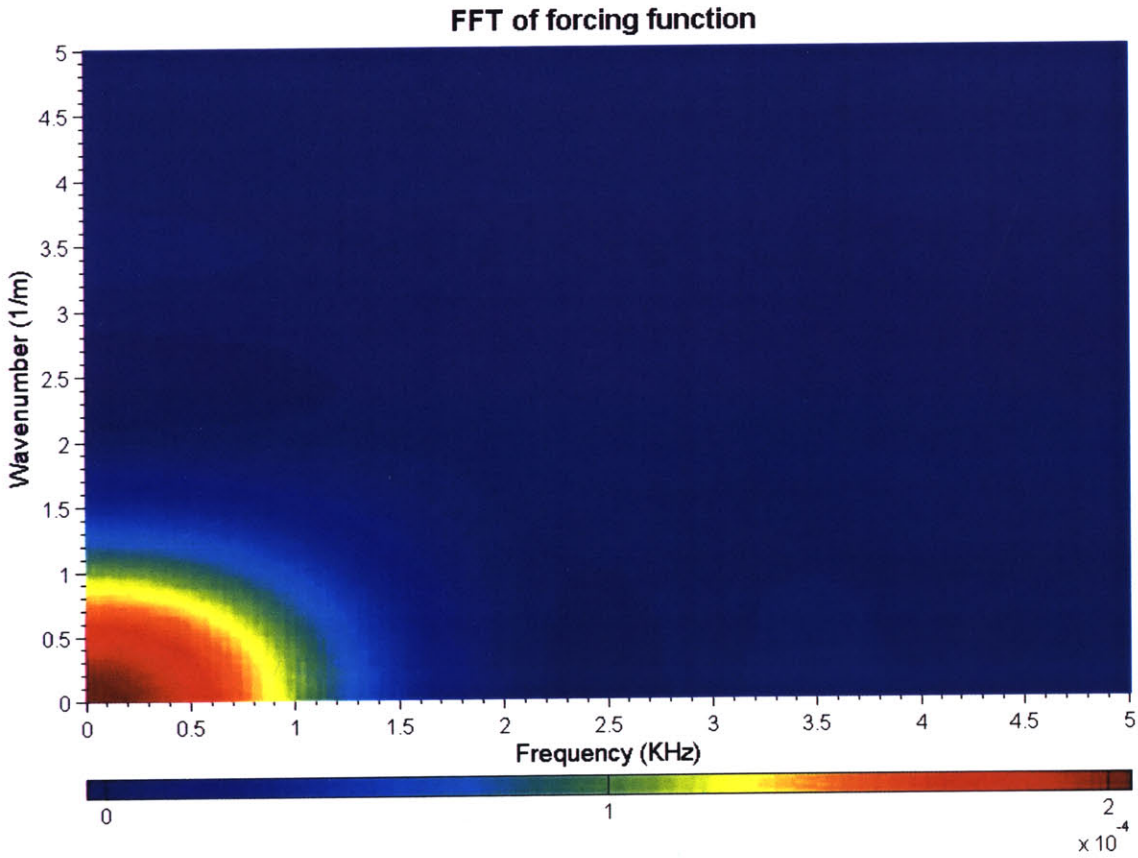

Figure 6.5: FFT of forcing function (1m, 1ms source)

In this graph one can see the value of the Fourier transformation of the forcing function for a range of frequencies and wavenumbers. The graph presenting as well as the solution can be normalized according to the inversed duration of the signal. A normalized graph would have the same axis divided by the total duration of the signal in (*time*, *space*) = (ms, m).

From this graph it can been seen that the FFT of the forcing function has a rather narrow bandwidth of up till ; 4 times the "frequency" of the signal in both space and time. This result can be analytically derived for this case as the Fourier transform of the force is:

$F(k,\omega)=\frac{\sin(kA)}{kA\left[1-\left(\frac{kA}{\pi}\right)^2\right]}\cdot\frac{\sin(\omega T)}{\omega T\left[1-\left(\frac{\omega T}{\pi}\right)^2\right]}$ for a forcing function of the form:

$F(k,\omega)=\frac{1}{AT}\cos^2\left(\frac{\pi x}{2A}\right)\cos^2\left(\frac{\pi t}{2T}\right)$

This bandwidth is then considered to be $(\omega_{max},k_{z\max})=\left(L/t_0,L/A_0\right)$ with L the ratio of the maximum frequency under consideration to the "frequency" (inversed duration) of the signal. Outside this bandwidth the value of the FFT is close to zero and, consequently, when the transfer function is multiplied by the FFT of the force the resulting value will be zero. At the same time, one can notice that the value of the FFT is close to zero not only outside this rectangular region, but also in a very large part inside it. The non-zero region is within an ellipse described by:

$\left(\frac{\omega}{\omega_{max}}\right)^2+\left(\frac{k_z}{k_{z\max}}\right)^2=1$, as it can be shown in the following graph.

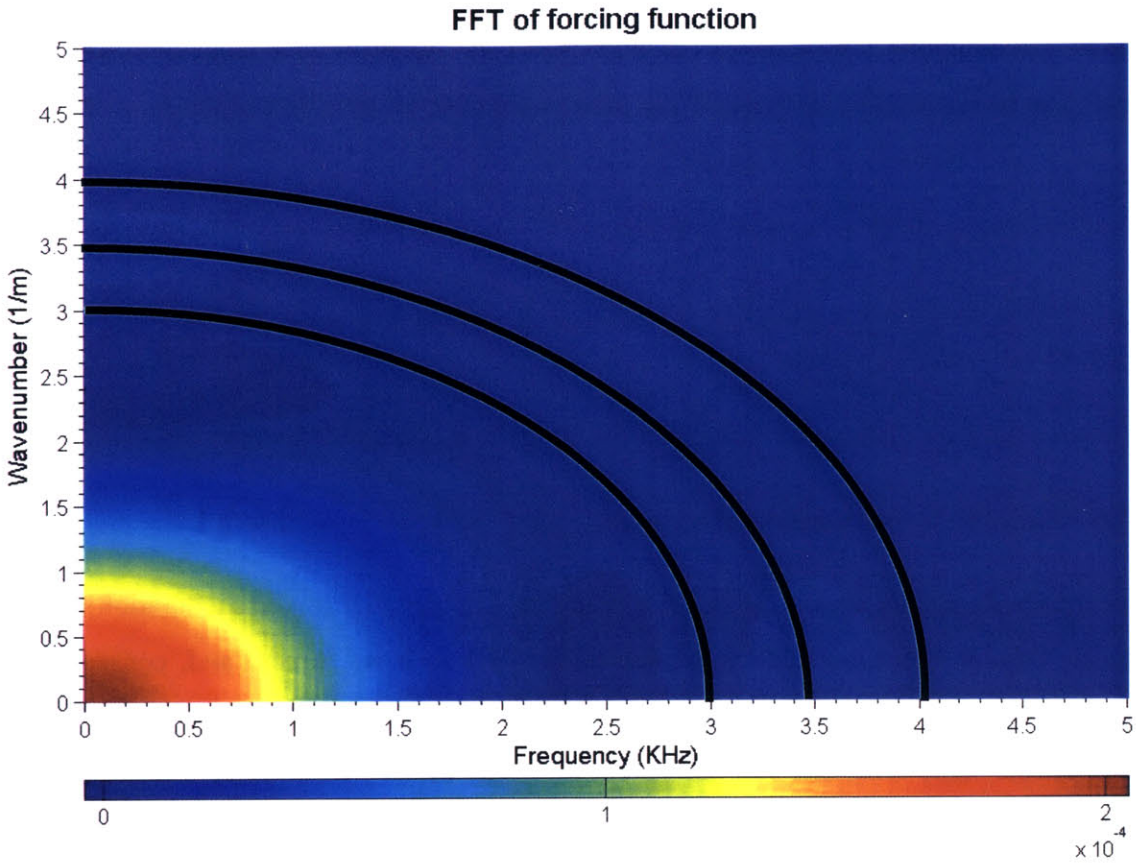

Figure 6.6: FFT of forcing function with bounding ellipses (1m, 1ms source)

If a desired level of accuracy is required then the ratio L can be derived from the following graph:

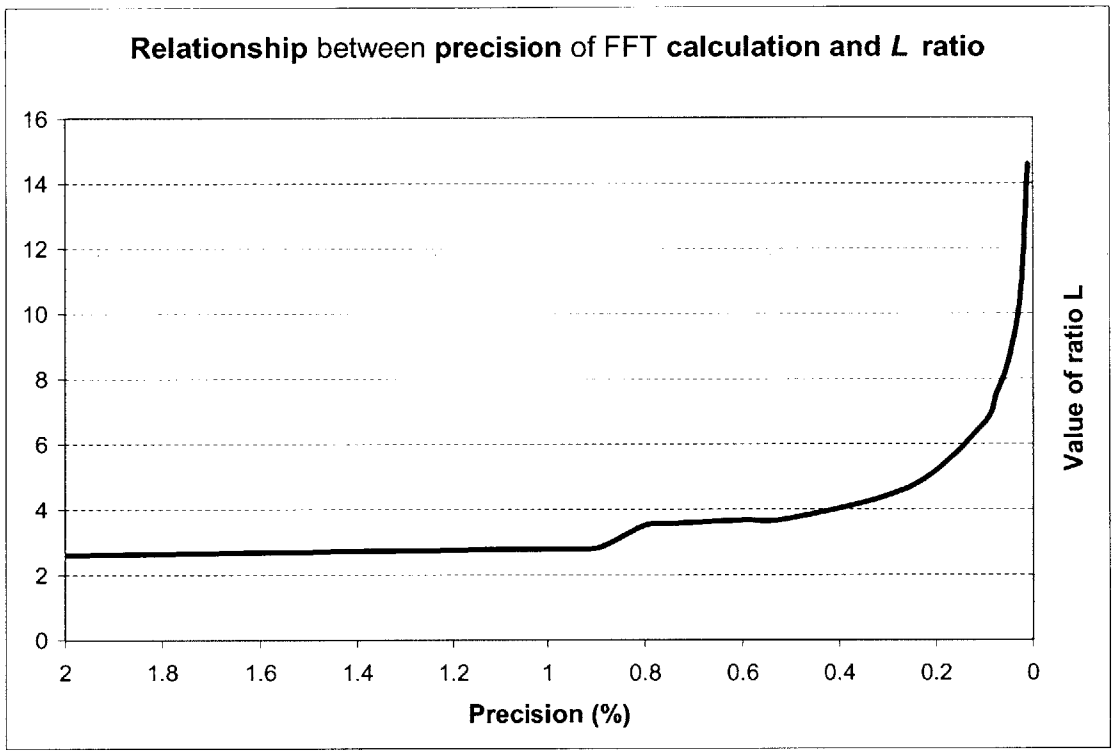

Figure 6.7: Required level of precision and S ratio value

This fact can be seen in the following 3D graphs of the forcing function FFT for different levels of precision. The graphs show the absolute normalized value of the FFT and the red area in each graph is where the value of the normalized FFT exceeds the prescribed limit.

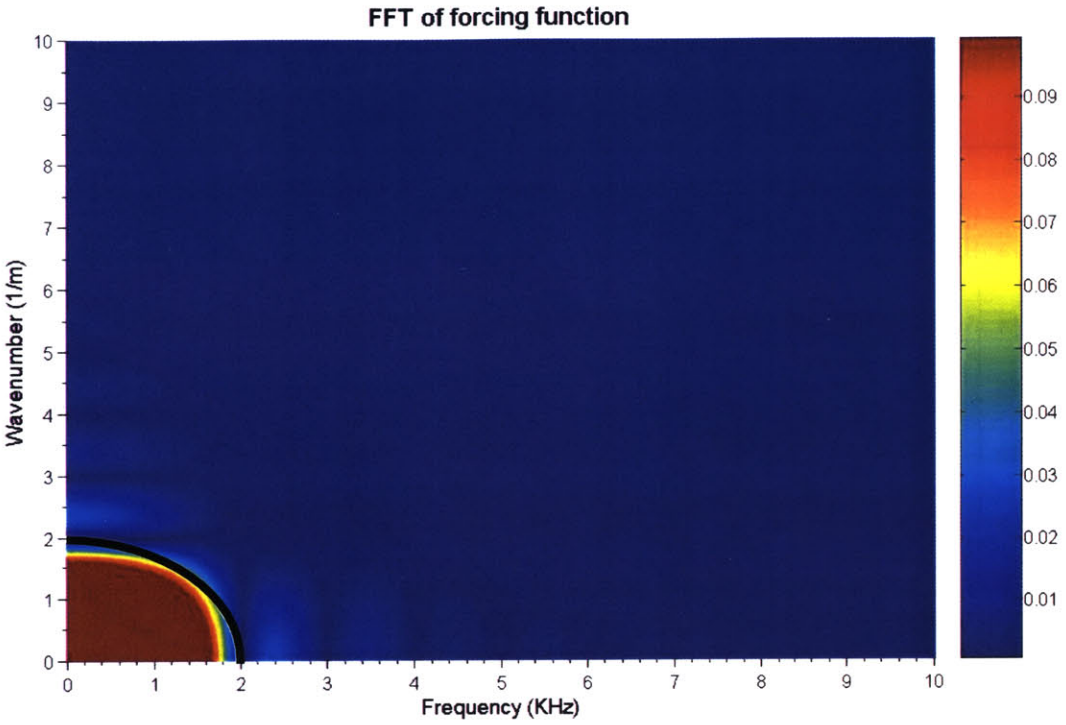

Figure 6.8: FFT of forcing function with 10% accuracy limit (L=1.65)

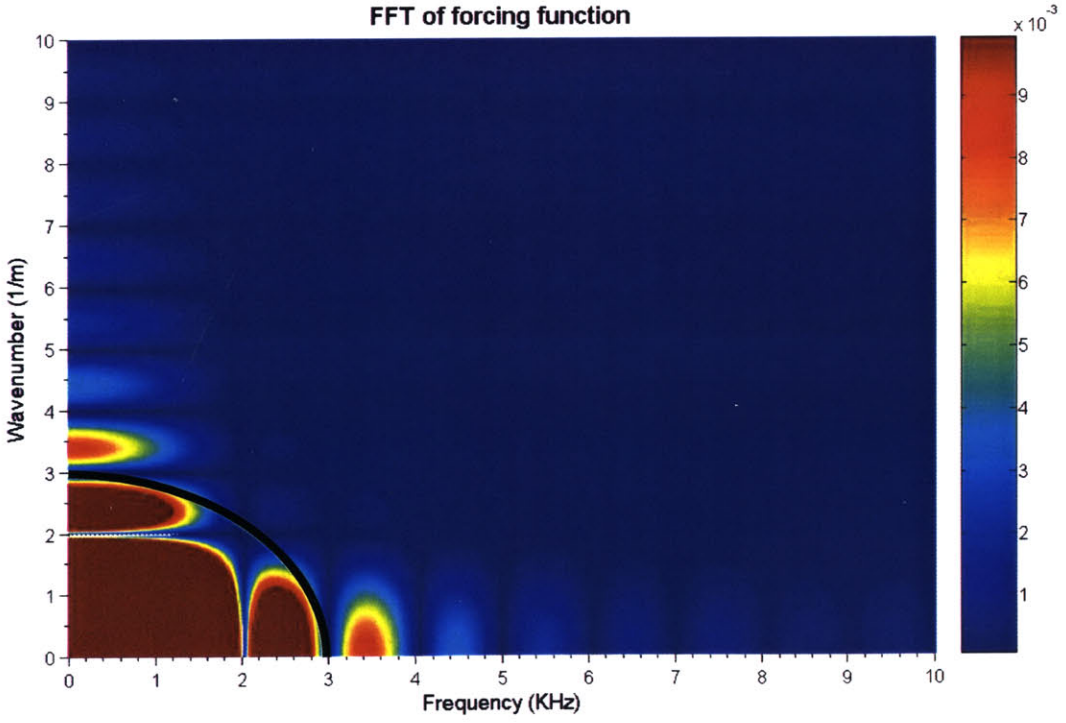

Figure 6.9: FFT of forcing function with 1% accuracy limit (L=2.8)

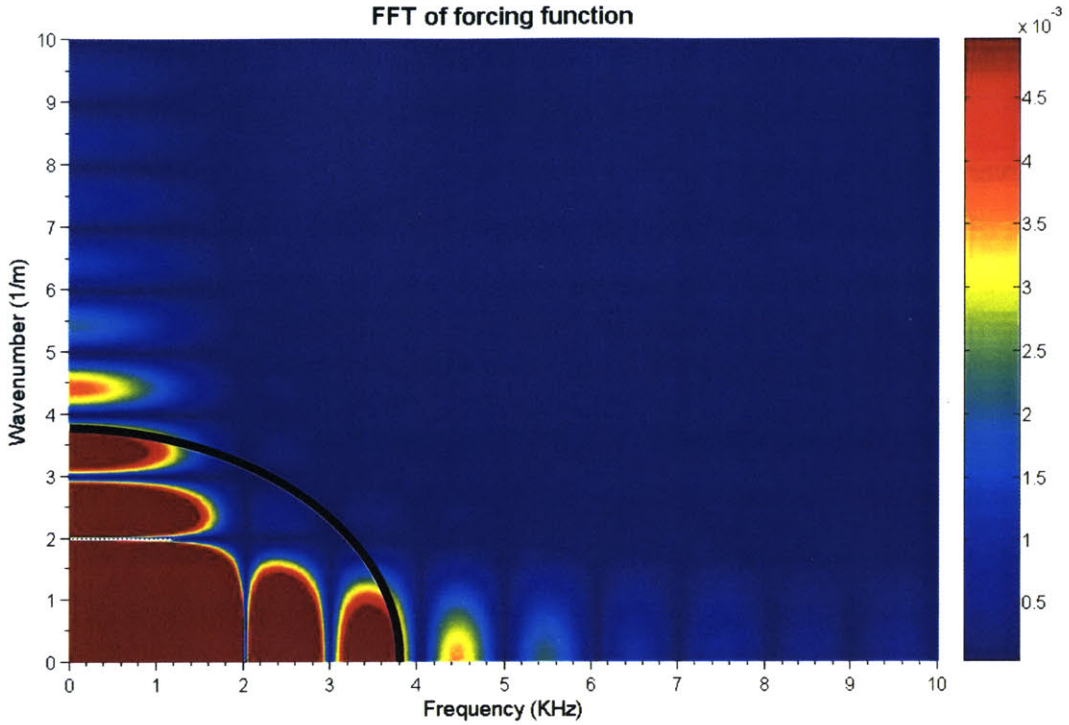

Figure 6.10: FFT of forcing function with 0.5% accuracy limit (L=3.73)

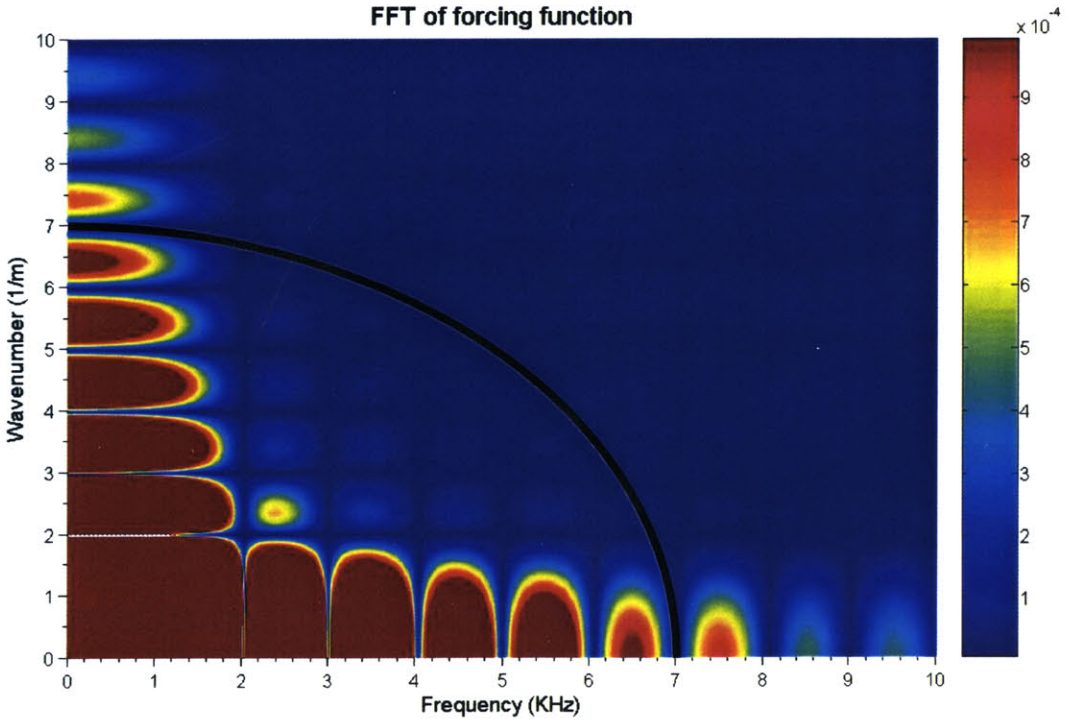

Figure 6.11: FFT of forcing function with 0.1% accuracy limit (L=6.64)

Note: The values of L come from a separate code written to calculate the maximum value of L after which the value of the FFT is lower than a certain accuracy level.

This very important property of the FFT can save up a lot of computational time, since the value of the transfer function needs not to be calculated outside this region. In general the amount of transfer function calculations (which are the most time consuming ones) will be reduced to about $\frac{\pi}{4}\cdot\left(n_{kactual}+1\right)\cdot\left(n_{factual}+1\right)$. The actual number of calculations will not be exactly this, because of the fact that the "bounding ellipsis" will be discretized in k and ω, but in general the decrease in time will be of the order of at least 20%. The following graphs provide an example of complete versus fractional computation of the transfer function to illustrate the aforementioned theory.

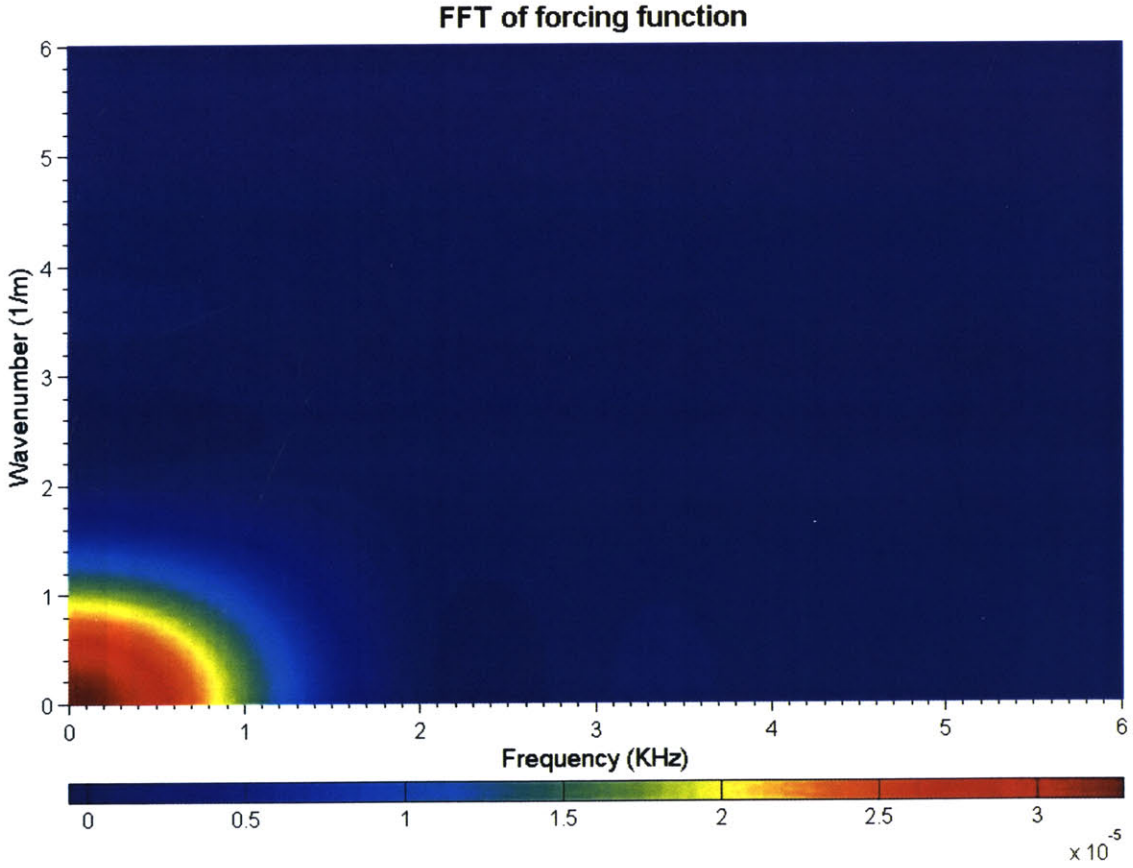

Figure 6.12: FFT of forcing function for a 1m,1ms excitation source

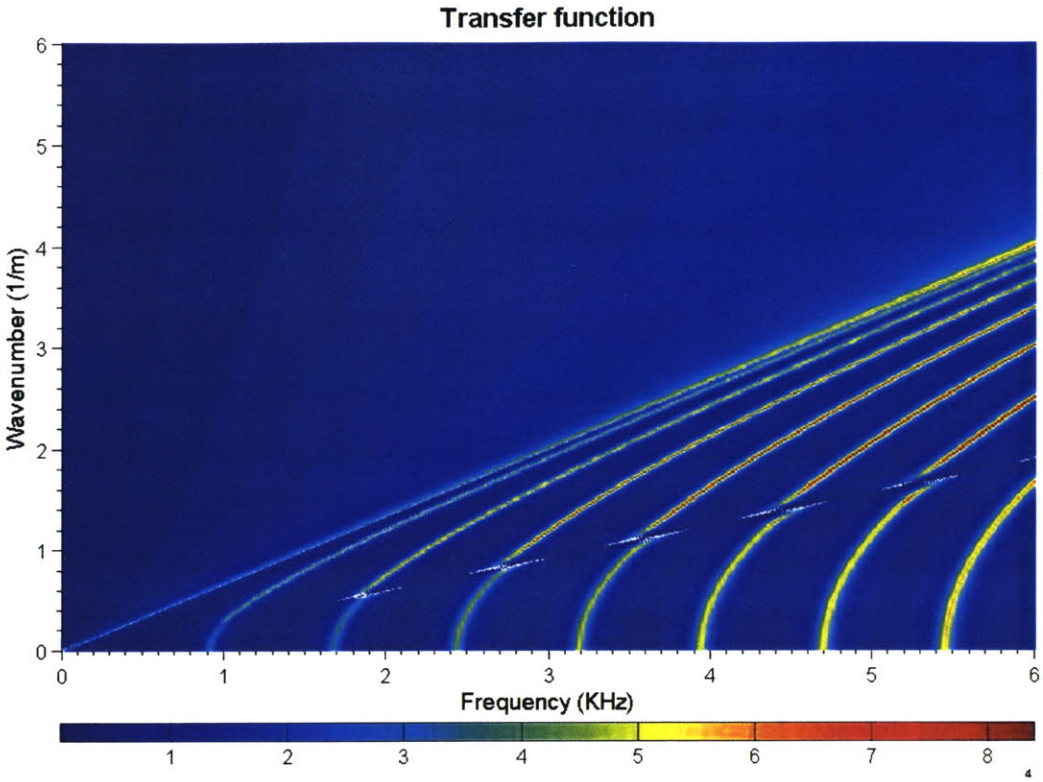

Figure 6.13: Transfer function (full analysis)

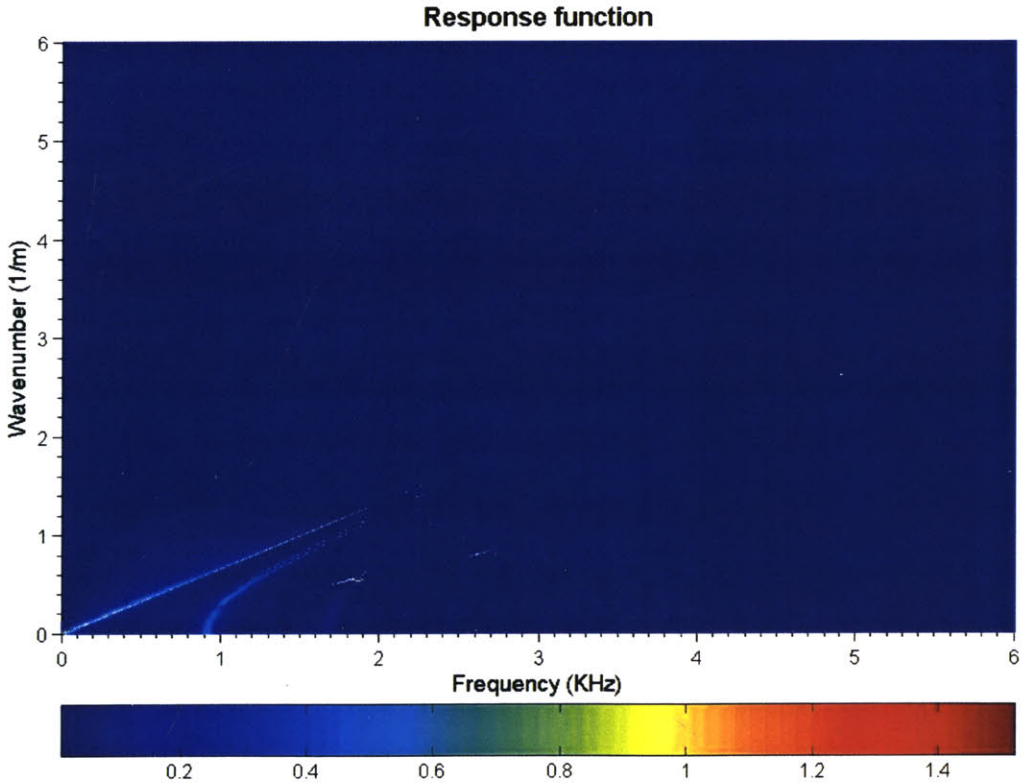

Figure 6.14: Response function (Product of FFT of force and transfer function)

In the above graphs one can see the FFT of the forcing function and how it affected the response function of the system. The above analysis was done with an excitation source, which spread over time and space 1ms and 1m respectively. The L ratio for the above analysis was 6 (way above the zero area of the FFT of the forcing function as shown in figure 6.14). The numbers were chosen arbitrarily to show the effect of the ellipsis and the bandwidth reduction.

Although the transfer function has substantial values across the whole bandwidth of analysis (up till an L value of 6) the resulting response function, coming from the multiplication of the transfer function with the FFT of the force, yields a zero result after an L of approximately 2.5. Consequently, the time-consuming calculations that were done outside this area were not needed and could have been omitted.

The effect that this note has on the system is not limited to the calculation of the transfer function. Since the response function of the system in the frequency-wavenumber domain is going to be zero over a certain area outside $\omega_{\max}$ and $k_{z\max}$, there is no need to calculate the inverse FFT (IFFT) over this area for the first step of the calculation. Consequently the routine for the calculation of the FFT of the forcing function will also change to store only the data, which are not going to be multiplied by zero.

In general the maximum amount of data needed to be stored for the calculation of the FFT of the forcing function will be $\left(n_{kactual}+1\right)\times\left(n_{factual}+1\right)$, or to be more precise where there is a n_m factor in columns it will be changed to $n_{kactual}$ and in the rows it will be changed to $n_{factual}$. The IFFT will follow the same rules starting from a matrix, which is $\left(n_{kactual}+1\right)\times\left(n_{factual}+1\right)$ and leading up to a matrix that is $N\times N$. Notice that, since the signal is periodic in time and space and that the sound travels in both directions after the initial signal pulse, the result needs to be studied only over half the length and half the time between excitations. This means the required result will be a $\left(n_m+1\right)\times\left(n_m+1\right)$ matrix.

6.5 Accuracy of the proposed code

In order to see the accuracy of the proposed method of analysis and the code as a whole, various easy to analytically predict cases will be simulated. All these simulations will deal with low frequency and wavenumber excitations, so that only the fundamental axisymmetric mode propagates in the fluid. However, these analyses will be split into the following categories:

- Surrounding medium with infinite stiffness (much larger than the fluid's)
- Infinite surrounding medium with finite stiffness (comparable to the fluid's)
- Finite surrounding medium with finite stiffness
- Multiple surrounding mediums with a mix of dimensions and stiffness

Infinitely stiff surrounding medium

The solution for the infinitely extending medium of infinite stiffness must match the solution of the infinitely rigid pipe for any kind of excitation. The dimensions of the surrounding medium will not affect the solution, given that its stiffness is many orders of magnitude higher than the fluid's.

The acoustic wave velocity of the fluid will be 1.5Km/s, a 0.1% damping ratio and a density of $1t/m^3$ in both cases, while the radius of the pipe will be equal to 1m. In order to simulate a very stiff pipe, the pipe was considered to have a compressional wave velocity of 100 Km/s and a density 100 times higher than the fluid's (giving the material of the pipe a Young's modulus of 10^6 GPa). This set numbers is used just for an equal comparison of the two methods and don't constitute the exact dimensions and properties of the real problem, being however very close to them.

The presented graphs will show the pressure distribution for excitations of 5ms (no noise – only "zero" mode excited), 1ms (intermediate noise – very few modes excited) and 0.5ms

(strong noise – at least seven modes excited given a $L \geq 3$) at mid-distance between the source and the surrounding shell (r=0.5).

Low frequency excitation

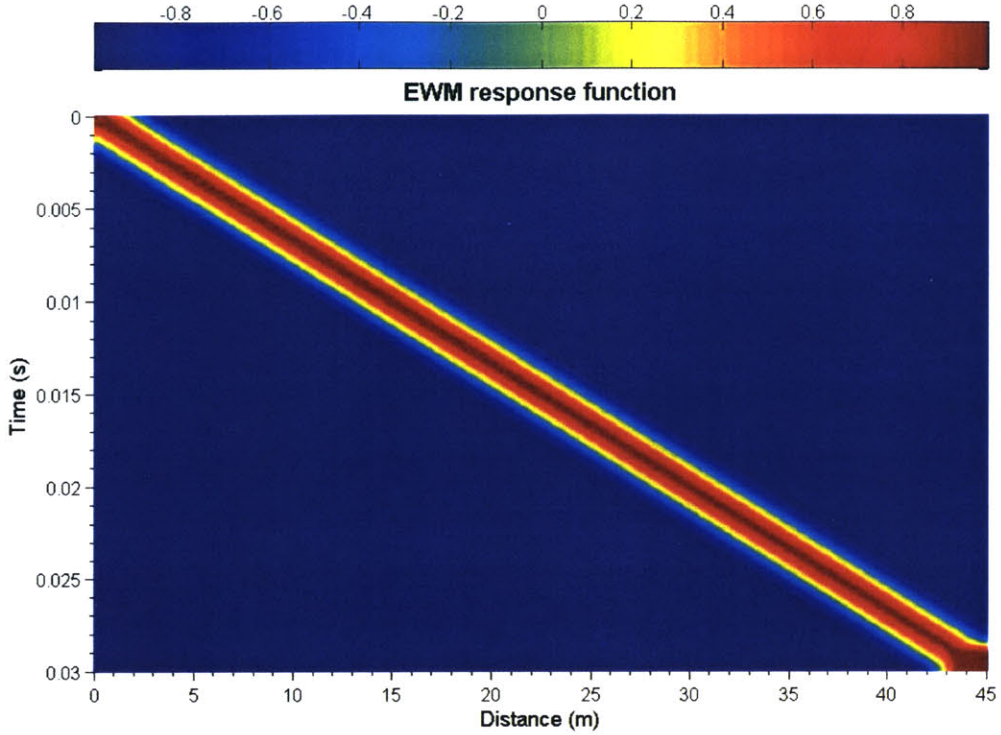

Figure 6.15: Pressure distribution for a 5ms pulse (complete analysis)

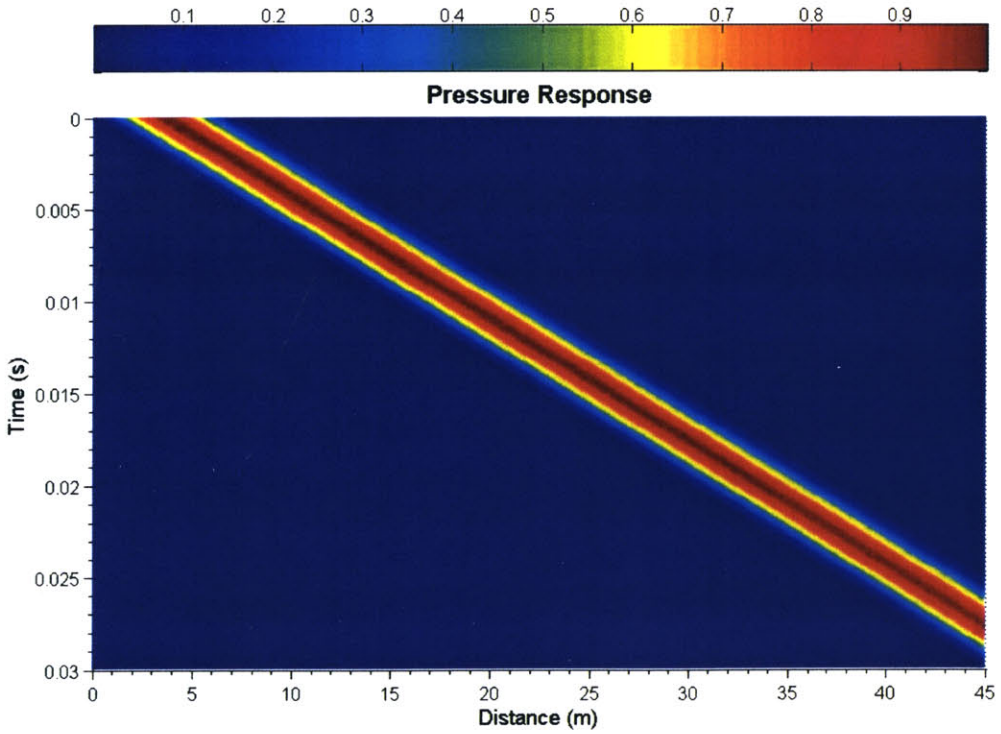

Figure 6.16: Pressure distribution for a 5ms pulse (simplified analysis)

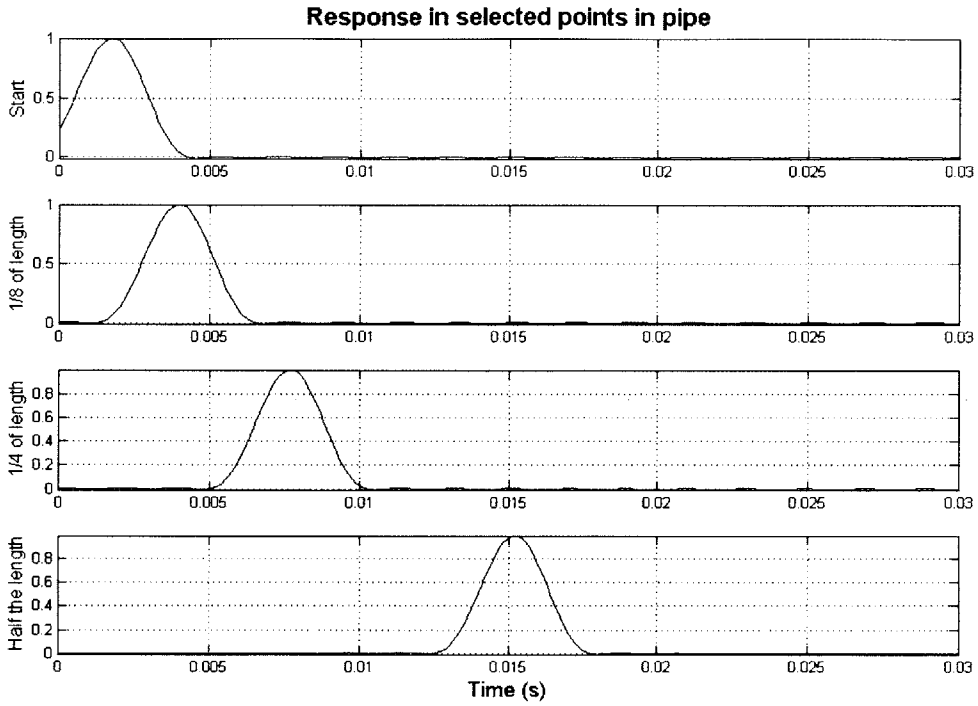

Figure 6.17: Pressures in selected points in pipe for a 5ms pulse (complete analysis)

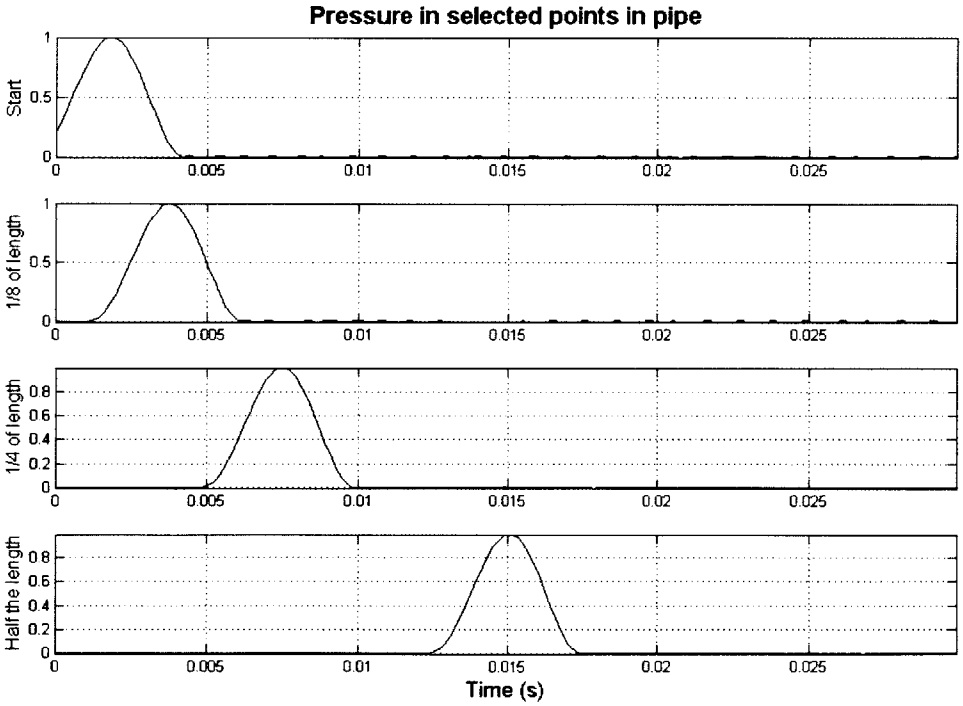

Figure 6.18: Pressures in selected points in pipe for a 5ms pulse (simplified analysis)

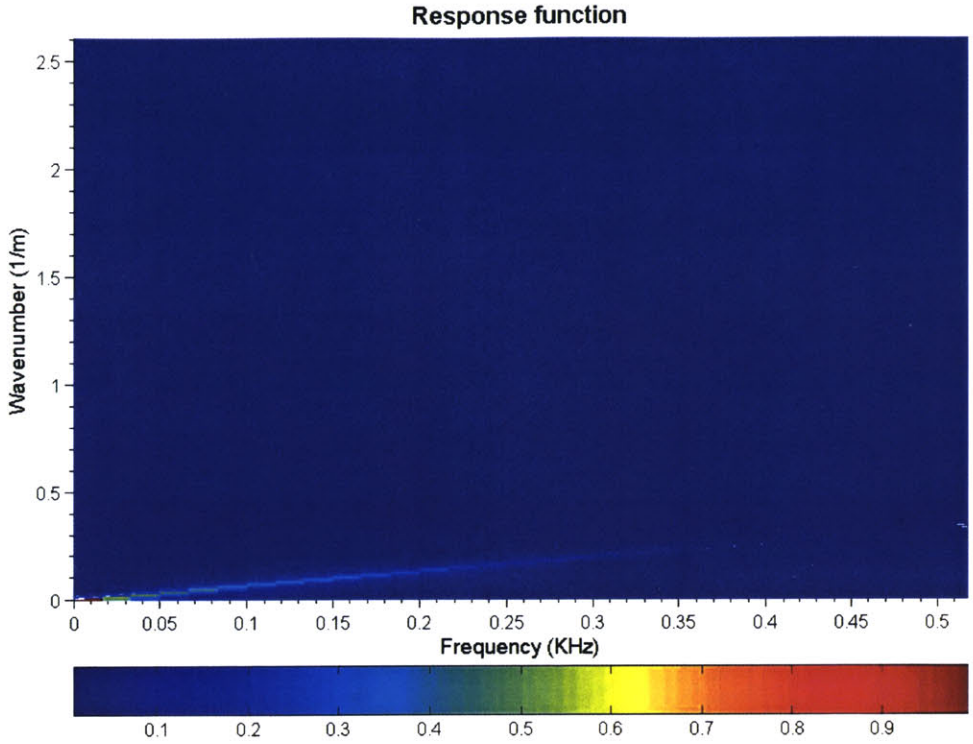

Figure 6.19: Response function in ω,k_z for a 5ms pulse (complete analysis)

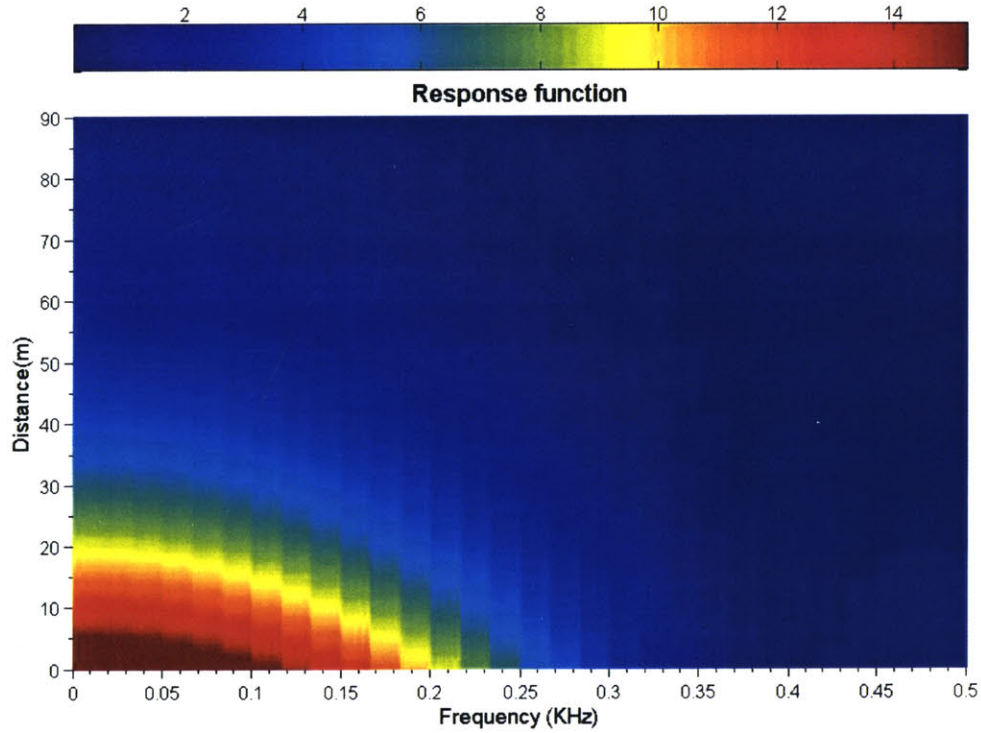

Figure 6.20: Response function in ω,z for a 5ms pulse (simplified analysis)

Medium frequency excitation

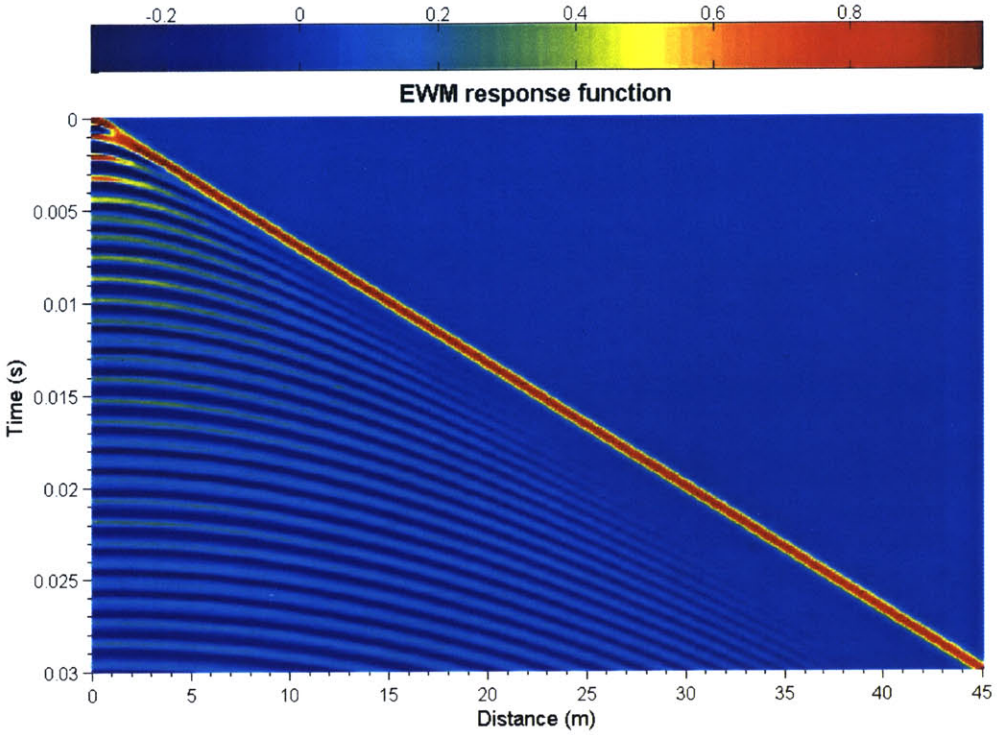

Figure 6.21: Pressure distribution for a 1ms pulse (complete analysis)

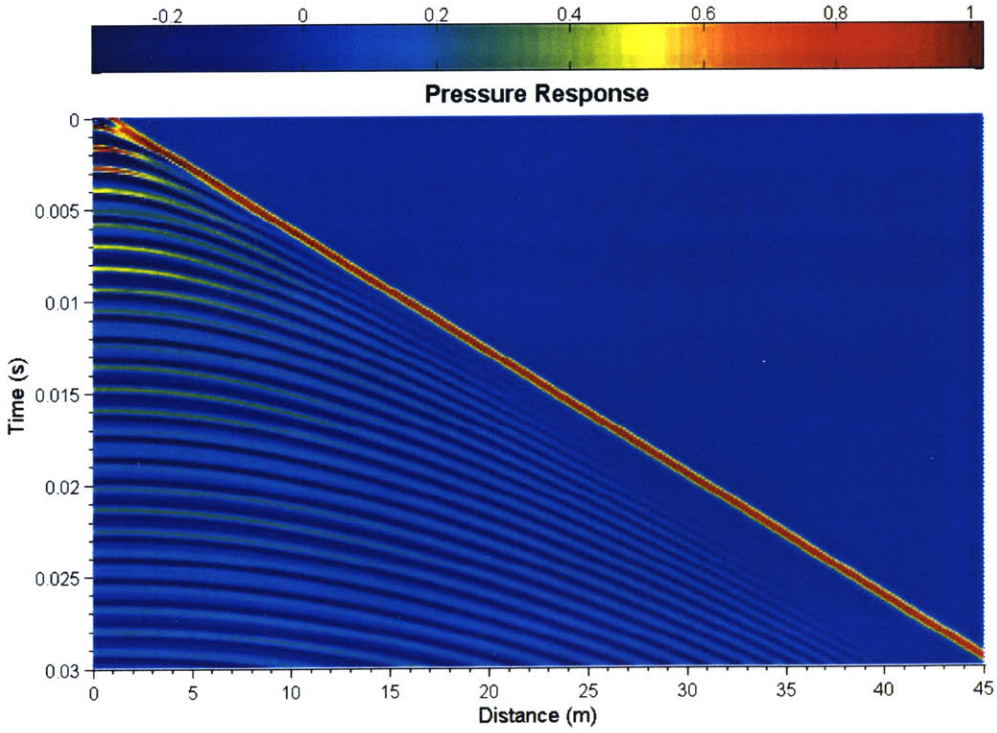

Figure 6.22: Pressure distribution for a 1ms pulse (simplified analysis)

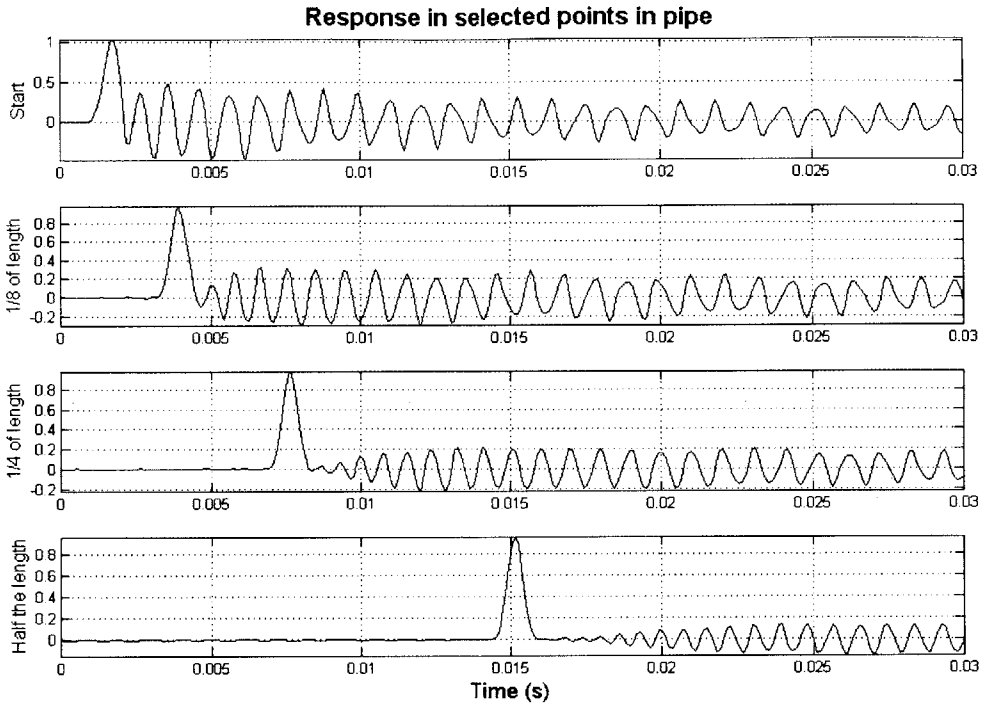

Figure 6.23: Pressures in selected points in pipe for a 1ms pulse (complete analysis)

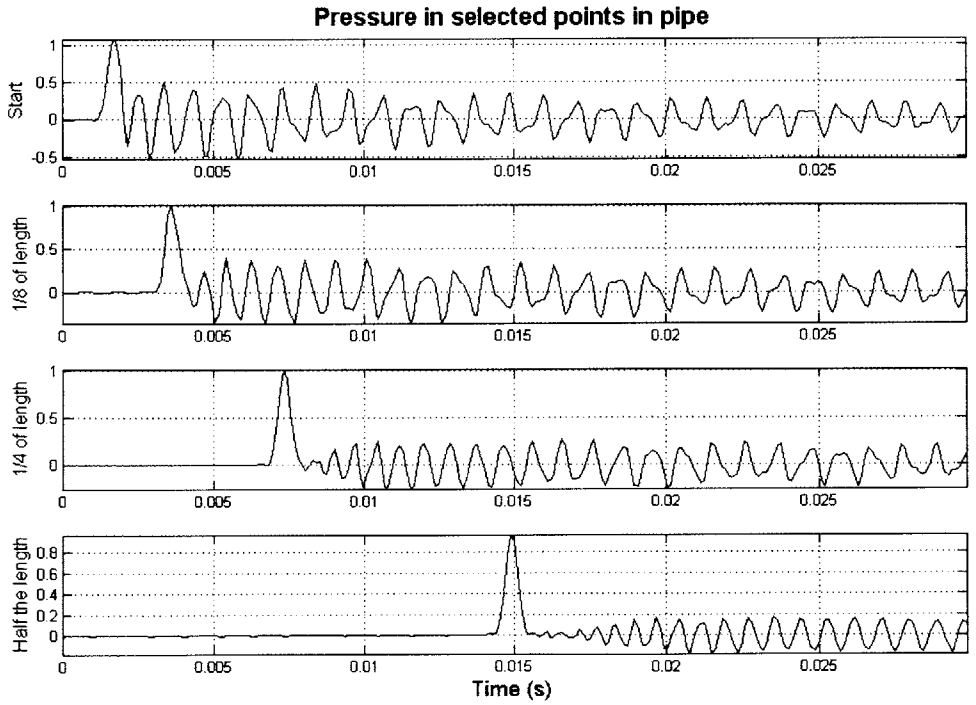

Figure 6.24: Pressures in selected points in pipe for a 1ms pulse (simplified analysis)

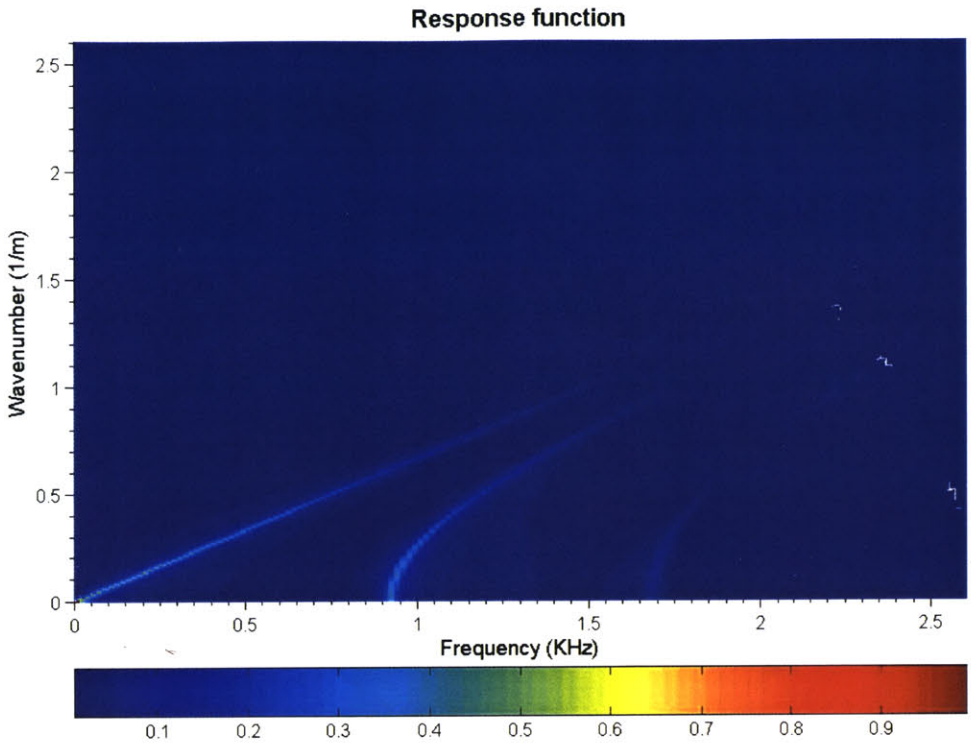

Figure 6.25: Response function in ω, k_z for a 1ms pulse (complete analysis)

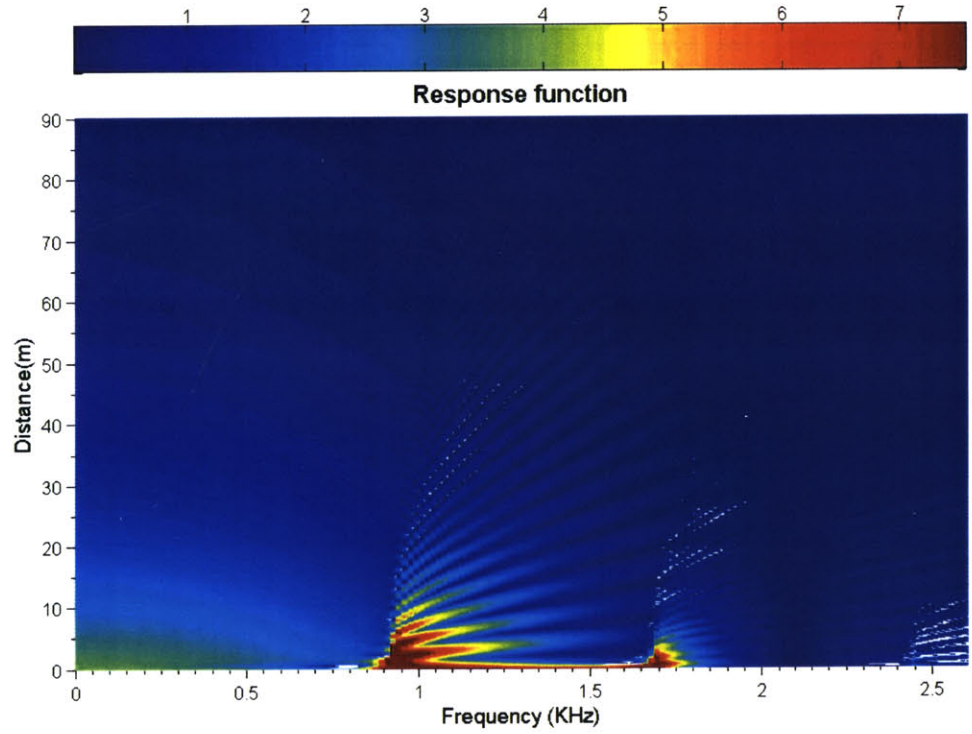

Figure 6.26: Response function in ω, z for a 1ms pulse (simplified analysis)

High frequency excitation

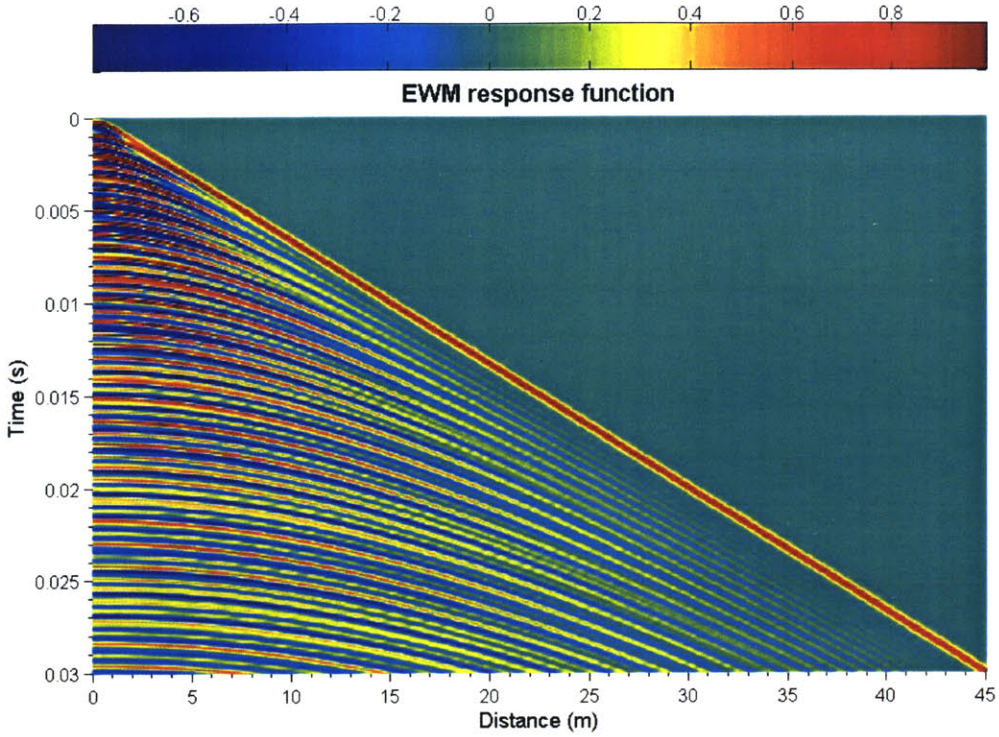

Figure 6.27: Pressure distribution for a 0.5ms pulse (complete analysis)

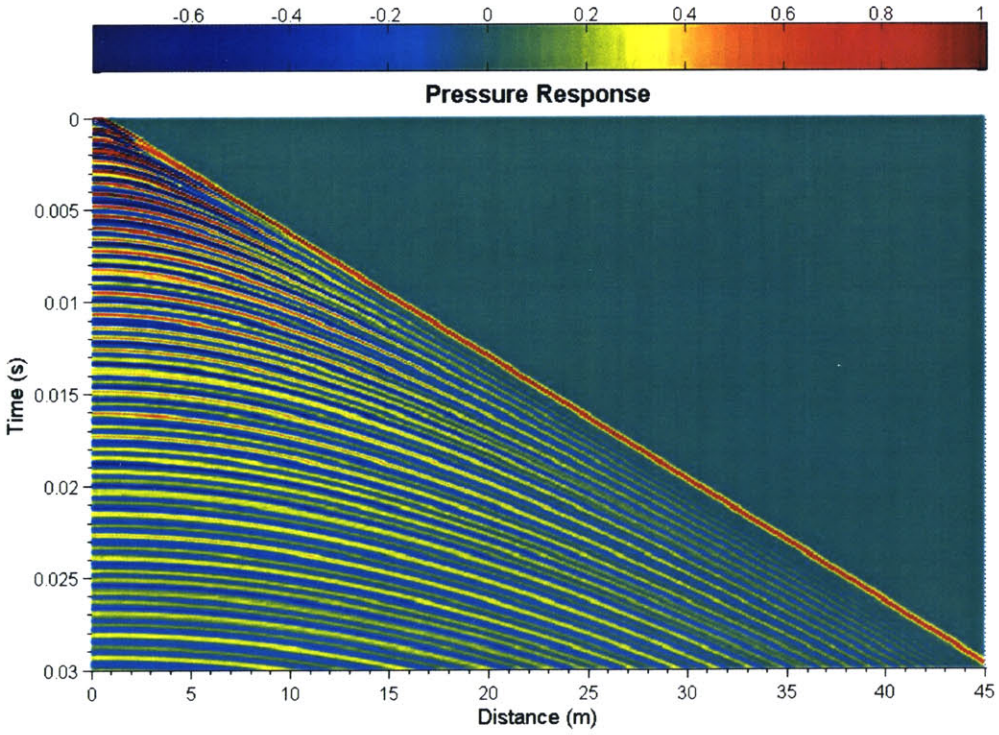

Figure 6.28: Pressure distribution for a 0.5ms pulse (simplified analysis)

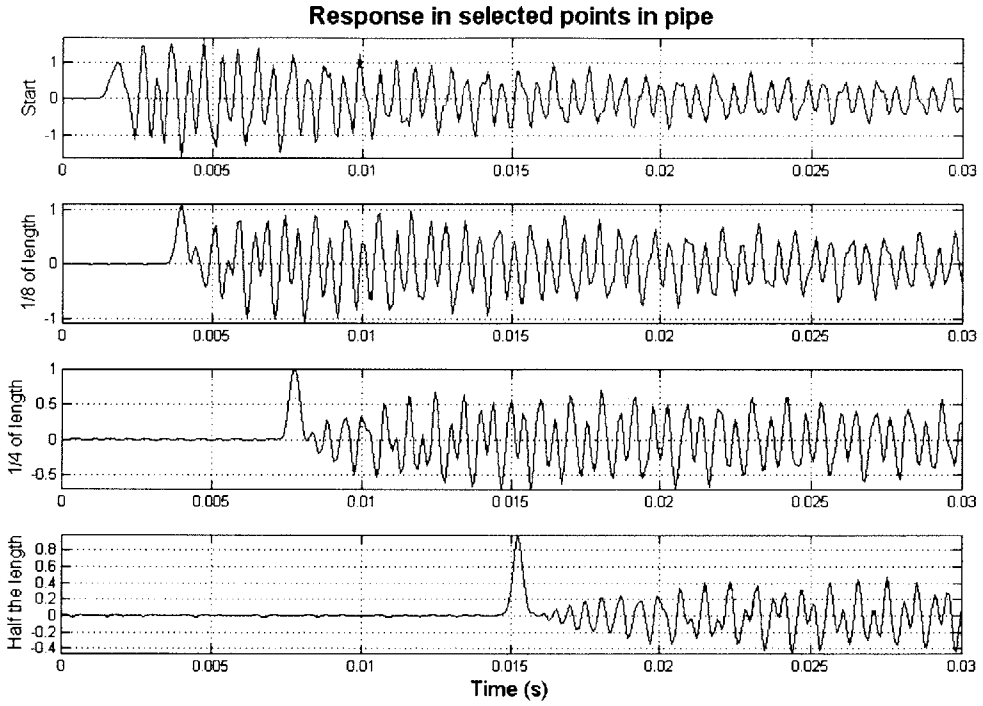

Figure 6.29: Pressures in selected points in pipe for a 0.5ms pulse (complete analysis)

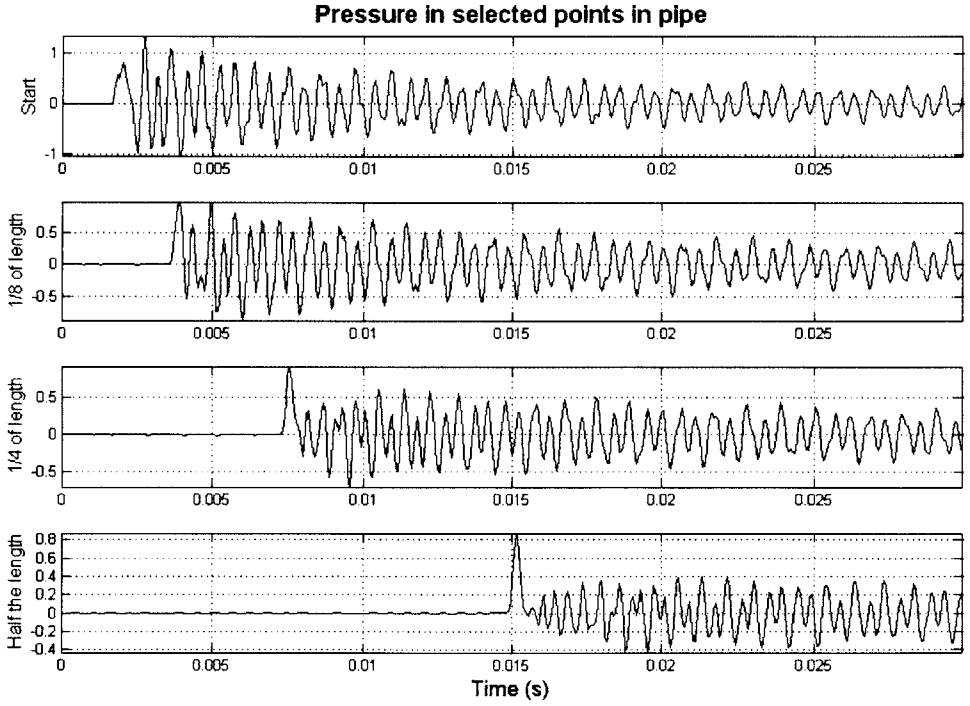

Figure 6.30: Pressures in selected points in pipe for a 0.5ms pulse (simplified analysis)

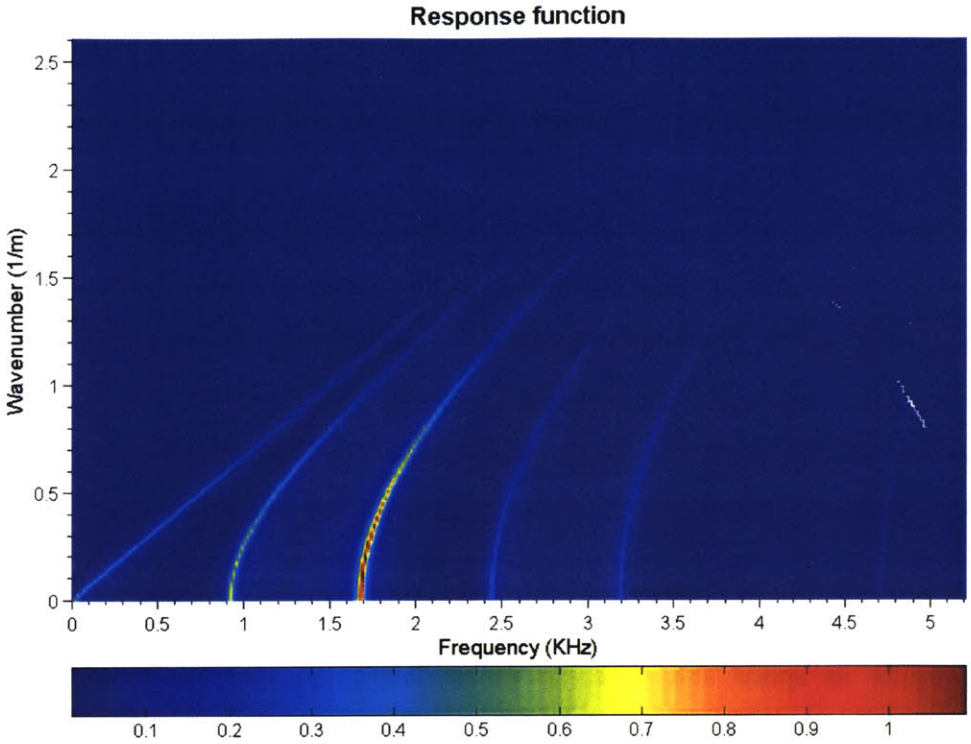

Figure 6.31: Response function in ω,k_z for a 0.5ms pulse (complete analysis)

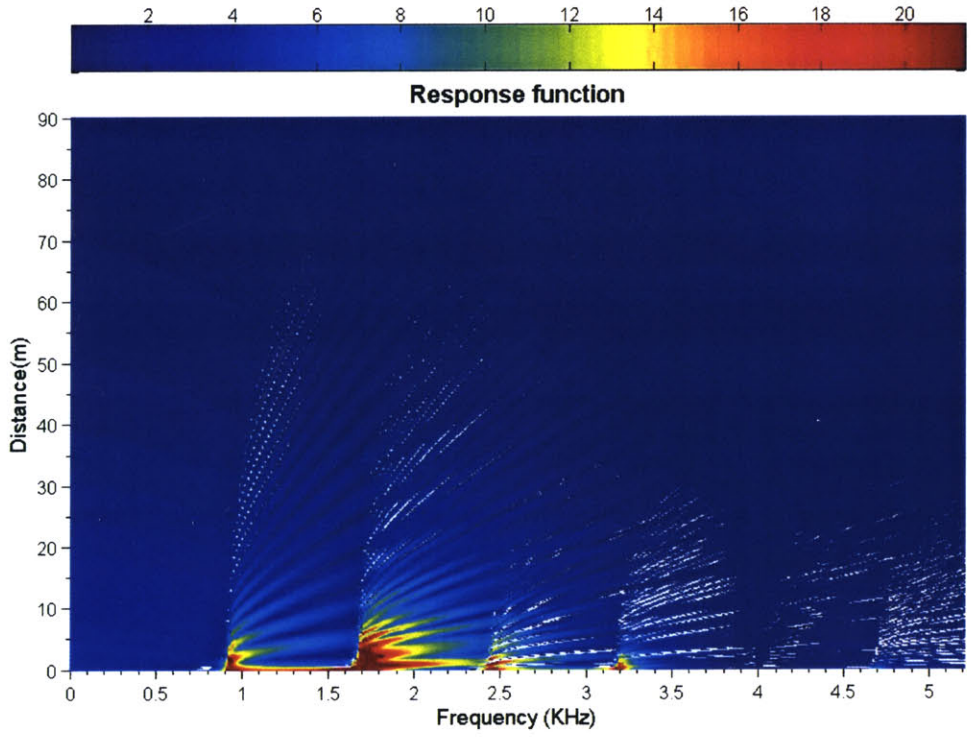

Figure 6.32: Response function in ω,z for a 0.5ms pulse (simplified analysis)

Notes:

a) The pressure signal has a phase shift of $\pi/2$ (or $t_d/2$) between the two analyses, since the simplified analysis is a $\sin^2$ signal, though the complete analysis signal, due to the reasons analyzed in chapter 6.4, is a $\cos^2$.

b) The response functions (product of Fourier transform of force and transfer function) were not graphed in the same manner, since there is no Fourier transform in k_z for the simplified analysis. Therefore, the complete analysis response function was graphed in the ω,k_z domain and the simplified analysis in the ω,z domain. Moreover, the response function of the complete analysis was normalized according to the response of the system of a permanent and globally applied forcing function ($\omega,k_z = 0$).

All of the above graphs demonstrate the absolute match of the simplified and complete analysis results in space and time. In more detail, the three-dimensional pressure distributions both show the same development of pressures. As noted in the simplified analysis, the noise propagates at a higher speed in relation to the main signal, while it gradually slows down to reach the acoustical wave velocity. The pressure-time history graphs show the exact match between the two ways of analysis (given the phase shift) in shape and magnitude. Finally, the response functions show the same characteristic frequencies of the system, which match the calculated ones in chapter 4.3 (table 4.1).

Surrounding medium with finite stiffness

According to White (1983) for frequencies below the first cut-off frequency of the pipe and wavelengths greater than the diameter of the pipe, the speed of the waves traveling in the fluid medium is lower than the actual speed of sound in the fluid. These "tube waves" have a speed of:

$$c_{tube} = \left[\rho_{fluid}\left(\frac{1}{B}+\frac{1}{M}\right)\right]^{-1/2} = \left[\frac{1}{c_{fluid}^2}+\frac{\rho_{fluid}}{M}\right]^{-1/2} \quad \text{with:}$$

$$M = \frac{E_{pipe}\cdot\left(a^2-b^2\right)}{2\left[\left(1+\nu_{pipe}\right)\left(a^2+b^2\right)-2\nu_{pipe}b^2\right]}$$

a : Outer radius of pipe

b : inner radius of pipe

ν_{pipe} : The Poisson's ratio of the pipe's material

E_{pipe} : The elasticity modulus of the pipe's material, which can be calculated by:

$E_{pipe} = 2\mu_{pipe}\left(1+\nu_{pipe}\right) = c_{s_{pipe}}^2 \cdot \rho_{pipe}\left(1+\nu_{pipe}\right)$, while it is known that:

$$c_s = c_p\sqrt{\frac{1-2\nu}{2(1-\nu)}}$$

If more than one solid are confining the fluid the above equation can be written as:

$$c_{tube} = \left[\frac{1}{c_{fluid}^2} + \frac{\rho_{fluid}}{\sum_{i=1}^{layers} M_i}\right]^{-1/2}$$, where layers is the number of solids.

As noted in White, for a thin tube $M = \frac{E_{pipe}h_{pipe}}{2b}$, where $h_{pipe} = a-b$ and for an infinite surrounding medium $M = \mu_{pipe}$.

Based on the above formulas, one can see the accuracy of the proposed method of analysis for a low frequency and large wavelength excitation. The excitation used will have a length of 10ms and is going to be generated by a 10m source. The numbers were chosen so that the resulting frequency and wavenumber spectrum are well below the cut-off values for the first mode in the pipe. In the following analyses the surrounding materials will have various properties, which may not be realistic. However, the purpose of the analyses is to observe the behavior of the proposed analysis under any kind of circumstances. Moreover, in order to check the final result, only the response of the system in time and space domain will be presented without any normalization.

The surrounding medium in this first case will be just one and the internal fluid will be water. For the purpose of analysis the following layout will be used:

Core fluid: Water with c_p = 1.5 Km/s, ρ=1t/m^3 and a radius of 1m

Surrounding solid: Steel with variable c_p, ρ=7.85 t/m^3 , v=0.3 and initially infinite radius

(Both materials will have a very small damping ratio of 0.01%)

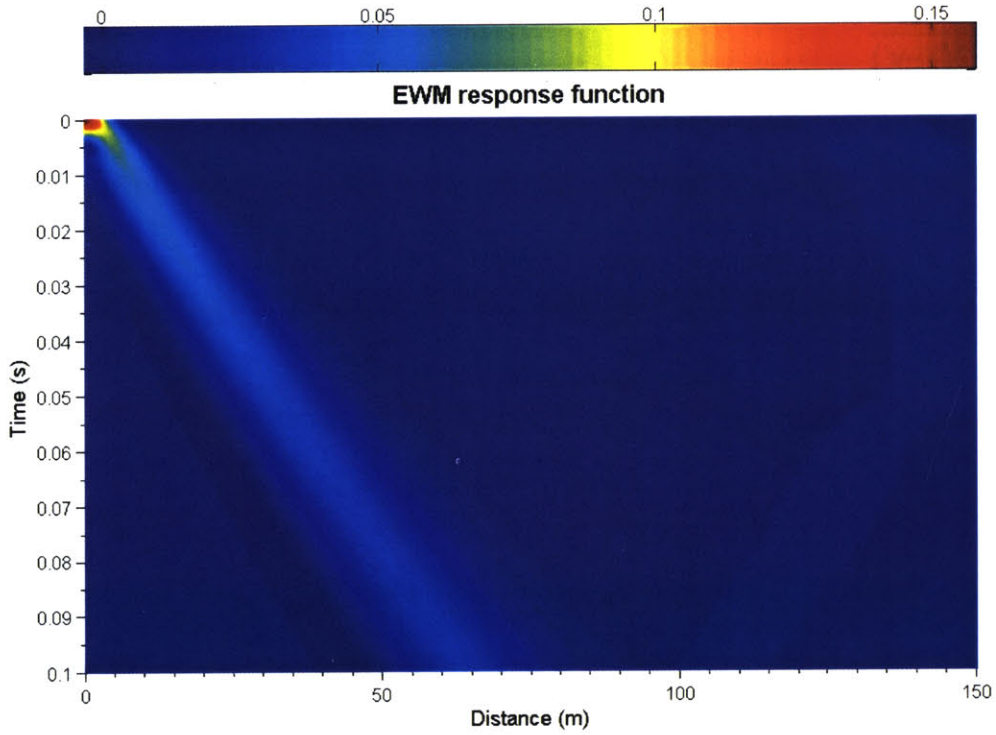

Figure 6.33: Response with c_p = 0.5 Km/s (Calculated c_{tube} = 0.67 Km/s)

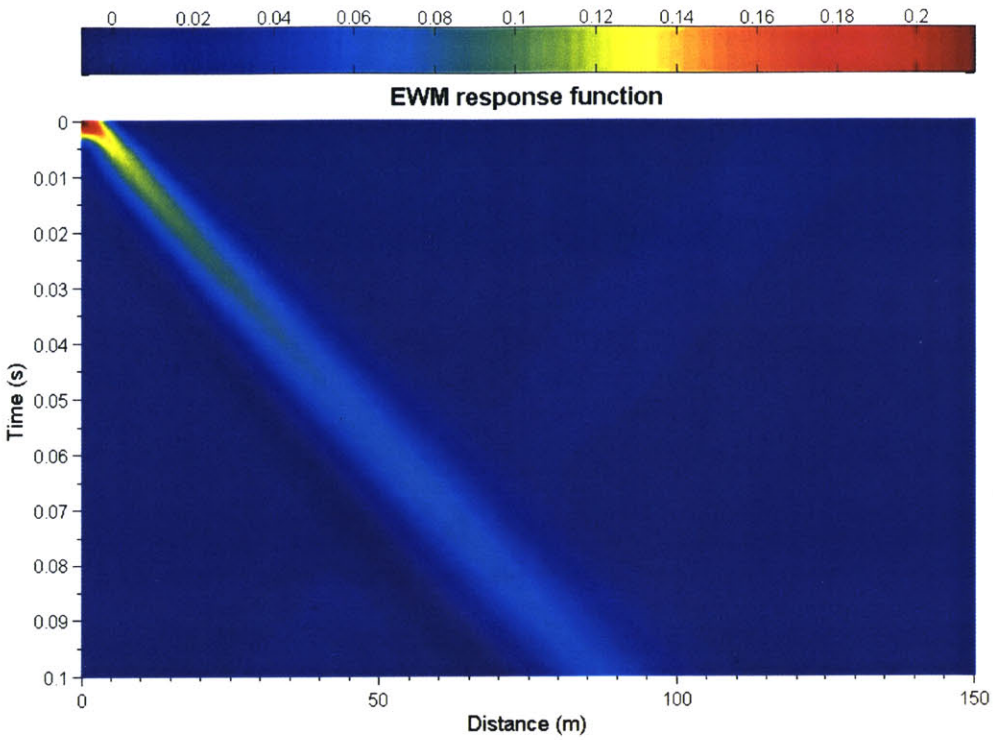

Response with $c_p = 0.75$ Km/s (Calculated $c_{tube} = 0.9$ Km/s)

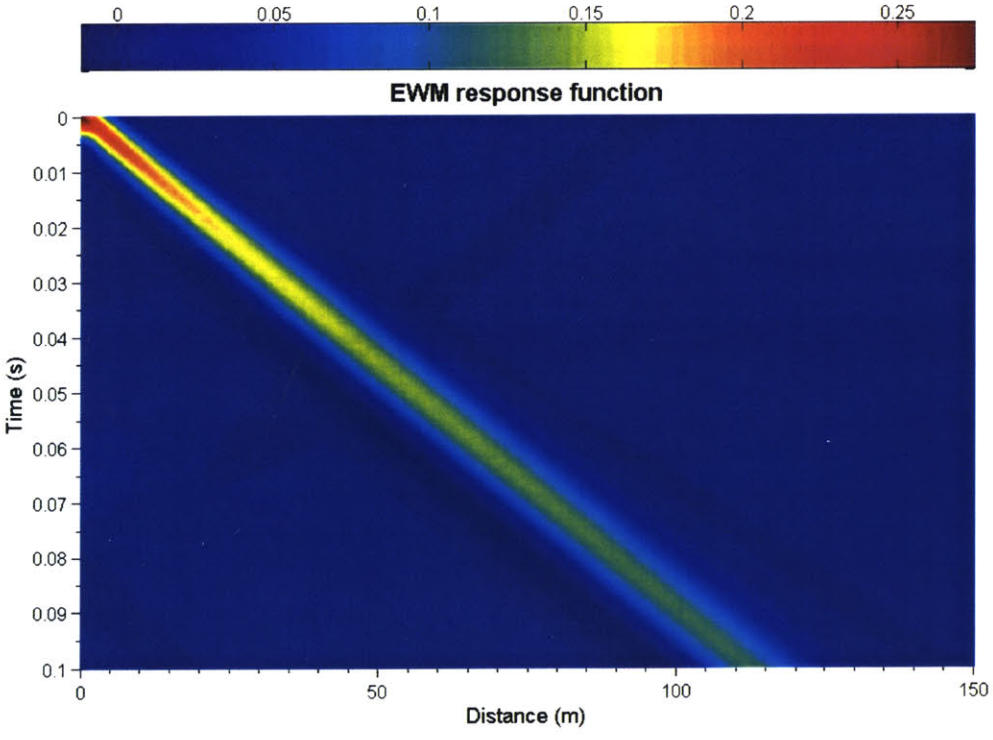

Figure 6.34: Response with $c_p = 1.2$ Km/s (Calculated $c_{tube} = 1.15$ Km/s)

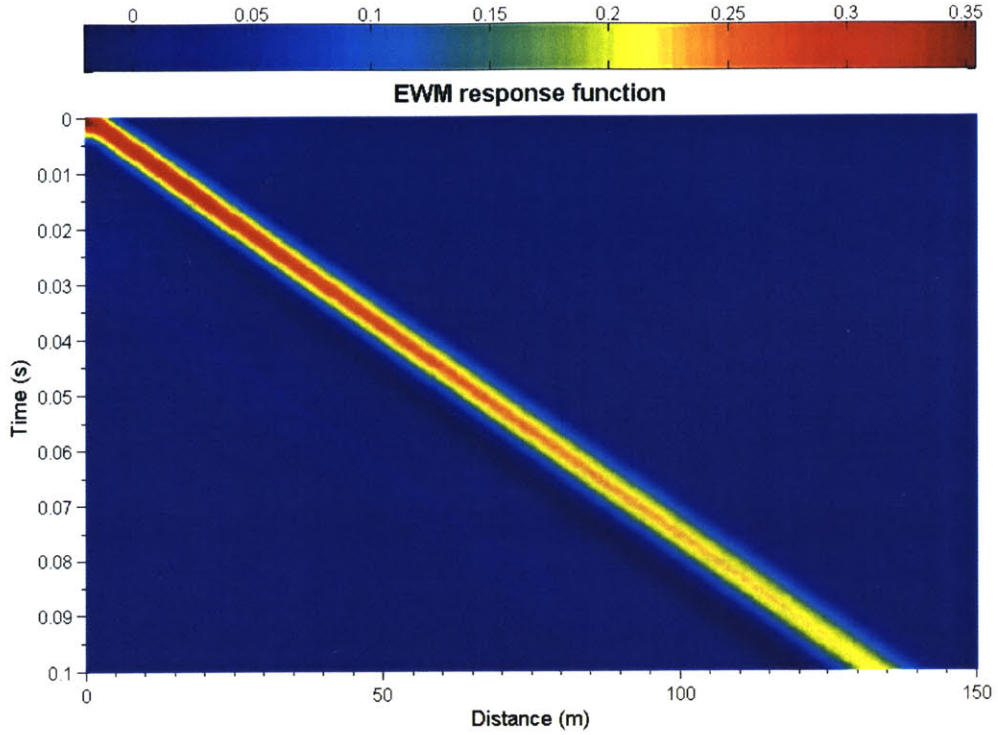

Figure 6.35: Response with $c_p = 2$ Km/s (Calculated $c_{tube} = 1.34$ Km/s)

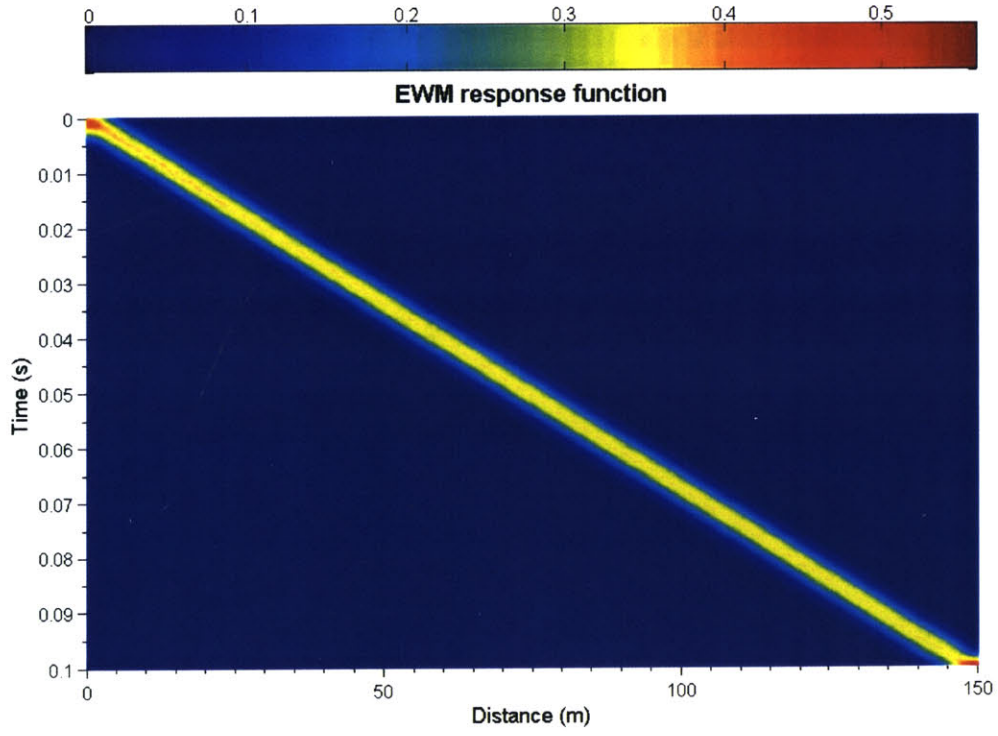

Figure 6.36: Response with $c_p = 6$ Km/s (Calculated $c_{tube} = 1.48$ Km/s)

In all of the above graphs, as it was expected the tube wave has a lower speed than the speed of sound in the fluid. The calculated speed of the tube waves according to White's theory is given below each graph and it matches the speed seen on the result in all cases. The absolute match of the analytical solution and the solution given by the code is apparent in all the graphs. The additional waves traveling in the pipe come from the signals fired in the previous period and from the other side of the pipe. These signals traveled all the way to the other side of the pipe (though of course having lost strength) and through the whole time span under consideration.

Moving on to a non-infinite surrounding medium, the same properties of the materials are going to be used with a fixed c_p of steel equal to 4 Km/s, while the thickness of the pipe will vary from 1cm to half a meter.

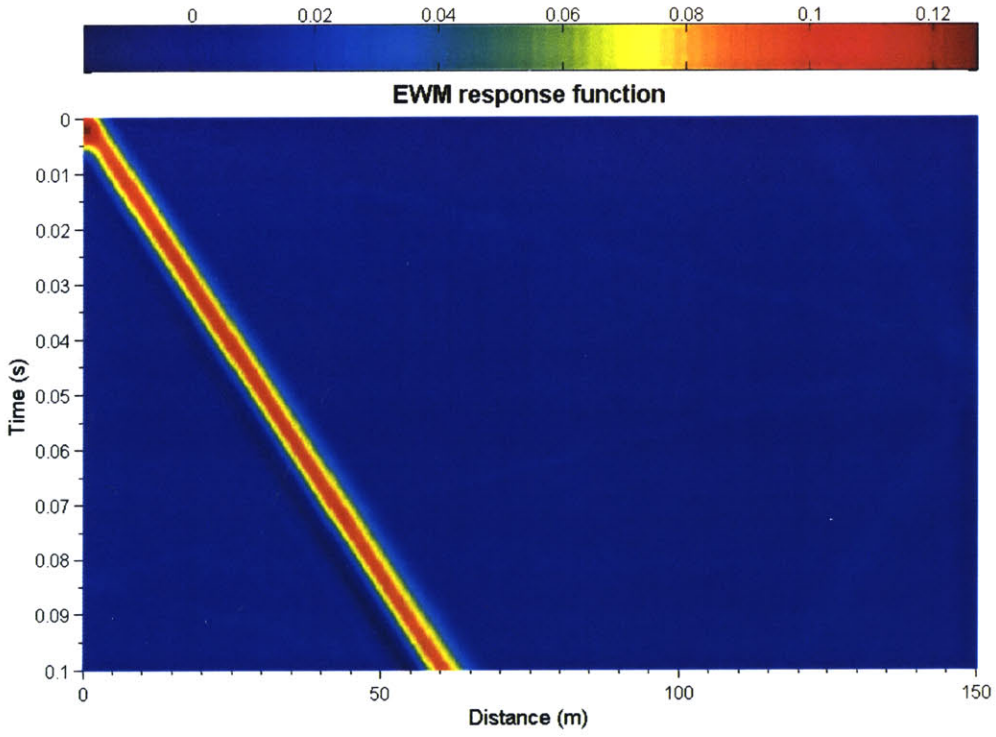

Figure 6.37: Response with $h = 1$ cm (Calculated $c_{tube} = 0.62$ Km/s)

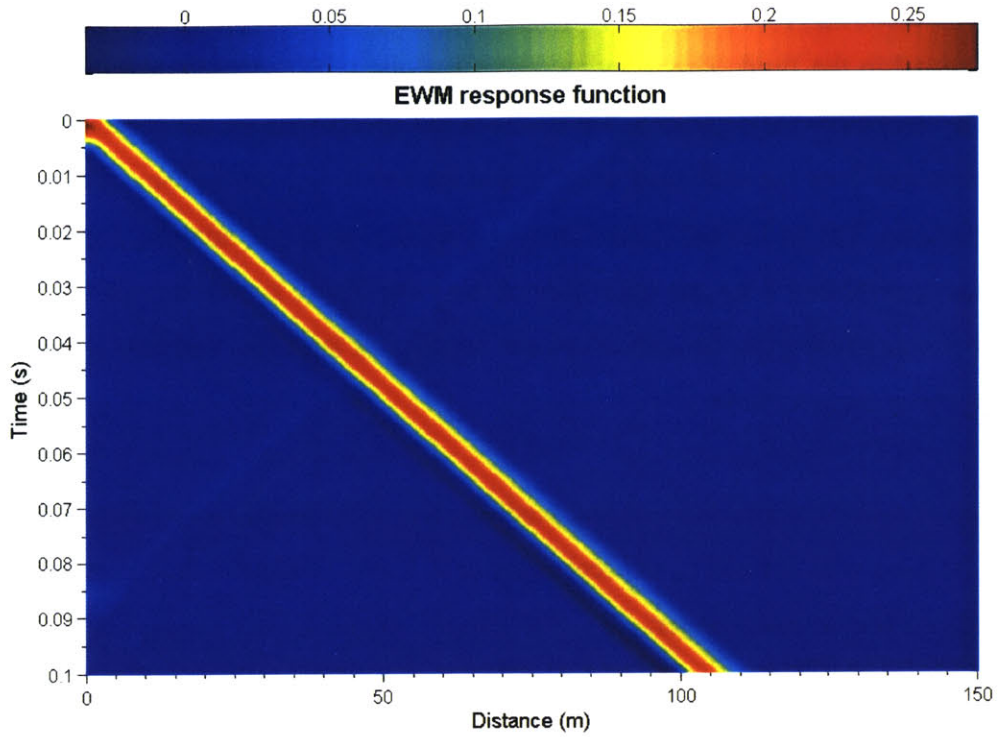

Figure 6.38: Response with $h = 5$ cm (Calculated $c_{tube} = 1.06$ Km/s)

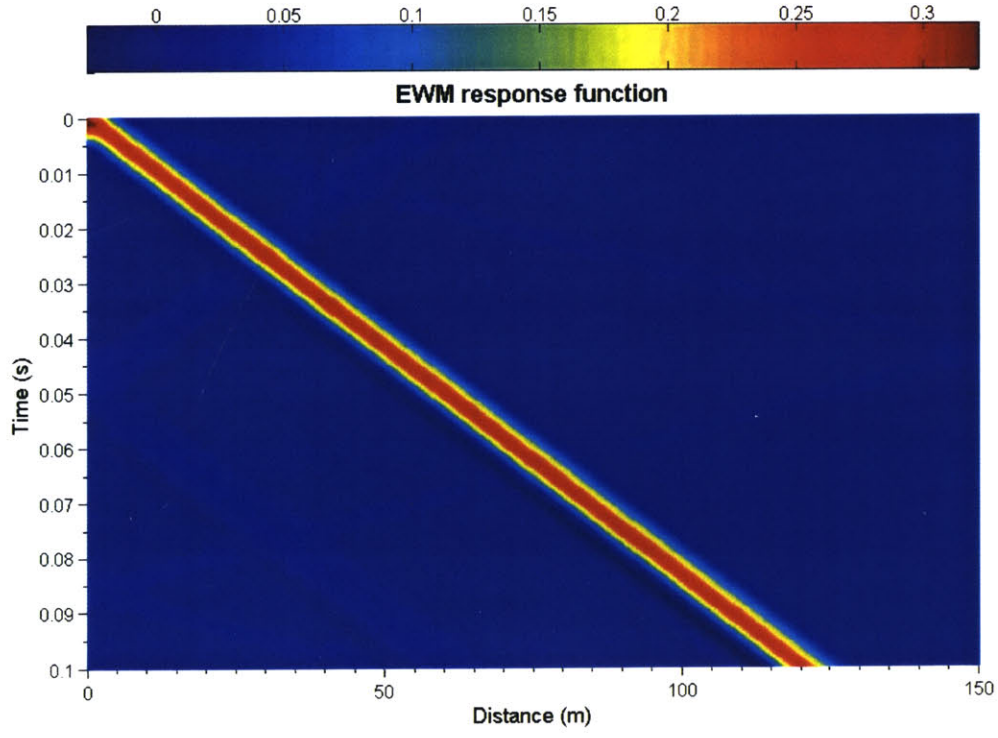

Figure 6.39: Response with $h = 10$ cm (Calculated $c_{tube} = 1.21$ Km/s)

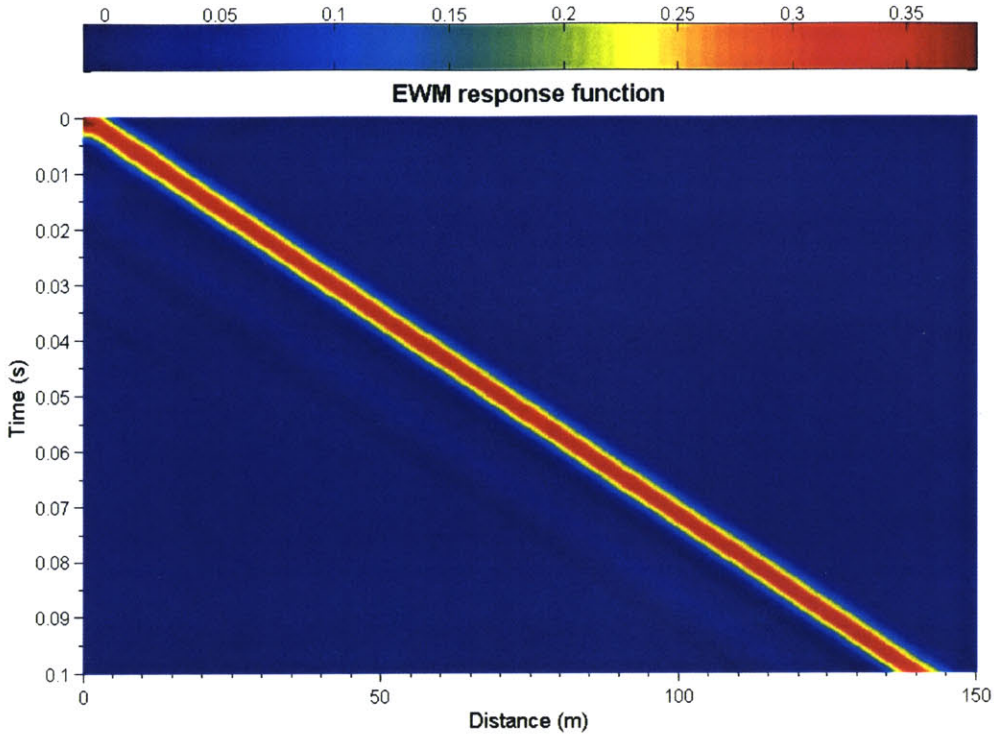

Figure 6.40: Response with $h = 50$ cm (Calculated $c_{tube} = 1.4$ Km/s)

From the above graphs one can easily see that the code's response in the case of the flexible pipe under low frequency and wavenumber excitation matches the theoretical response. Given these results, more complicated systems can be simulated. The system that is of special interest is a water filled steel pipe embedded in a soil. For this analysis the material properties of the steel will be considered fixed (c_p=5.8 Km/s) and the variability will be focused on the properties of the soil and the thickness of the pipe.

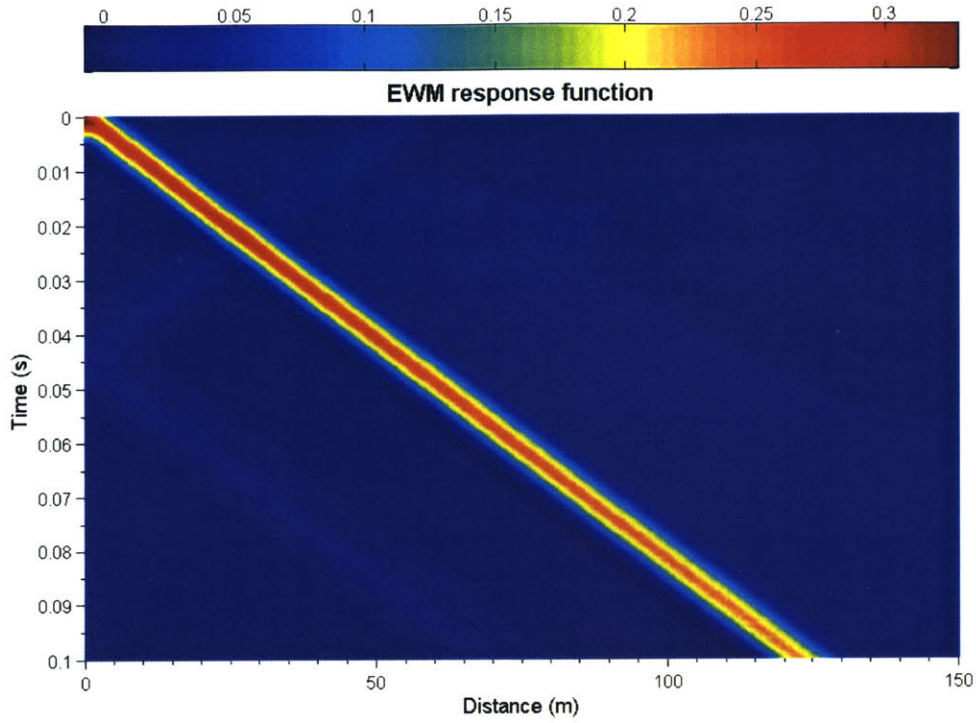

Figure 6.41: Response with $h = 5$ cm, $c_{p\text{-}soil}$=0.5 Km/s, $c_{s\text{-}soil}$=70m/s, ρ_{soil}=1.8t/m^3

(Calculated $c_{tube} = 1.23$ Km/s)

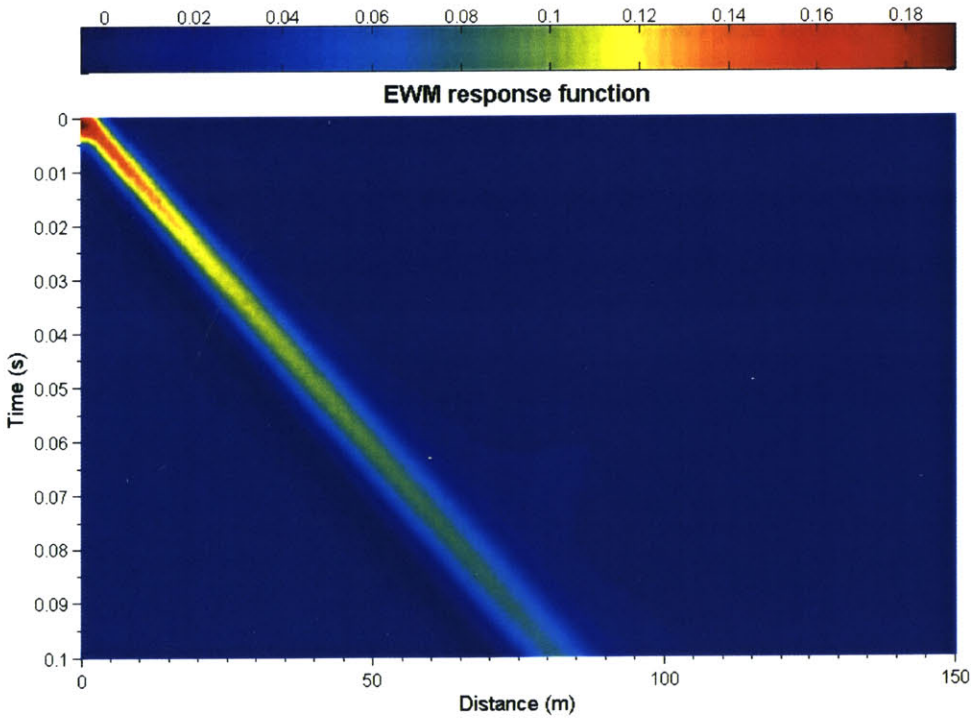

Figure 6.42: Response with $h = 1$ cm, $c_{p\text{-}soil}$=0.5 Km/s, $c_{s\text{-}soil}$=70m/s, ρ_{soil}=1.8t/m^3

(Calculated $c_{tube} = 0.83$ Km/s)

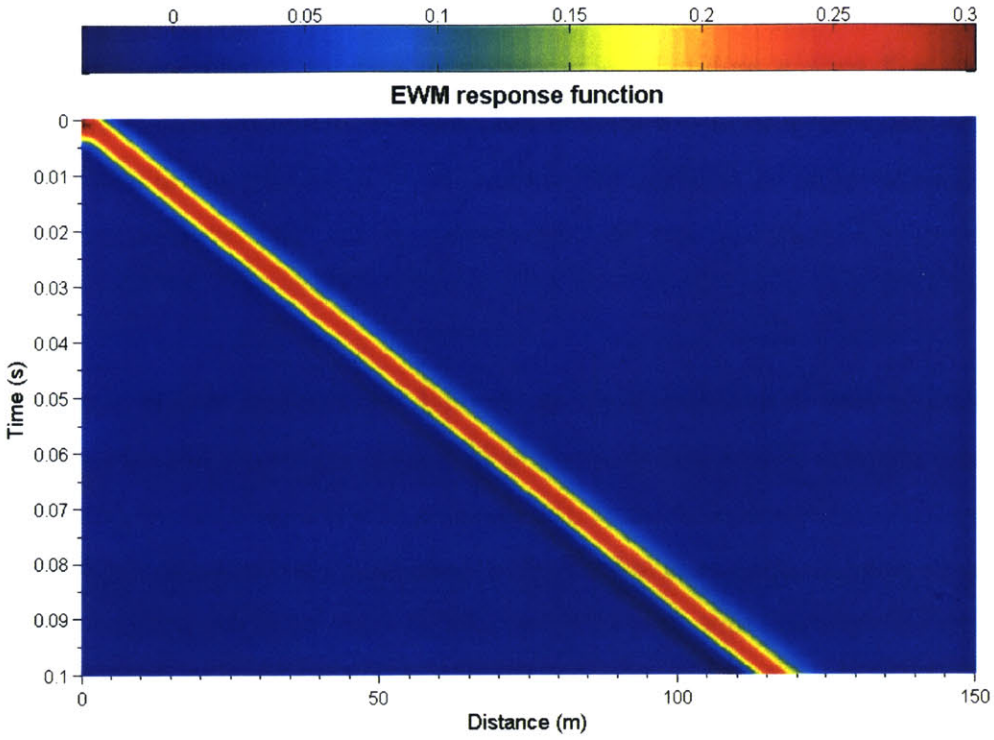

Figure 6.43: Response with h = 1 cm, $c_{p\text{-}soil}$=3 Km/s, $c_{s\text{-}soil}$=1.22Km/s, ρ_{soil}=1.8t/m^3 (Calculated c_{tube} = 1.18 Km/s)

As seen in the graphs above, the code works in complete agreement with the theoretical model for the low frequency and long wavelength case. However, the most interesting part is the analytical simulation of the same fluid-pipe-soil system for high frequencies and short wavelengths. This will be analyzed in the next chapter, where realistic values will be assigned to the dimensions of the system and the properties of the materials comprising it.

6.6 Practical uses

As shown in the previous chapter the stiffness matrix formulation can provide an exact solution to low frequency and low wavenumber excitation or the infinitely stiff pipe case. This chapter will use realistic values for the material properties and the dimensions of the system to simulate the response of the system under any kind of excitation and any system layout. The system under consideration will be a complete three-layered fluid-pipe-soil

system. The material properties will remain the same for the fluid (water) in the pipe, but the pipe's material (concrete or steel) and the surrounding soil (variety of soils and soil conditions) will have a multitude of properties in each of the different analyses. The purpose of this chapter is to use the proposed method to find the exact solution of the pressure distribution in cases where there is no analytical solution and to observe how the properties of the materials and the dimensions of the pipe will affect the signal transmission.

The excitations used in this chapter will be the high and medium frequency ones used in the previous chapters (0.5ms and 1ms), while the source will be considered to have a total area of pressure impact equal to 0.5m. The distance between the two consecutive sources will be up to 300m, in order to investigate the system for a maximum propagation distance of 150m and a maximum time-span of 100ms, without mixing of the signals coming from subsequent firings or sources.

The water will have the typical properties used in the previous chapters (c_p = 1.5 Km/s, ρ=1t/m^3, ξ=0.1%). The properties of the pipe's material which will remain the same will be its density (7.85 t/m^3 if steel, 2.5 t/m^3 if reinforced concrete) and its Poisson ratio (0.3 in any case), while its damping ratio will vary from 0.1% to 5%, which are both extreme values (base case value: 0.5%). The soil properties will all vary according to its type and according to the depth of the pipe (keeping Poisson's ratio equal to 0.498), while it will be considered to extend infinitely away from pipe. The thickness of the pipe will vary from 1cm to 20cm (base case value: 5cm) and its radius from 0.25m to 2m (base case value: 1m). For each set of properties and dimension a set of parametric analyses will be run, keeping all the other variables constant. The following table shows the base case value and the limits of all the properties and dimensions of the system:

Property/Dimension	Minimum	Maximum	Base case
Pipe radius (m)	0.25	3	1m
Pipe thickness (cm)	1	15	5cm, ; 2in
c_p of pipe (Km/s)	4	10	6
ξ_{pipe} (%)	0.5	5	0.5
ξ_{soil} (%)	2	10	2
soil density (t/m^3)	1.1	2.2	1.8
c_p of soil (Km/s)	0.01(10m/s)	2	0.8

Table 6.1: Base case properties and property limits for all other analysis

Note:

When the combined acoustic velocity of the system (tube waves) will be equal to the water's the analysis can be done with the simplified method, as proven in chapter 6.3 and so there will be no analysis of this kind in this chapter. For comparison, the tube waves speed of the base case have a velocity of 1.25 Km/s, so there is enough latitude for a stiffer formation, given that the base case already considers a pipe made of steel. At the same time, only the base case will be excited with a low frequency signal, since this case can be solved analytically, as proven in chapter 6.3.

Base case scenario (c_{tube} = 1.25Km/s)

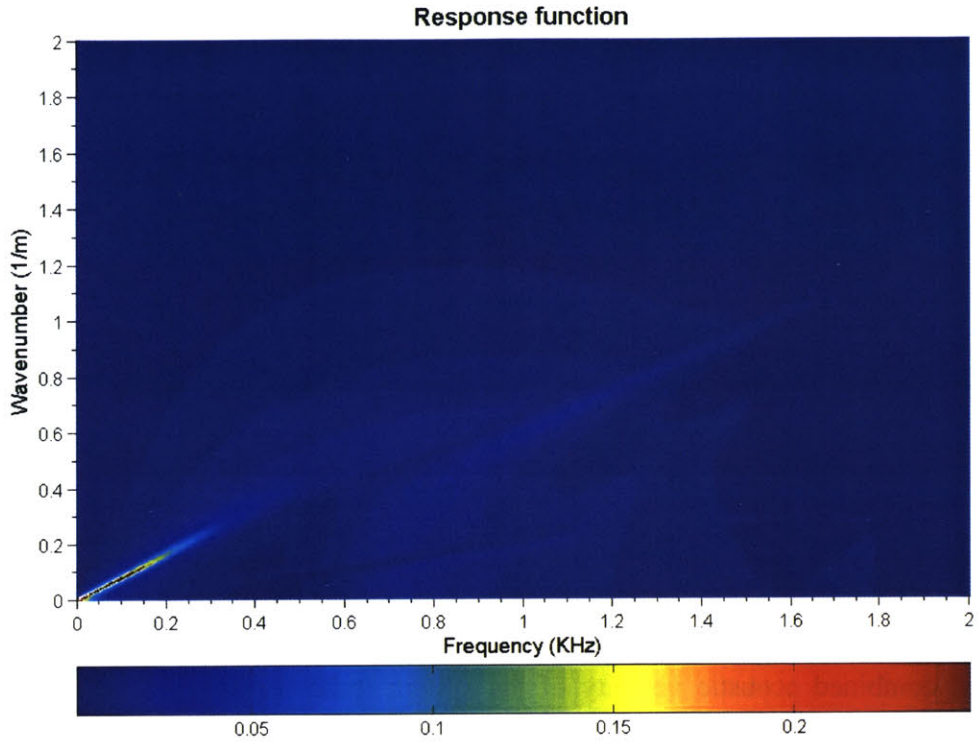

Figure 6.44: Response function of base case (1ms pulse)

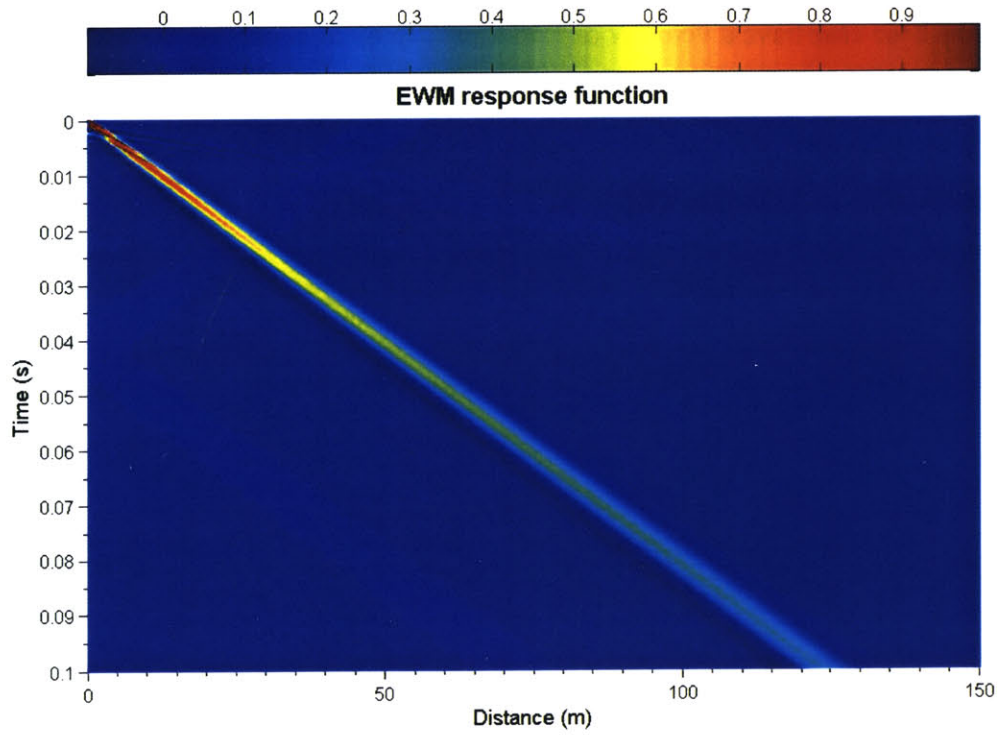

Figure 6.45: Pressure distribution of base case, c_{tube}=1.25Km/s (1ms pulse)

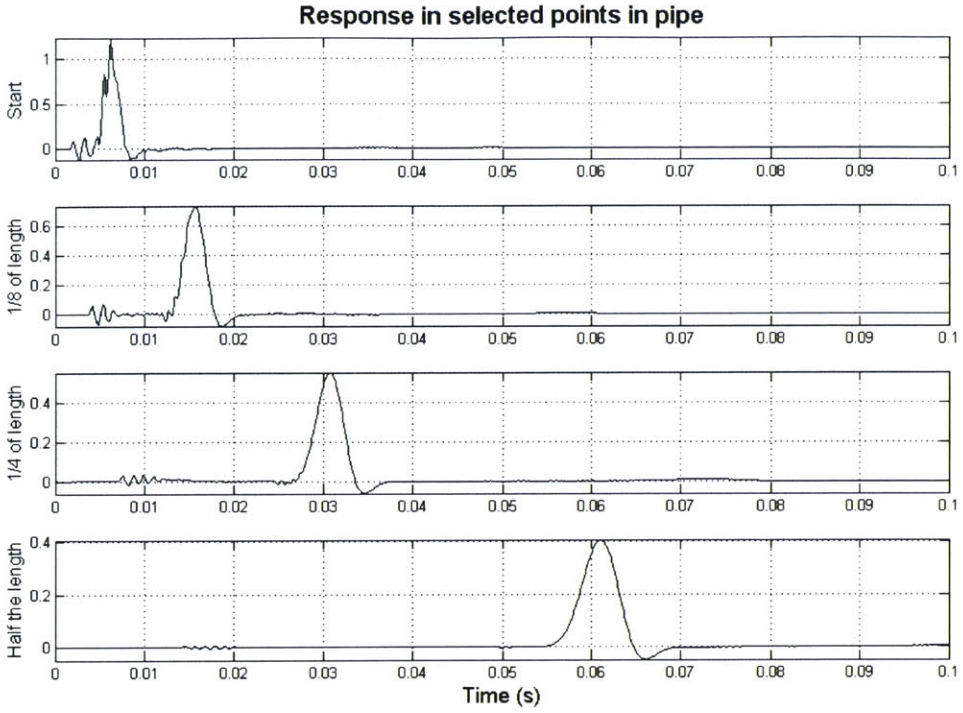

Figure 6.46: Pressures in selected points in pipe (1ms pulse)

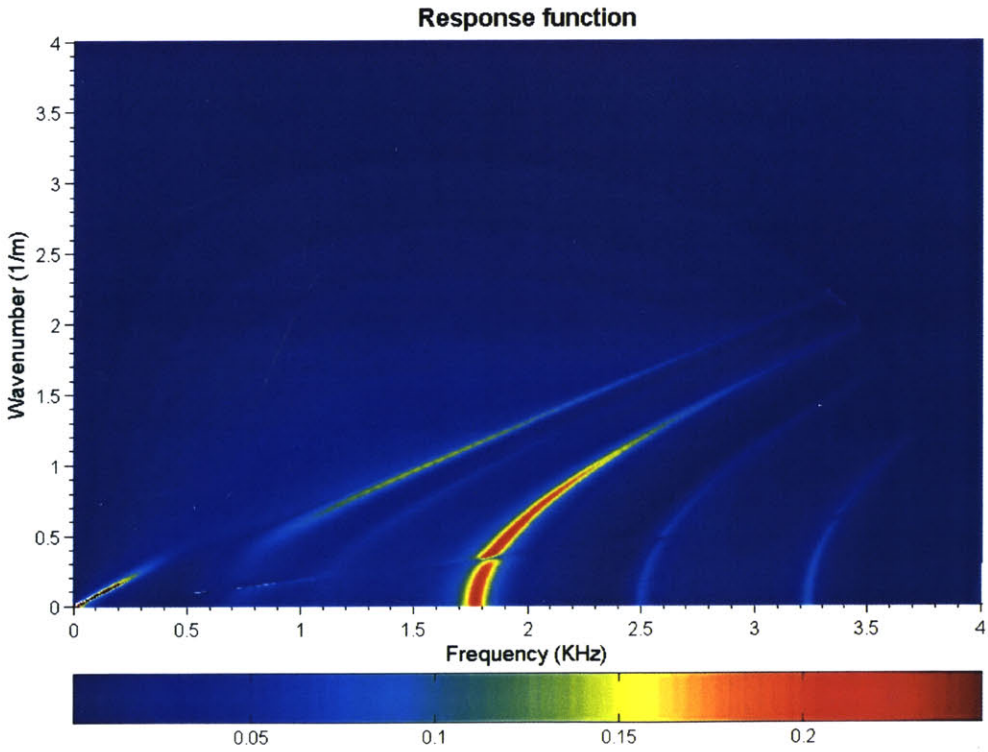

Figure 6.47: Response function of base case (0.5ms pulse)

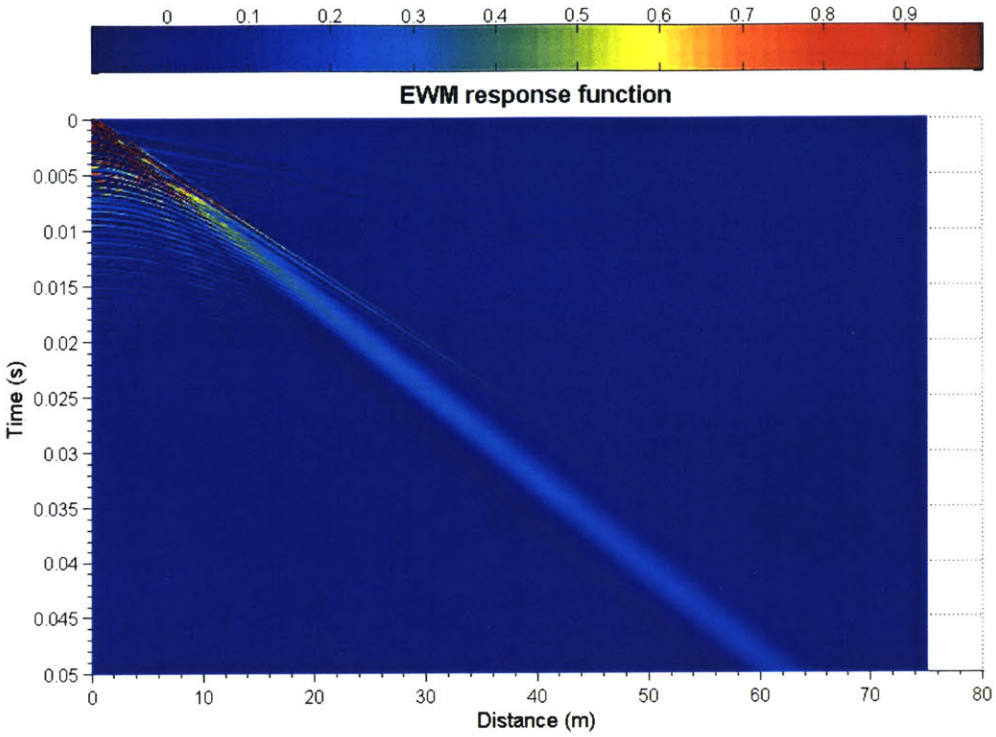

Figure 6.48: Pressure distribution of base case (0.5ms pulse)

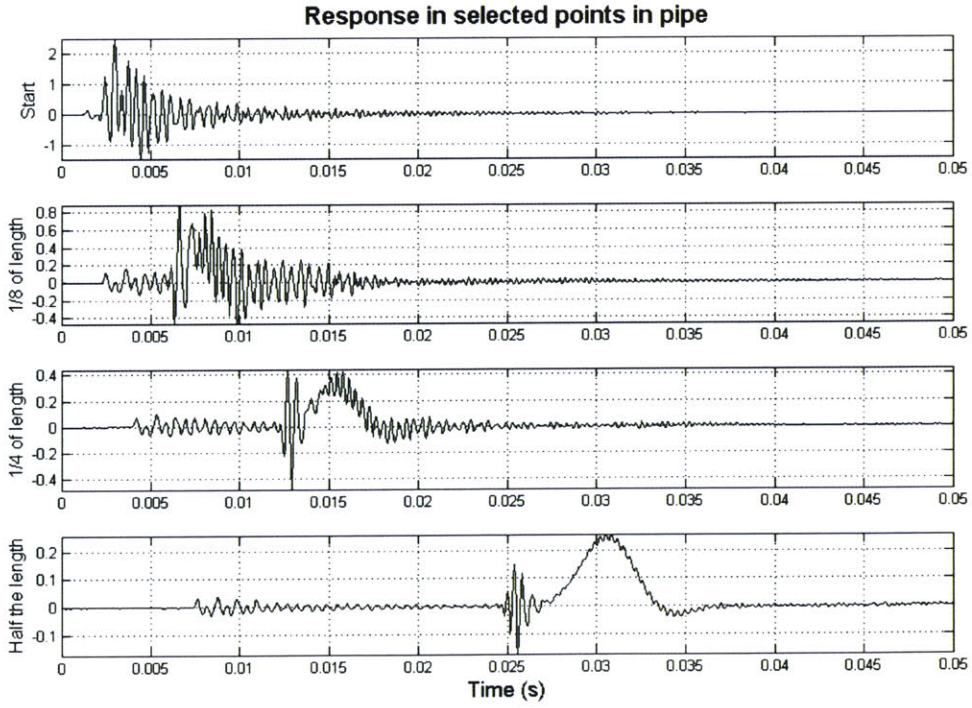

Figure 6.49: Pressure in selected points in pipe (0.5ms pulse)

In the case of the 1ms excitation the graphs show low noise levels in general, but at the same time there are waves traveling inside the pipe with velocities higher than the water's. This phenomenon is the result of waves re-entering the fluid, after propagating faster through the pipe shell. However, these waves die out very fast and cannot be seen after 50-60m of propagation. At the same time, the main signal attenuates much faster than in any rigid pipe case, due to the high damping ratio of the system. The 0.5ms excitation case shows analogous results, but in this example the noise levels are much higher and there is a wave traveling with the speed of water, which is sustained for much longer.

Effect of pipe dimensions

Given the formula of the tube wave speed, it is easy to see that increasing the thickness of the pipe will make the system even stiffer, resulting in the simplified analysis approximation. For this set of analysis, in order to keep the velocity of the tube waves constant, the pipe is going to be scaled down according to its internal dimension.

The following graphs show the behavior of a pipe with an internal diameter of 3m (15cm thickness). In this extreme case, one can see that there is a lot of noise generated, because of the shifting of the characteristic frequencies of the pipe. As it can be seen by the response function, the cut-off frequencies of the pipe were scaled down according to its diameter change. In this case the cut-off frequencies were scaled down by a factor of three and this means that for a given signal with a given frequency bandwidth, approximately three times more modes can propagate in the pipe system.

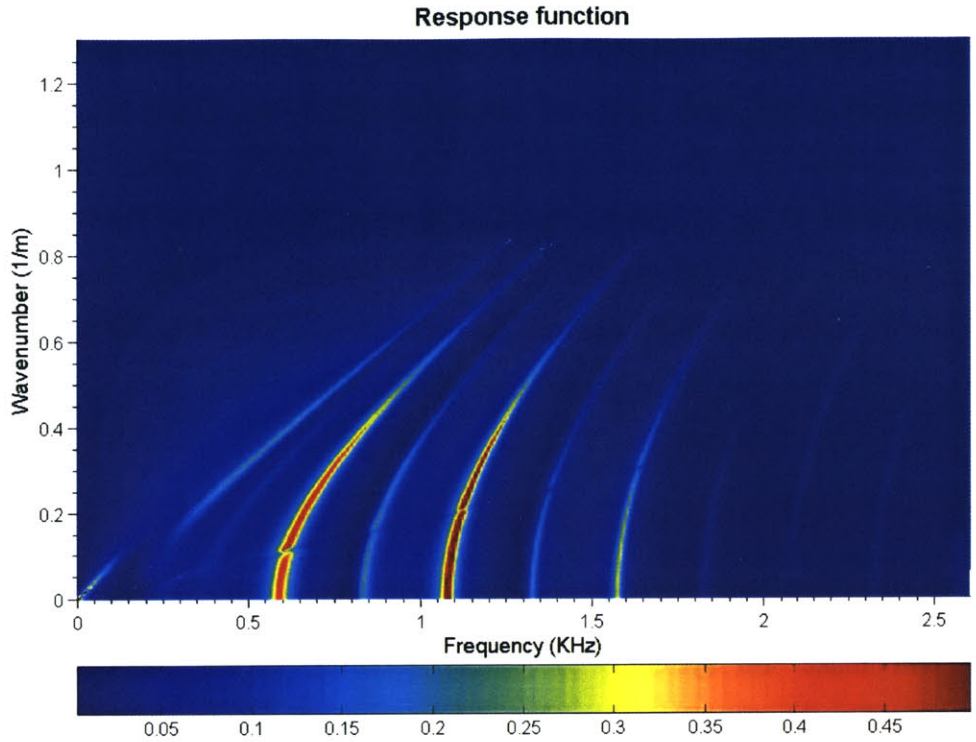

Figure 6.50: Response function of a 3m radius pipe (1ms pulse)

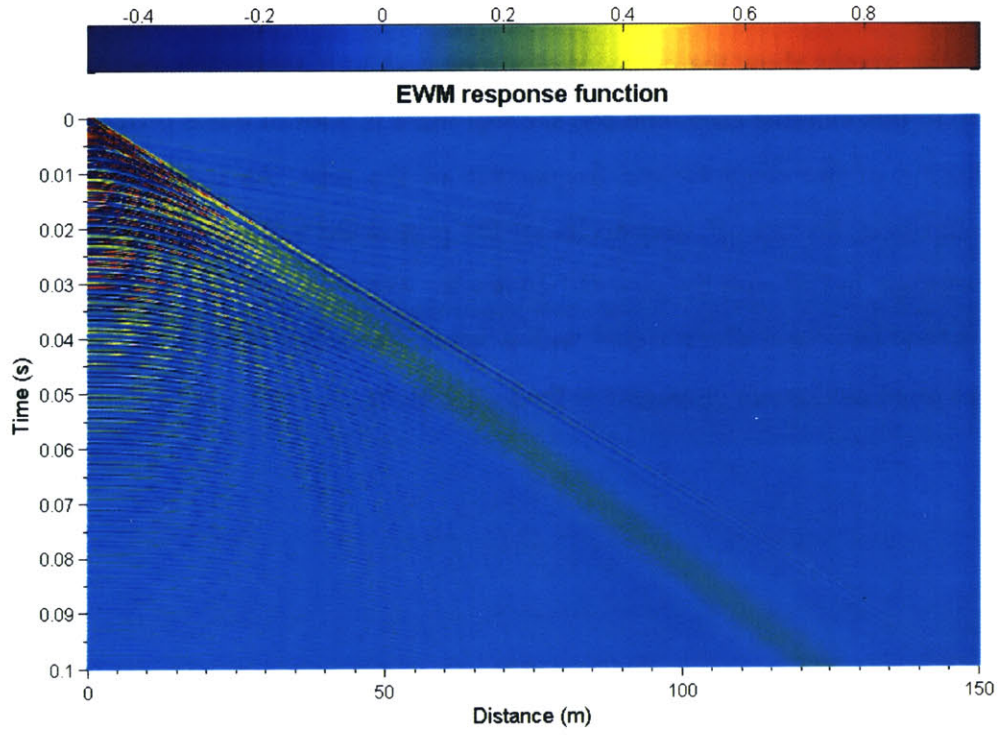

Figure 6.51: Pressure distribution of a 3m radius pipe (1ms pulse)

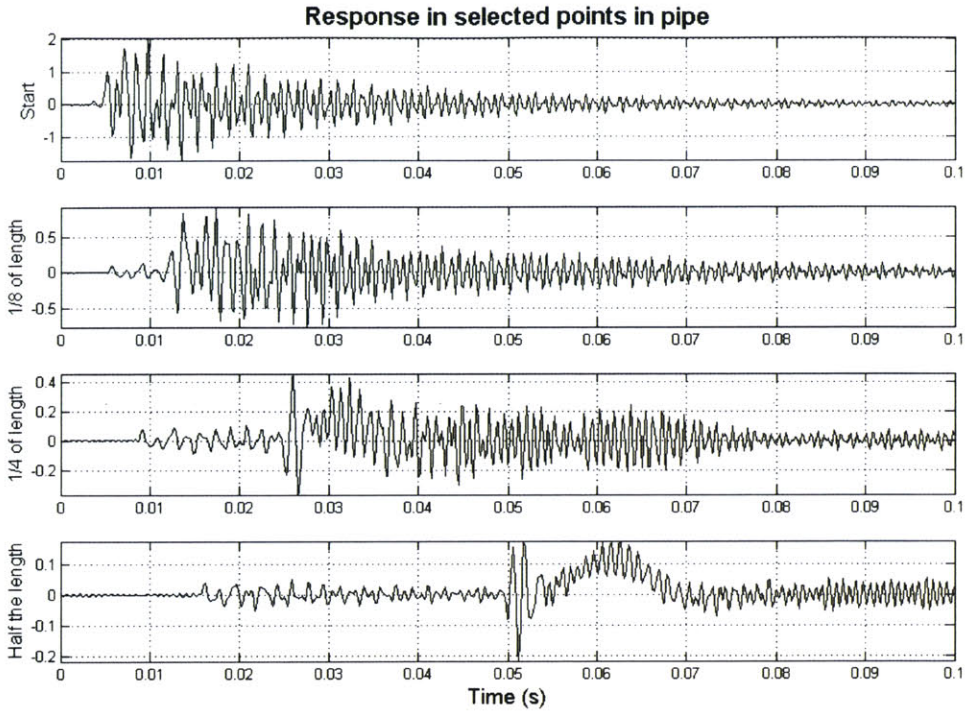

Figure 6.52: Pressures in selected points in 3m radius pipe (1ms pulse)

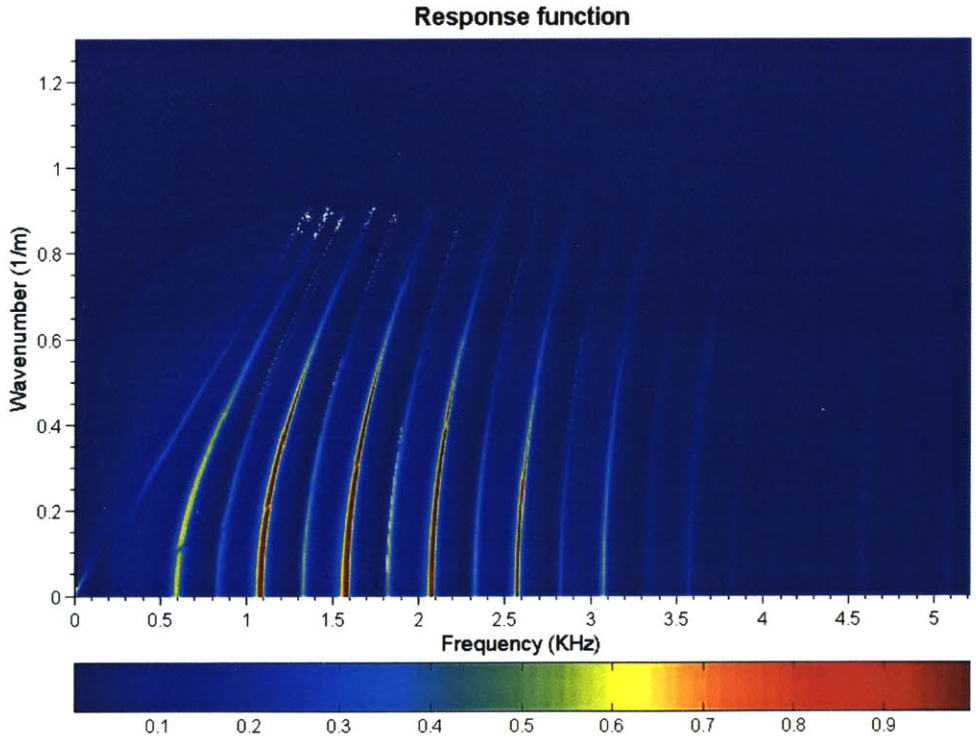

Figure 6.53: Response function of a 3m radius pipe (0.5ms pulse)

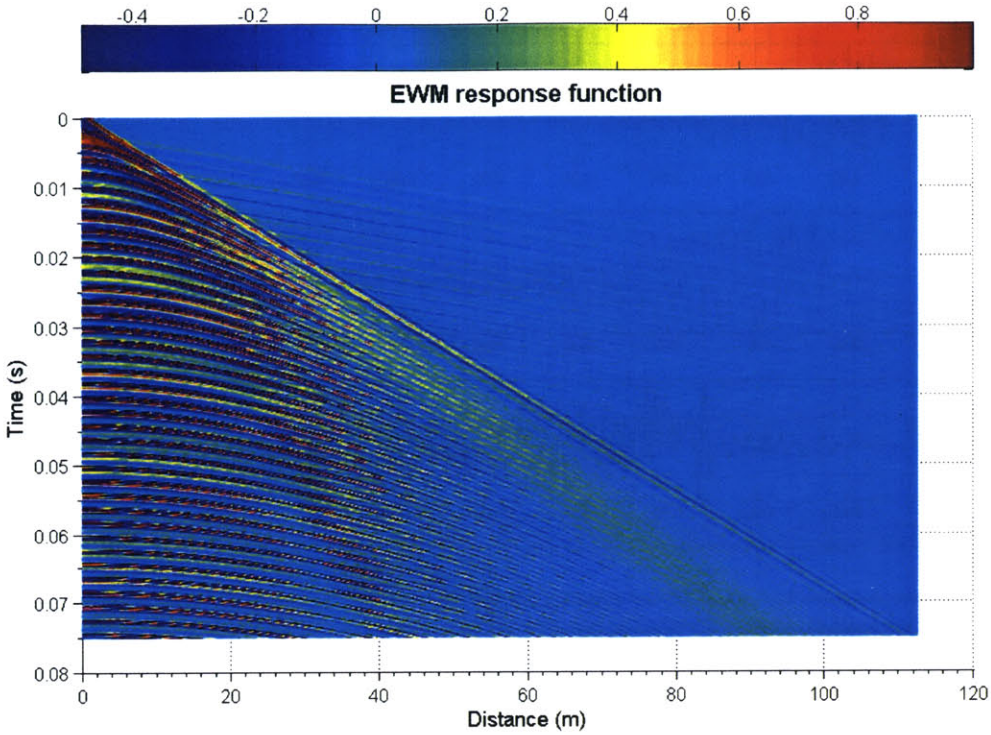

Figure 6.54: Pressure distribution of a 3m radius pipe (0.5ms pulse)

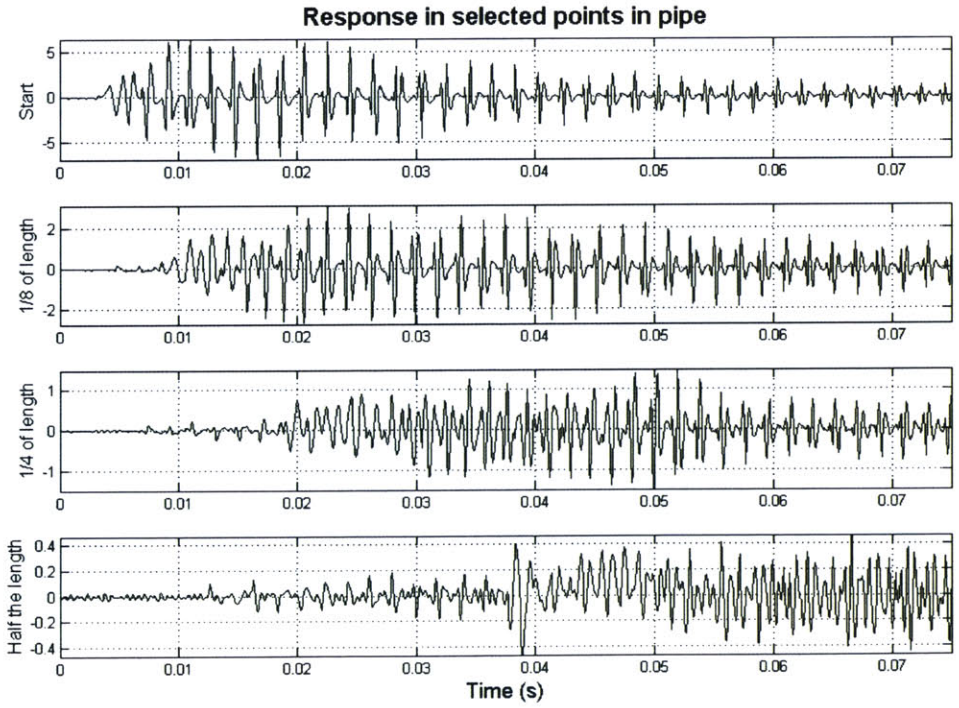

Figure 6.55: Pressures in selected points in 3m radius pipe (0.5ms pulse)

The inverse effect is seen when the pipe radius decreases. The following graphs present the pressure distribution for a pipe with internal diameter of 0.25m (1.25cm thickness). One can see that, even for a high frequency signal (according to the 1m radius pipe), there is no noise generated in the pipe, because the cut-off frequencies of the higher modes have been increased by a factor of four.

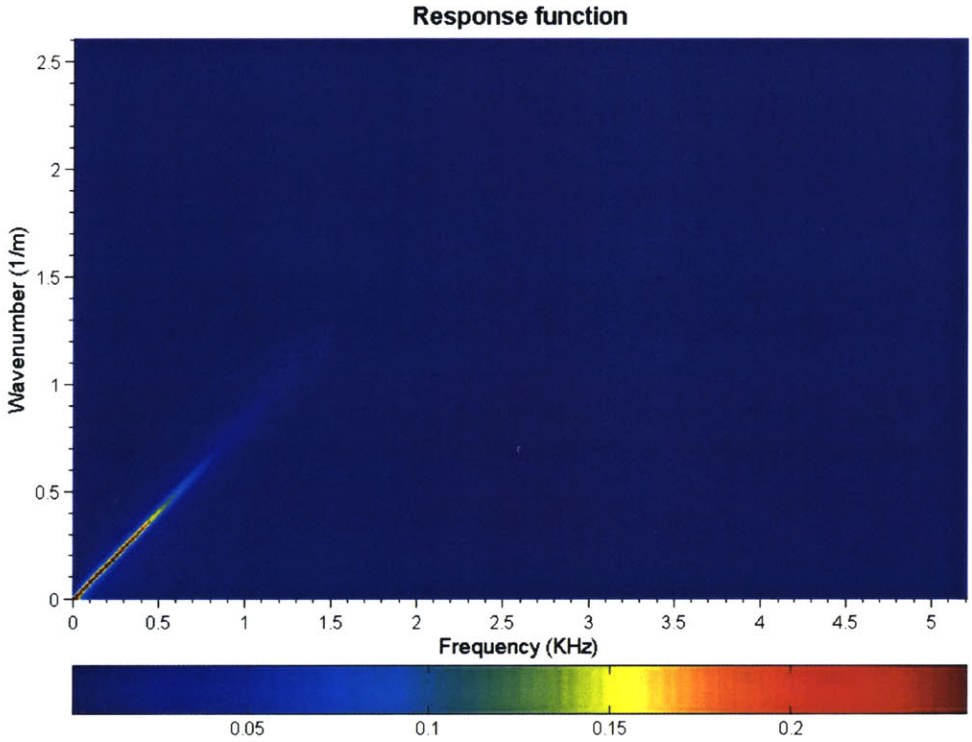

Figure 6.56: Response function of a 0.25m radius pipe (0.5ms pulse)

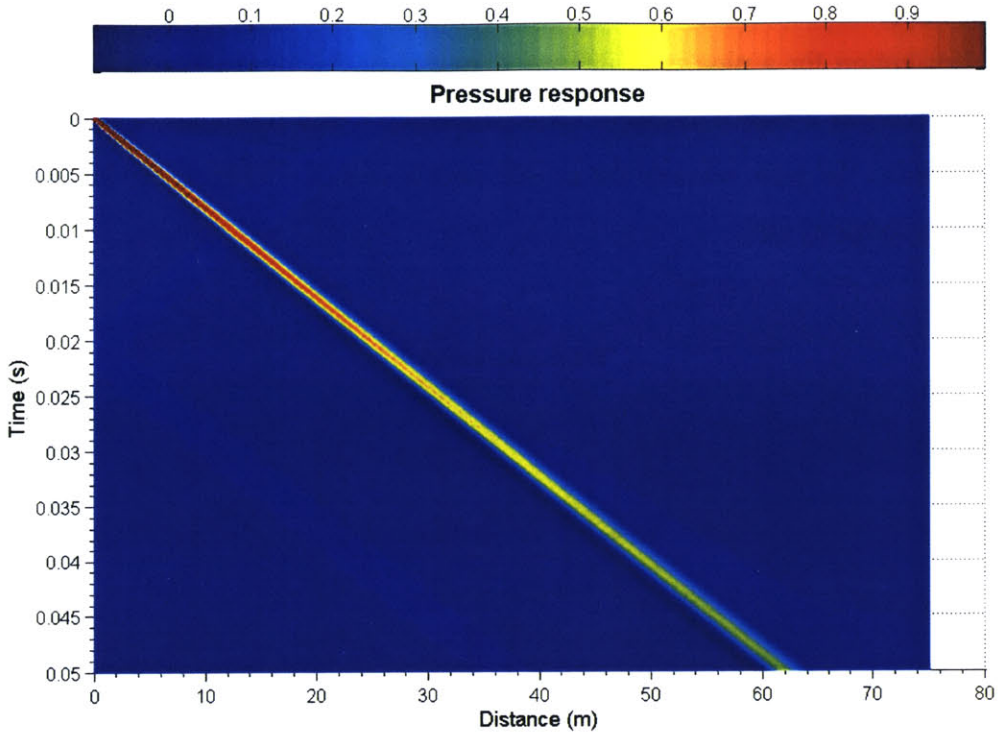

Figure 6.57: Pressure distribution of a 0.25m radius pipe (0.5ms pulse)

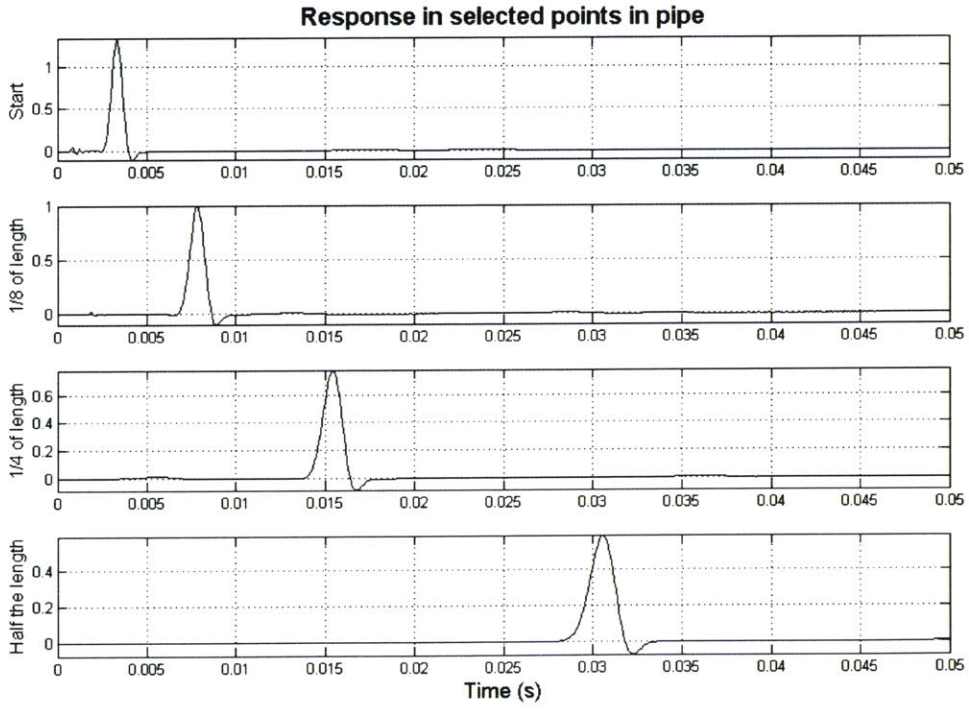

Figure 6.58: Pressures in selected points in 0.25m radius pipe (0.5ms pulse)

As it was expected by the findings of the simplified analysis, which stated that the cut-off frequencies of the rigid pipe were $\omega_{nj} = z_{nj}\frac{c}{R}$, the complete analysis showed the same relationship between radius and characteristic frequencies. In conclusion, it was proven that the effect of the pipe radius is to shift the characteristic frequencies of the system, so that higher modes can or cannot propagate in the pipe.

Effect of pipe stiffness

Instead of the steel pipe of the base case scenario, this set of analysis will deal with a lower stiffness pipe, as would be, for example, a concrete pipe having a thickness of up till 10 times the thickness of the steel pipe. The density of the concrete will be taken equal to 2.5t/m^3 and its compressional wave velocity equal to 4Km/s, while the Poisson's ratio will be kept the same as in the steel case (0.3). This set of analyses will demonstrate the effect of the pipe stiffness on the noise level and the dying out of the signal noise in relation to distance traveled in the pipe.

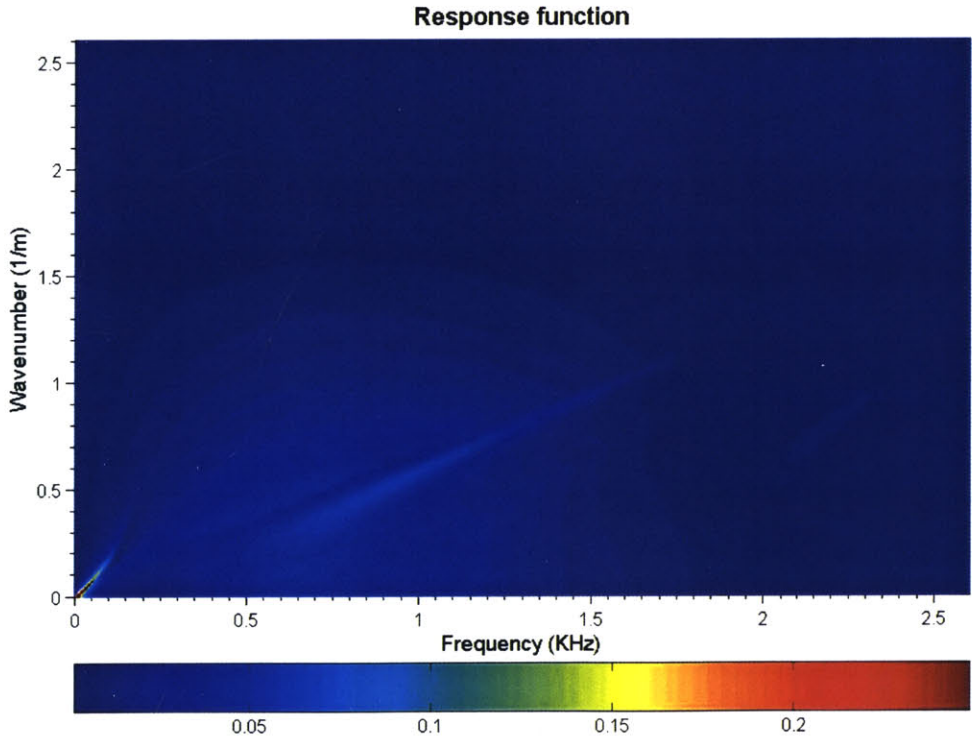

Figure 6.59: Response function of a concrete 5cm thick pipe (1ms pulse)

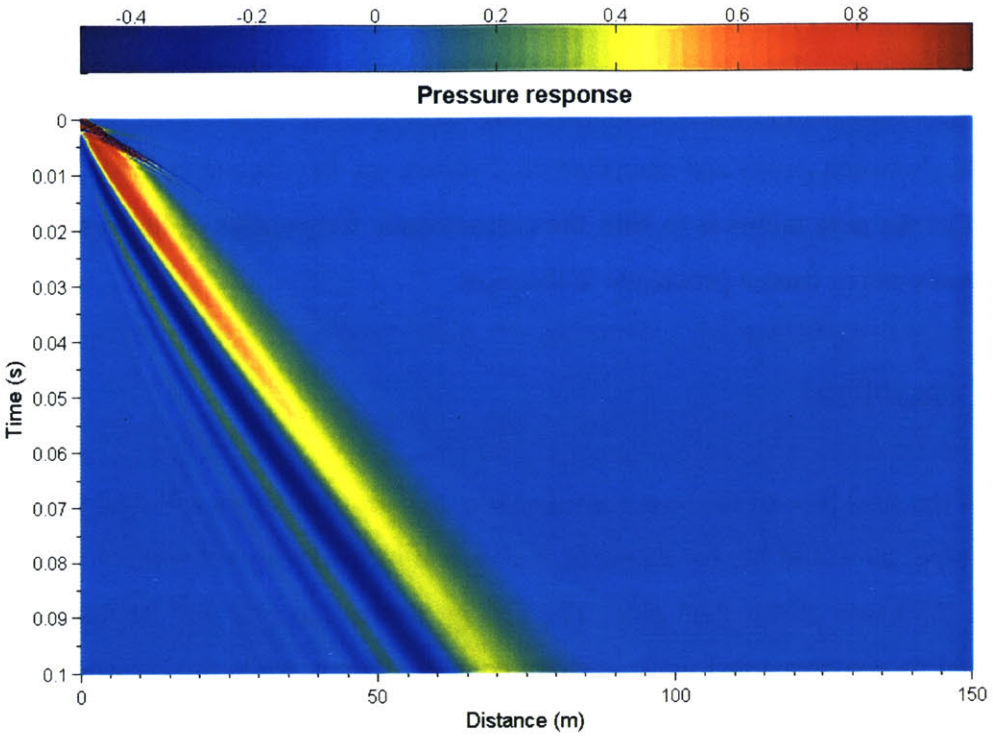

Figure 6.60: Pressure distribution of a concrete 5cm thick pipe (1ms pulse)

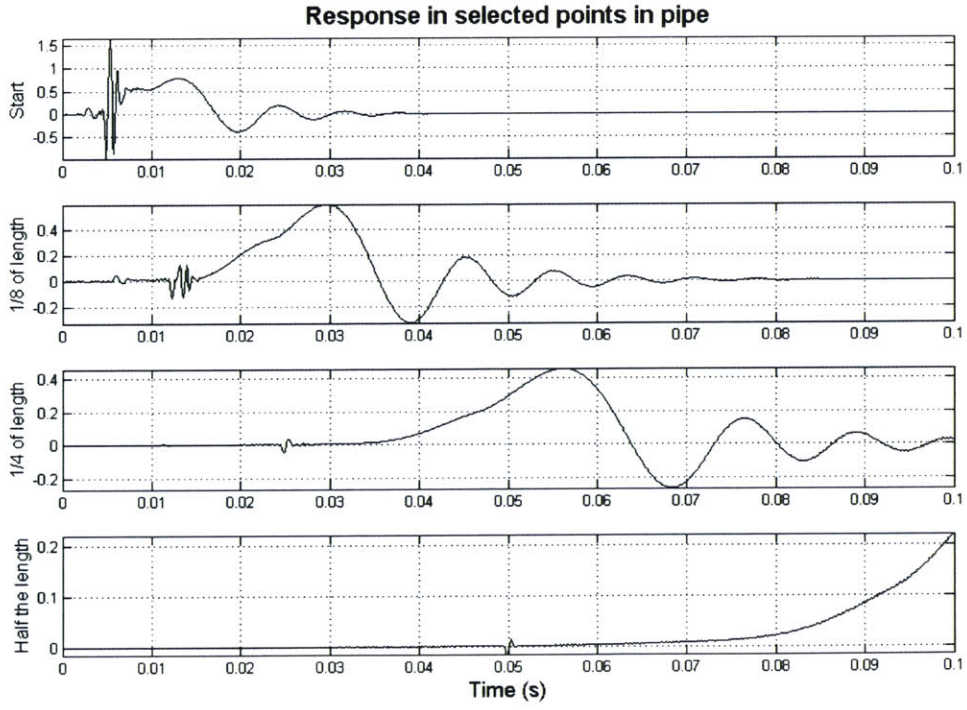

Figure 6.61: Pressure in selected points in a concrete 5cm thick pipe (1ms pulse)

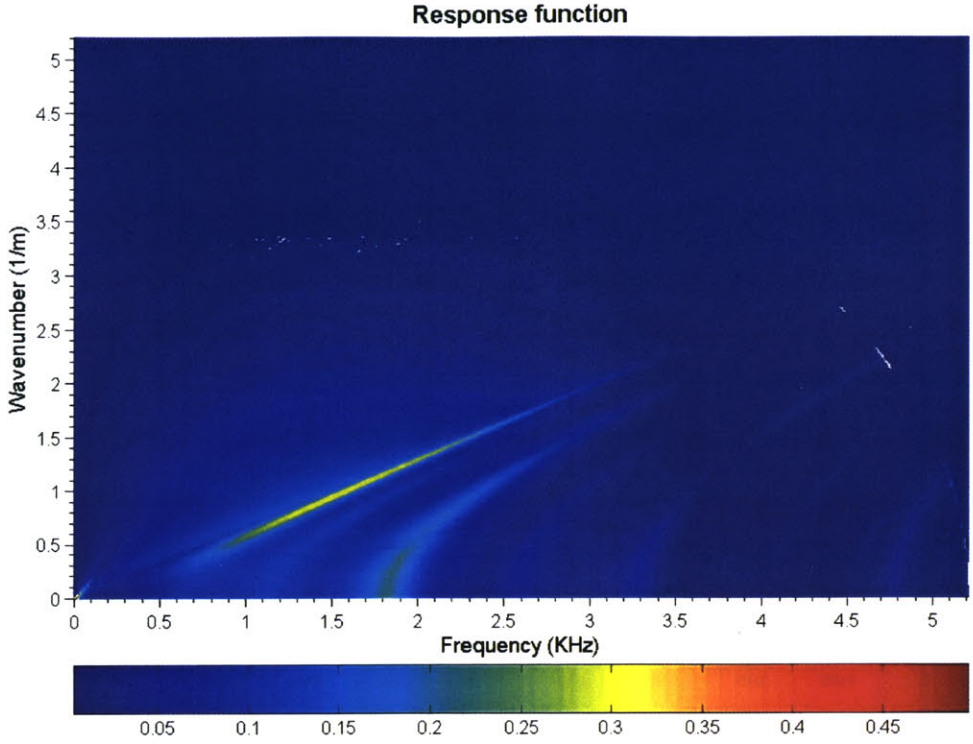

Figure 6.62: Response function of a concrete 5cm thick pipe (0.5ms pulse)

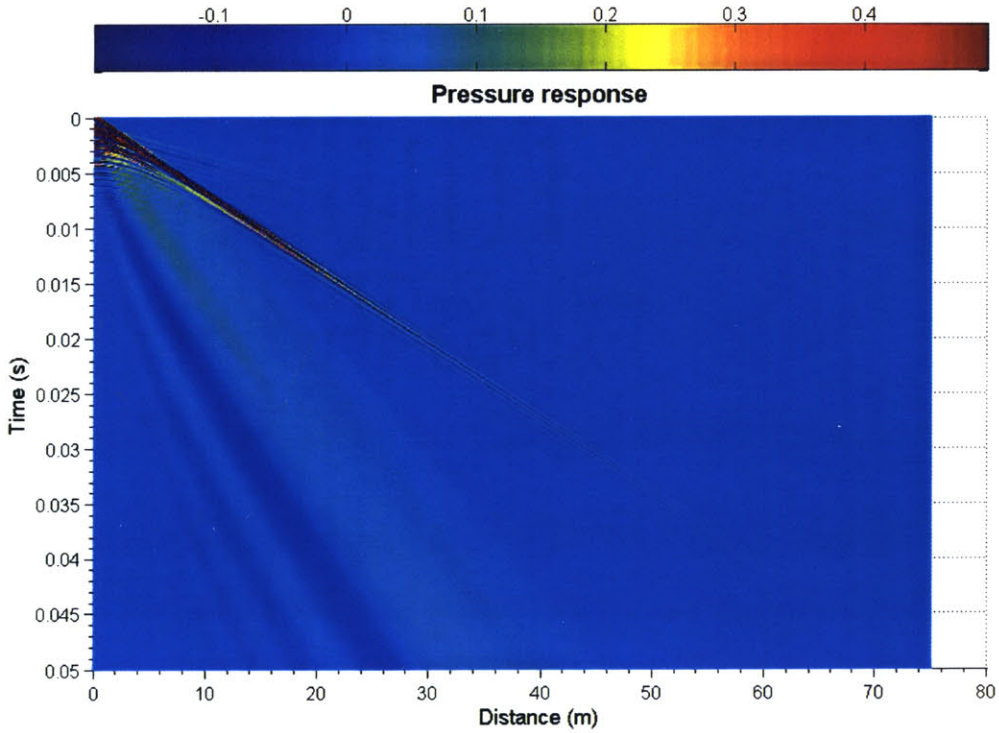

Figure 6.63: Pressure distribution of a concrete 5cm thick pipe (0.5ms pulse)

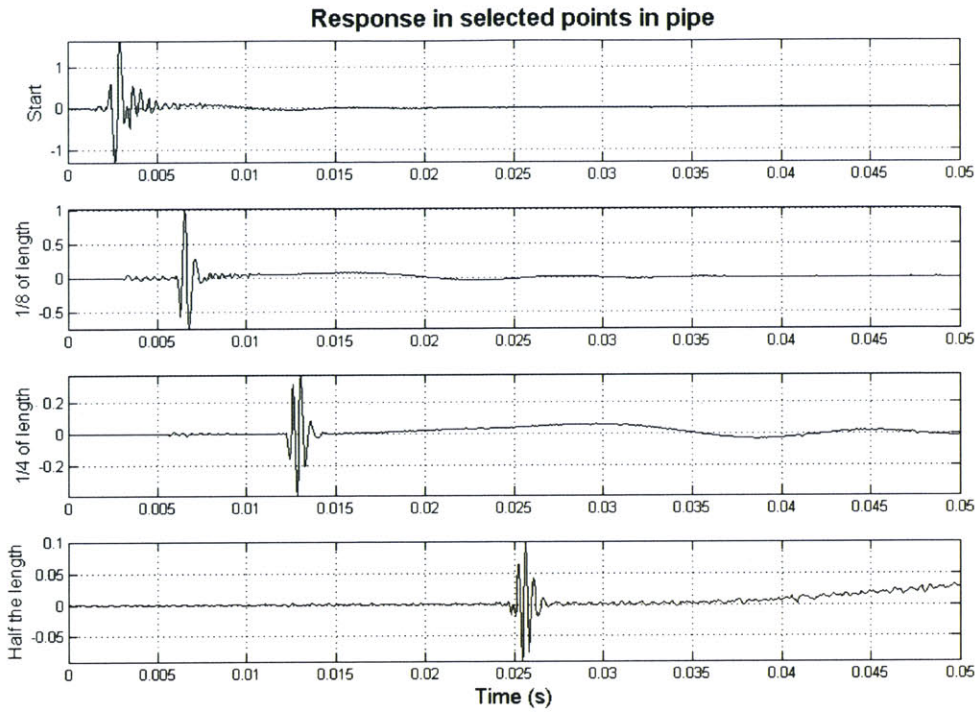

Figure 6.64: Pressure in selected points in a concrete 5cm thick pipe (0.5ms pulse)

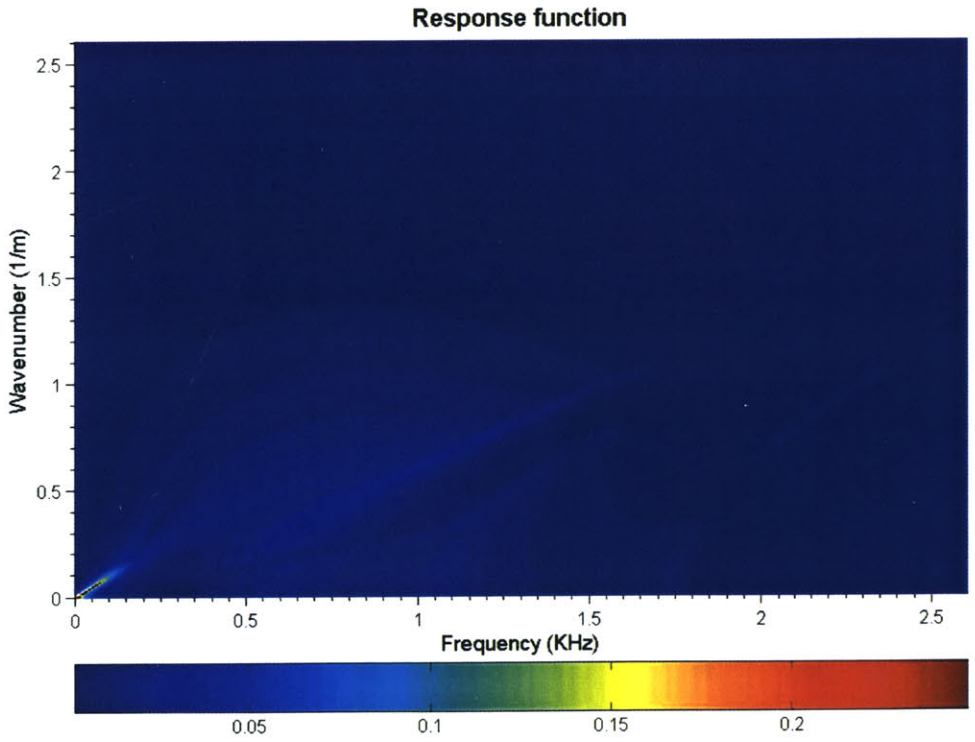

Figure 6.65: Response function of a concrete 15cm thick pipe (1ms pulse)

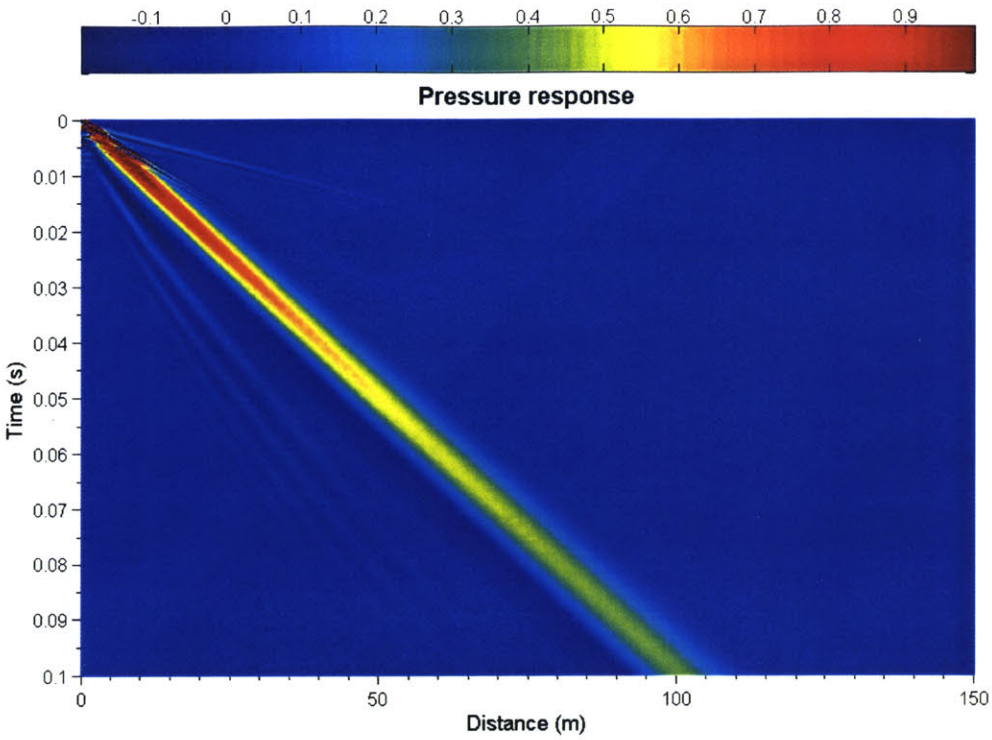

Figure 6.66: Pressure distribution of a concrete 15cm thick pipe (1ms pulse)

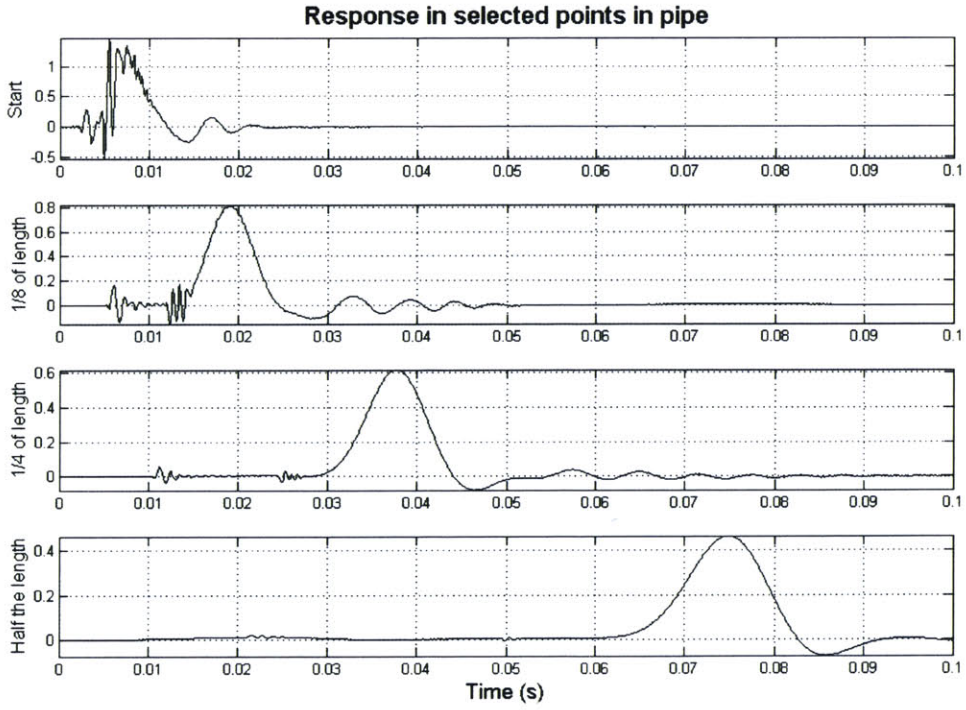

Figure 6.67: Pressure in selected points in a concrete 15cm thick pipe (1ms pulse)

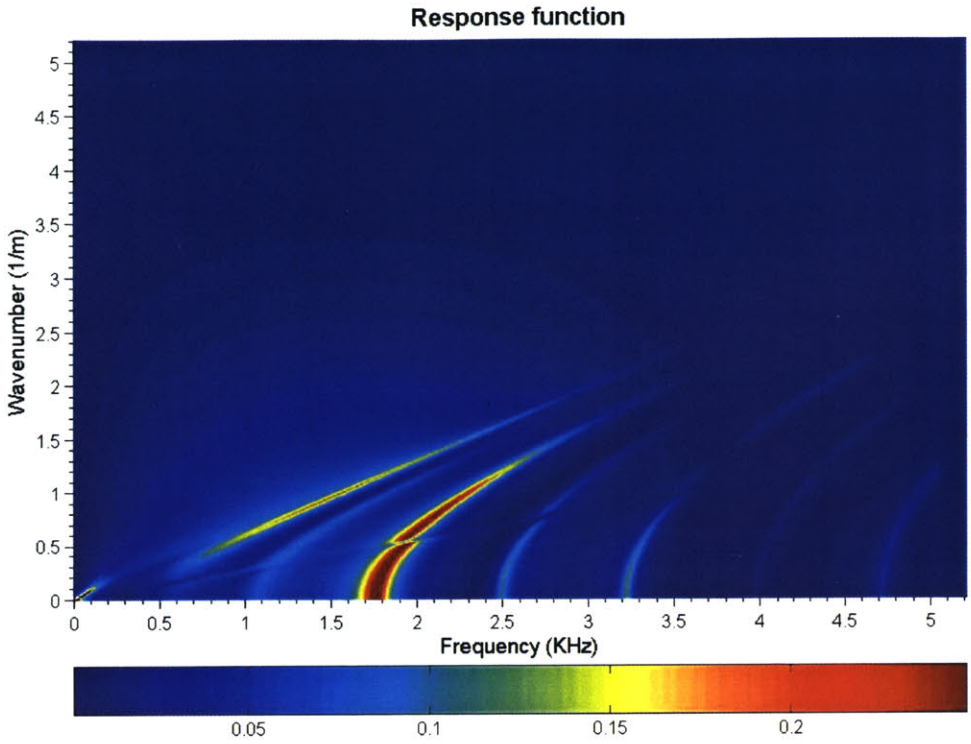

Figure 6.68: Response function of a concrete 15cm thick pipe (0.5ms pulse)

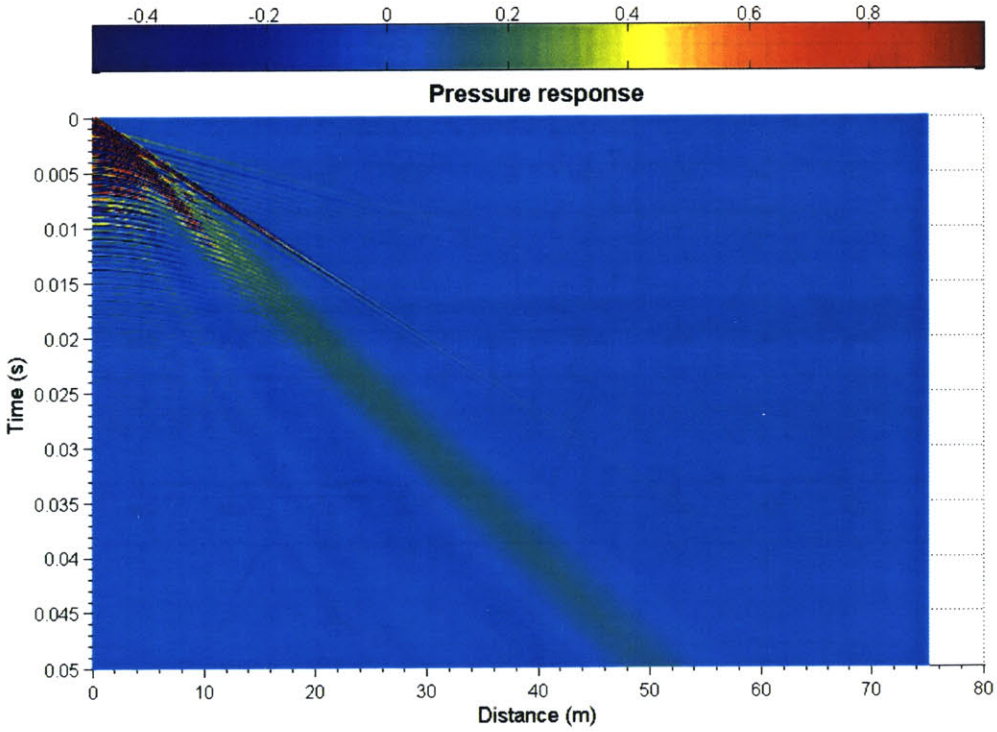

Figure 6.69: Pressure distribution of a concrete 15cm thick pipe (0.5ms pulse)

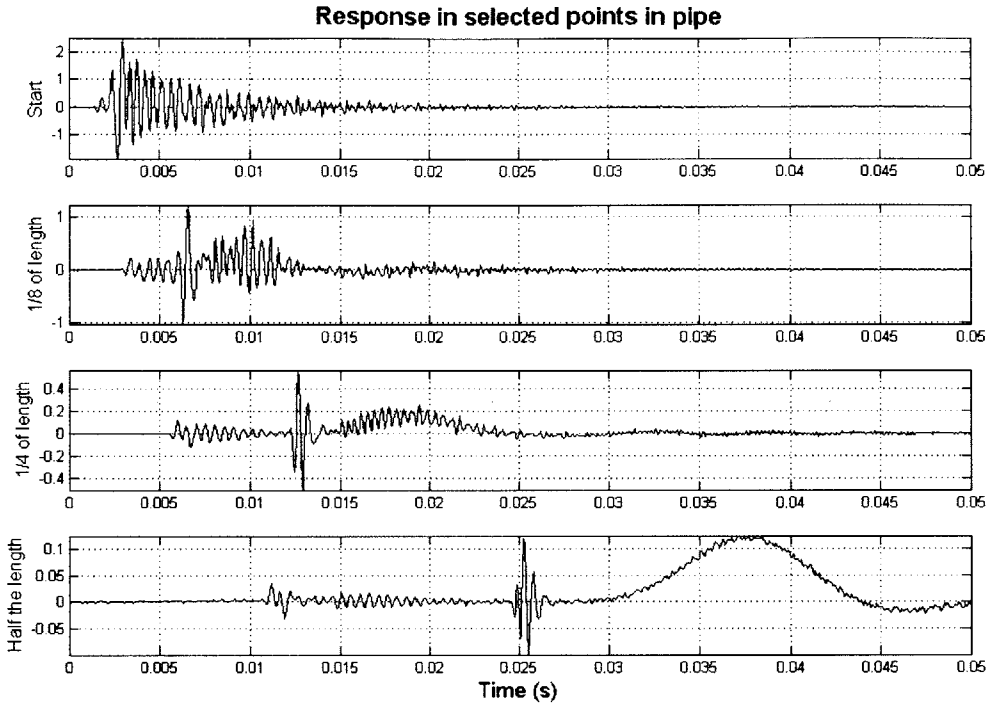

Figure 6.70: Pressure in selected points in a concrete 15cm thick pipe (0.5ms pulse)

This set of analysis showed that when the pipe stiffness approaches the stiffness of the water (5cm pipe), the system attenuation increases substantially, due to the coupling of the pipe and the water and due to the higher overall damping ratio, since the pipe deforms much more and takes up much more of the overall energy. However, if the pipe has substantial stiffness (15cm pipe), the overall response resembles the base case.

Running the same analysis with a higher stiffness pipe (c_p=10Km/s, ρ=7.85t/m^3) will result in the solution that resembles more the one for the rigid pipe, as it can be seen by the following graphs:

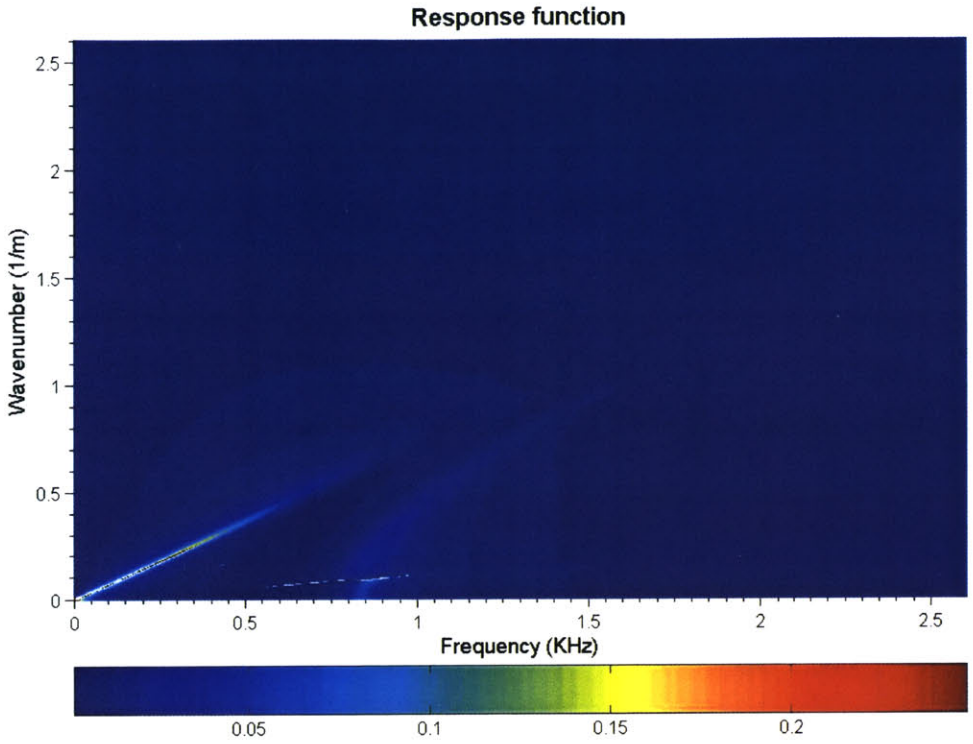

Figure 6.71: Response function of a high stiffness steel pipe (1ms pulse)

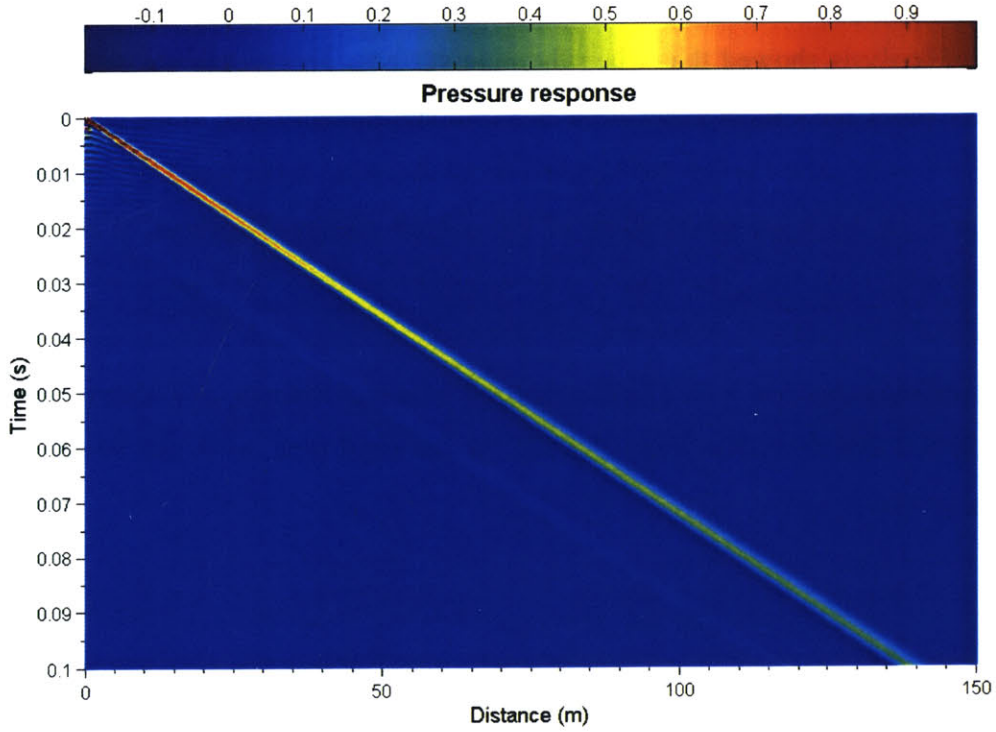

Figure 6.72: Pressure distribution of a high stiffness steel pipe (1ms pulse)

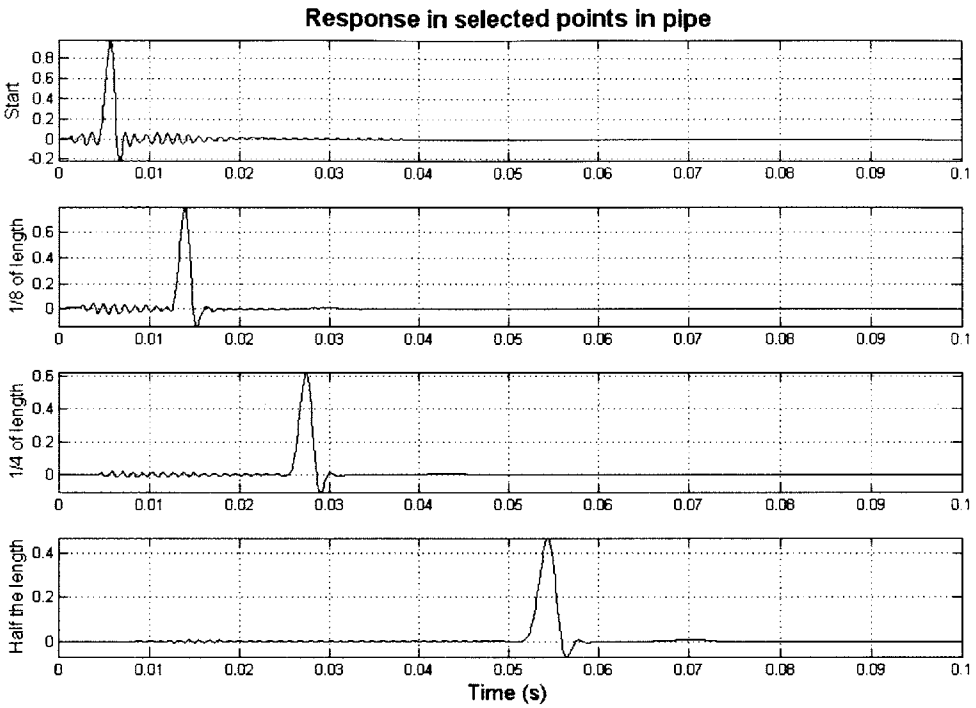

Figure 6.73: Pressures in selected points in a high stiffness steel pipe (1ms pulse)

Effect of soil stiffness

Given that the properties of the soil cannot be known with the same accuracy as the ones relating to the pipe's material due to many kinds of uncertainties, it is interesting to see in what extent these properties affect the solution and if it is worthwhile to investigate them. The first set of analysis will deal with the extreme case of a soil without any significant stiffness (c_p=10m/s, ρ=1.1t/m^3) or equivalently the case where there is no other medium surrounding the pipe. The following graphs show substantial difference between this case and the base case, although White's formula gave a tube wave velocity very similar to the base case one. The response function graphs (figures 6.74 and 6.77) show difference in the characteristic frequencies between the base case and the case of a low stiffness surrounding soil. Given these differences, one can expect that the response of the system is very different.

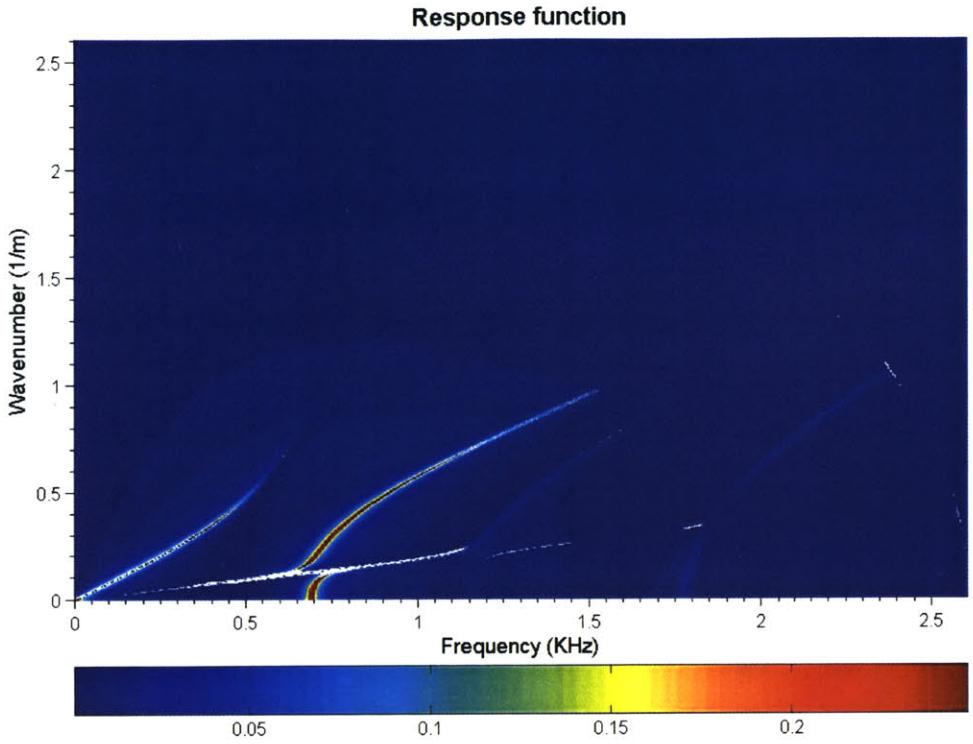

Figure 6.74: Response function of a low stiffness soil (1ms pulse)

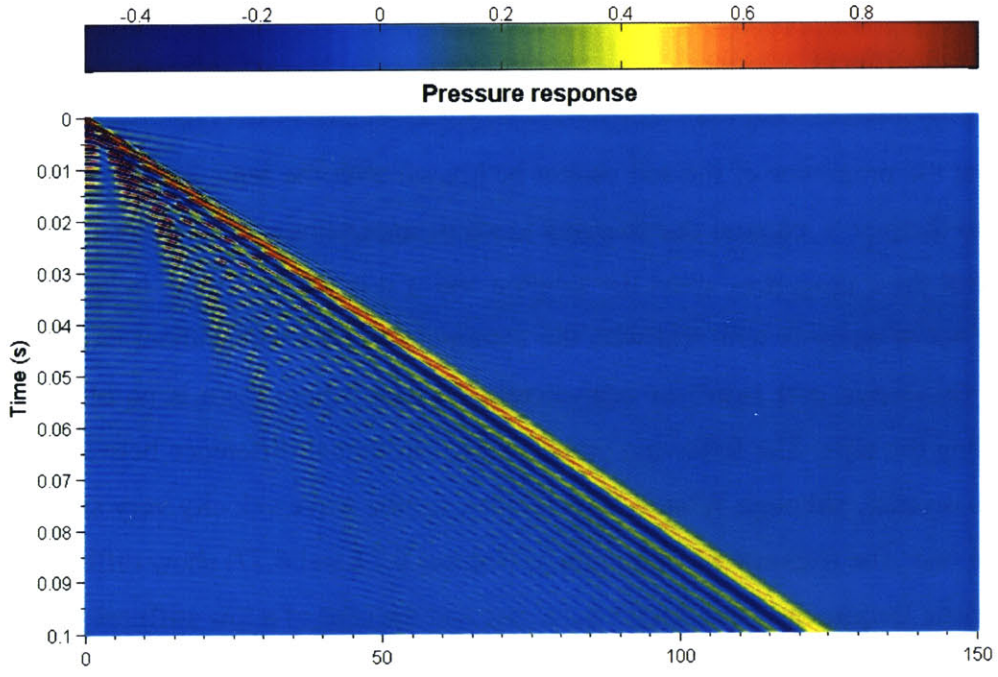

Figure 6.75: Pressure distribution for a very low stiffness soil (1ms pulse)

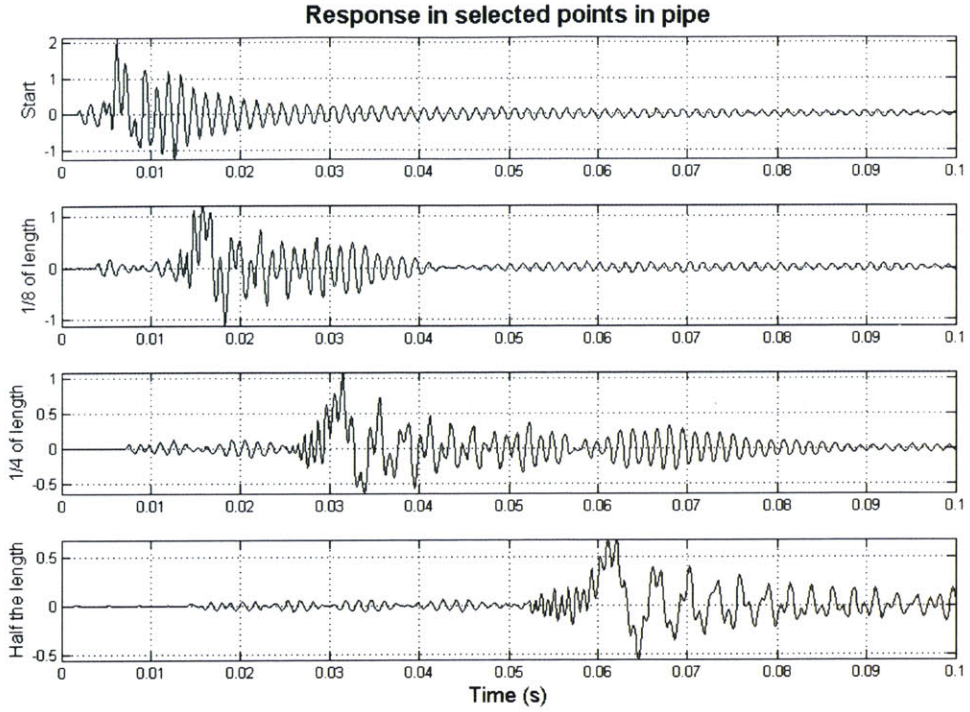

Figure 6.76: Pressures in selected points in pipe for a low stiffness soil (1ms pulse)

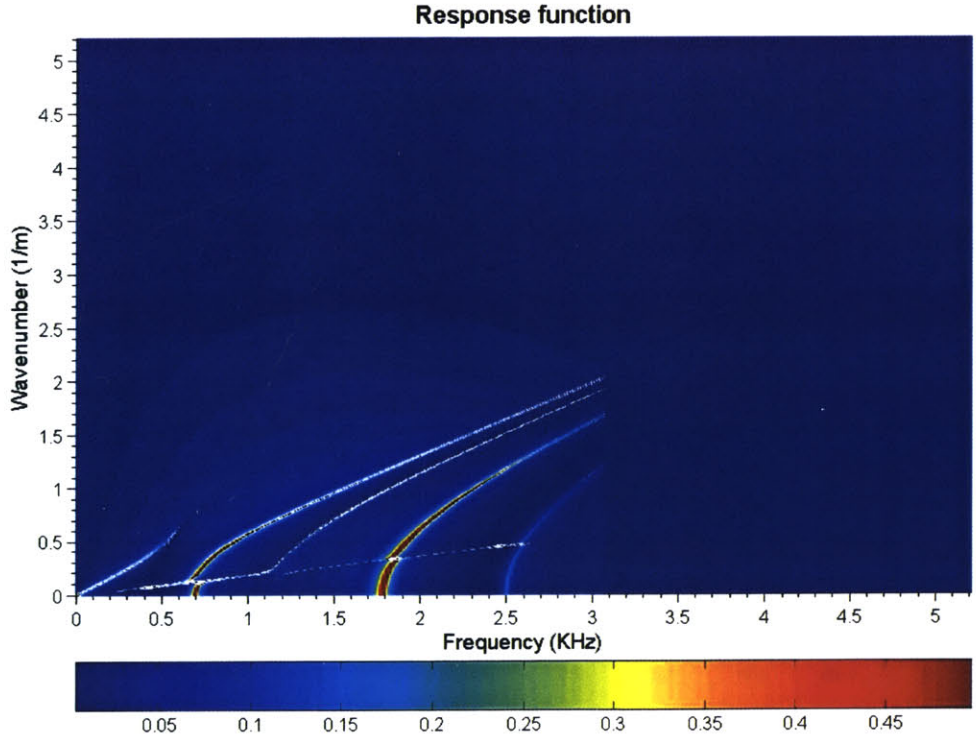

Figure 6.77: Response function for a low stiffness soil (0.5ms pulse)

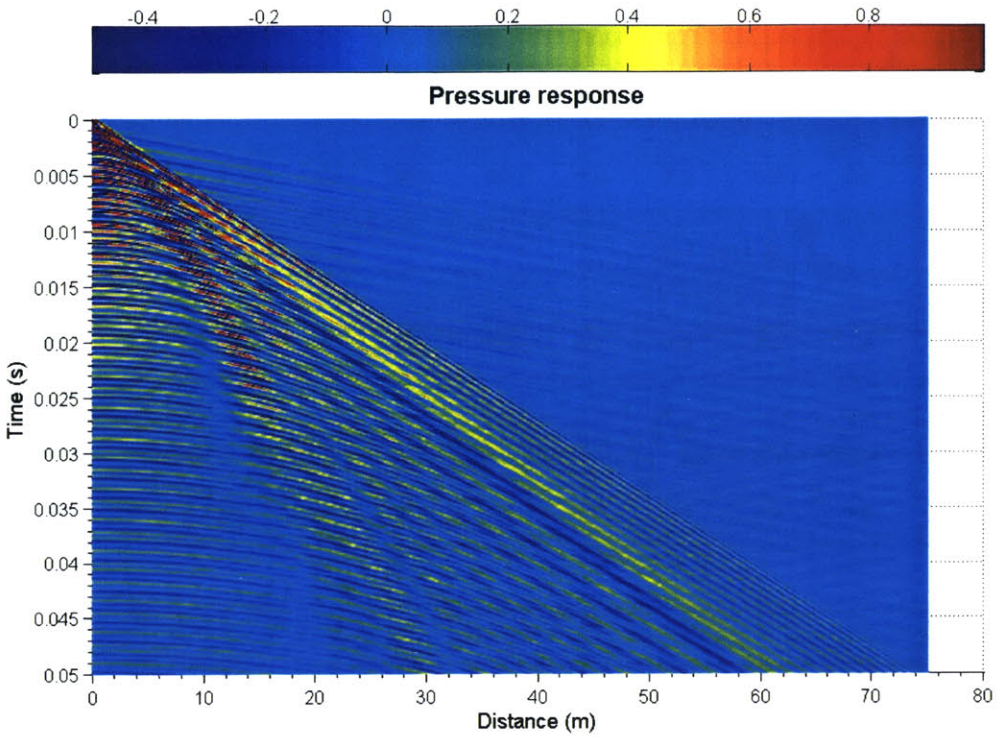

Figure 6.78: Pressure distribution for a low stiffness soil (0.5ms pulse)

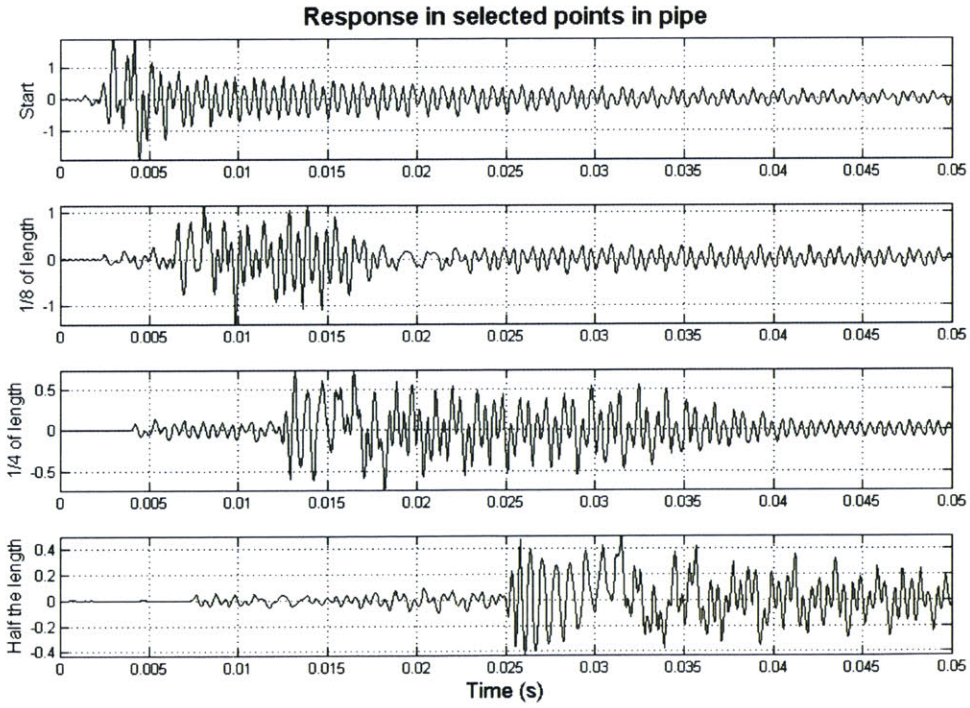

Figure 6.79: Pressures in selected points in pipe for a low stiffness soil (0.5ms pulse)

In the case of a very stiff soil (c_p=2Km/s, ρ=2.5 t/m^3), White's formula predicts the base case results. However, an interesting case would be the existence of a very stiff soil around a low stiffness concrete pipe. A concrete pipe of 1m radius and 5 cm thickness and a soil with a c_p of 2Km/s give the following results:

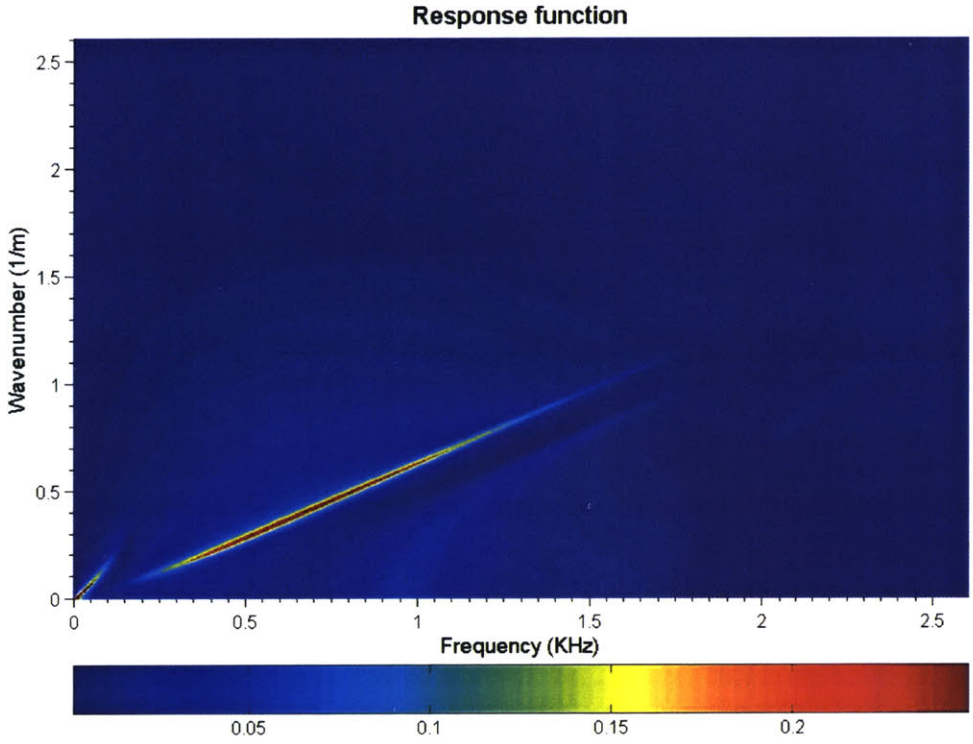

Figure 6.80: Response function for a very stiff soil (1ms pulse)

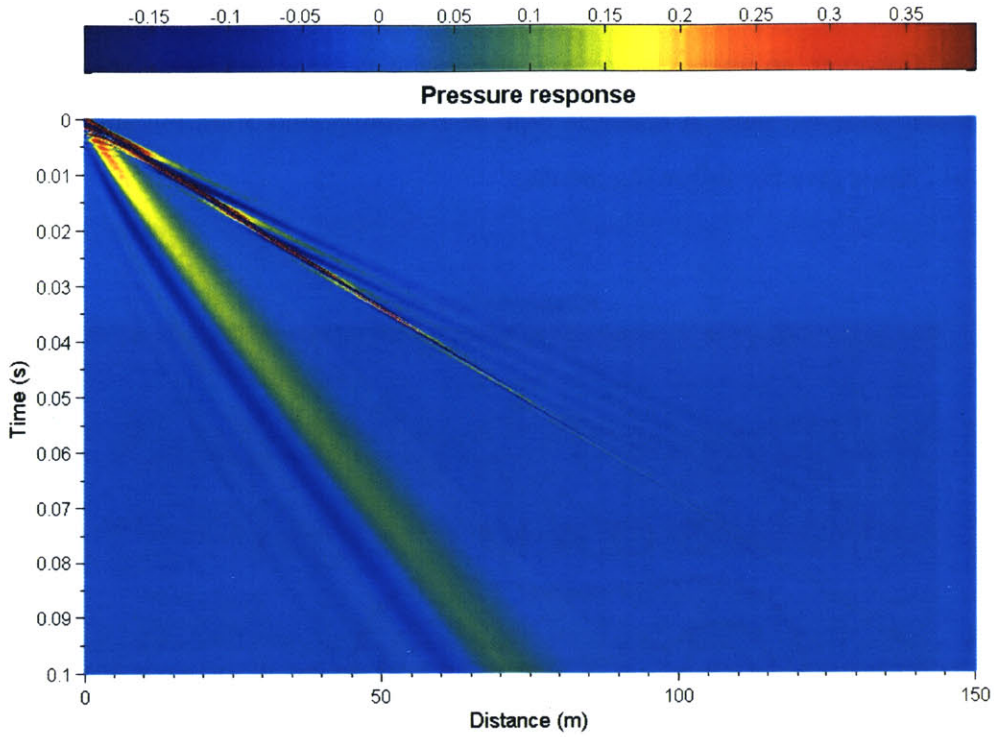

Figure 6.81: Pressure distribution for a very stiff soil (1ms pulse)

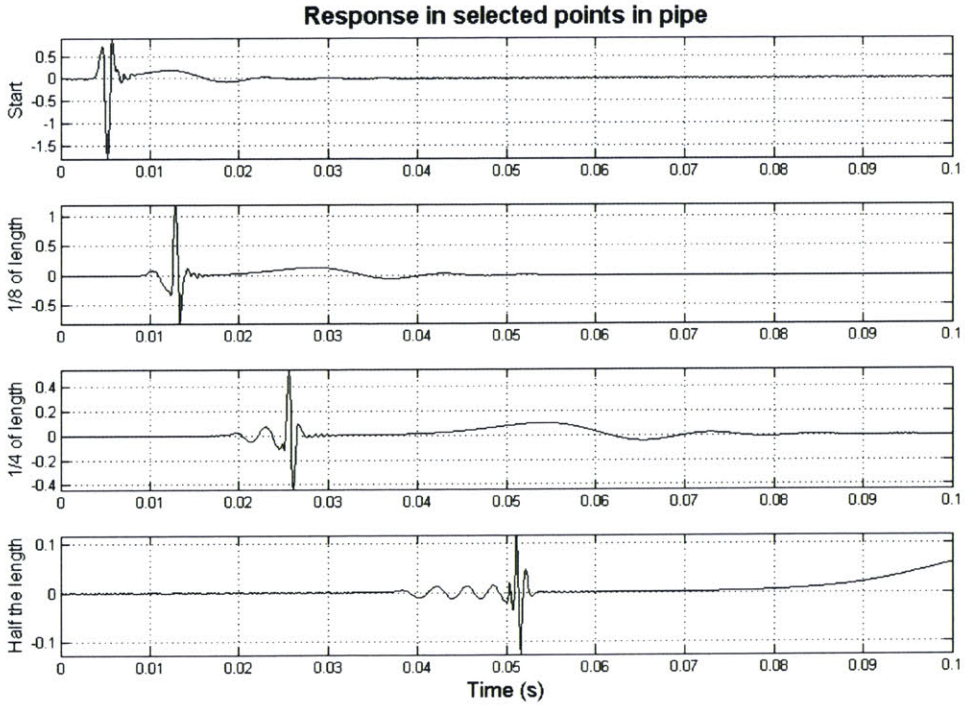

Figure 6.82: Pressures in selected points in pipe for a very stiff soil (1ms pulse)

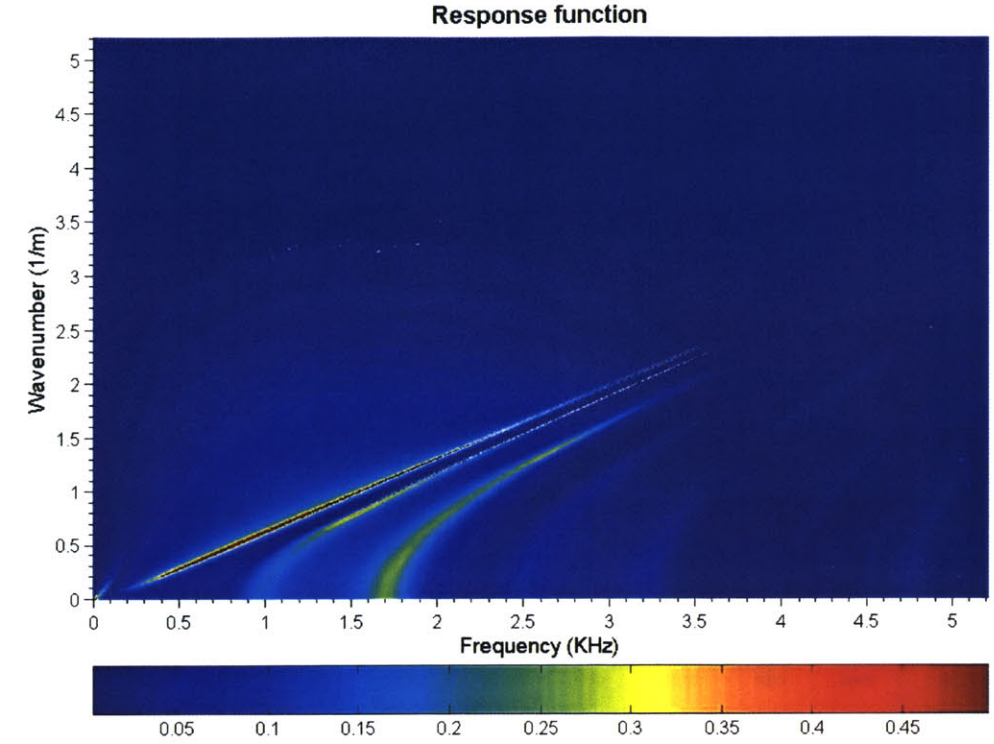

Figure 6.83: Response function for a very stiff soil (0.5ms pulse)

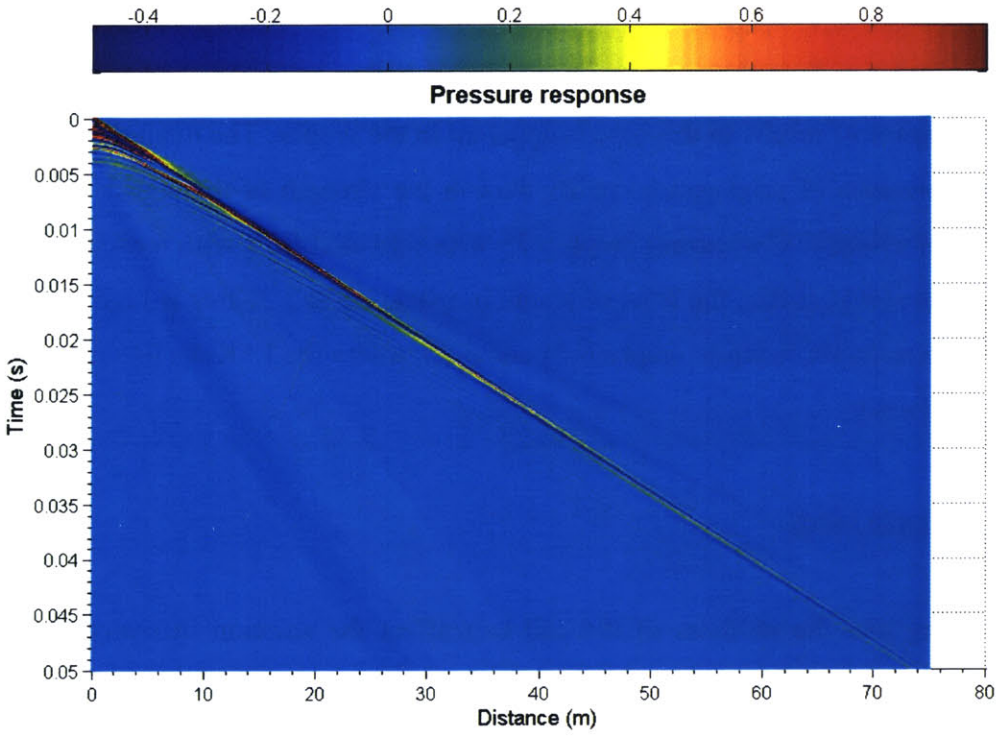

Figure 6.84: Pressure distribution for a very stiff soil (0.5ms pulse)

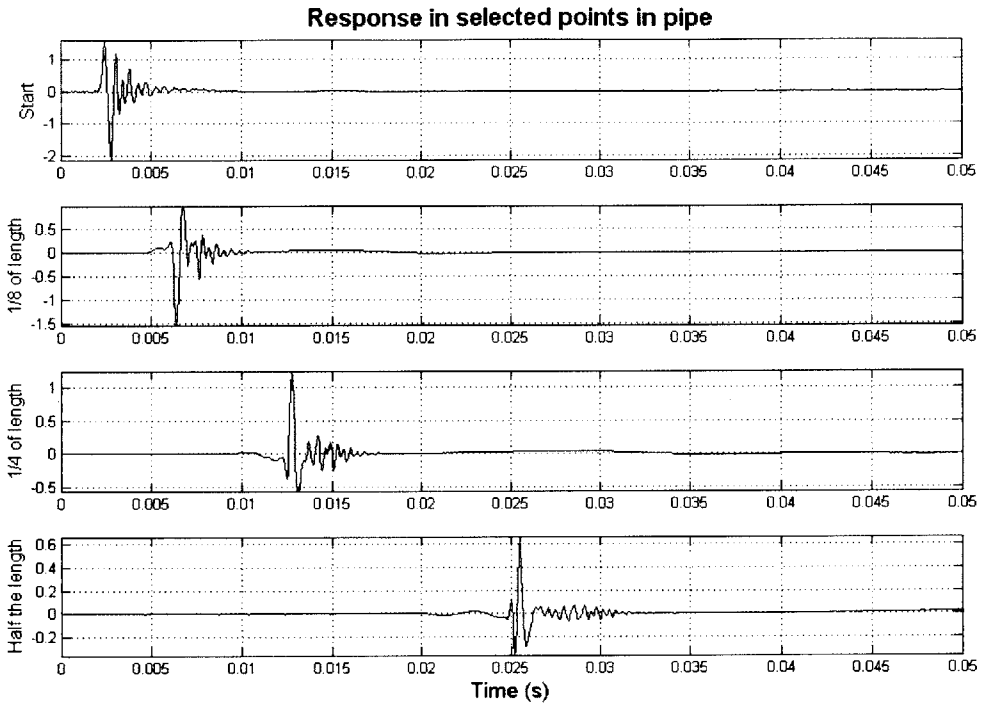

Figure 6.85: Pressures in selected points in pipe for a very stiff soil (0.5ms pulse)

For this case White's formula predicted a wave speed different that the one of the base case, and the difference of results in this case is apparent in the graphs. The main differences are not in the velocities of propagation, rather than in the strength of the signal propagating with the fluid velocity. Comparing graph 6.75 with 6.81 and 6.78 with 6.84, one can see that, when the soil is stiffer, the level of sound propagating at 1.5Km/s is higher. This can be seen in the response function graphs 6.74 and 6.80, where the 1.5Km/s line is stronger in the stiffer soil case.

Effect of damping ratios

After showing that the stiffness of the soil can affect the solution in many cases it is interesting to see if its substantially higher damping ratio (in relation to the pipe's material) can reduce the noise levels in the pipe. For this case the soil will be considered to have a high damping ratio of 10%. The system will be excited by a high frequency excitation of 0.5ms.

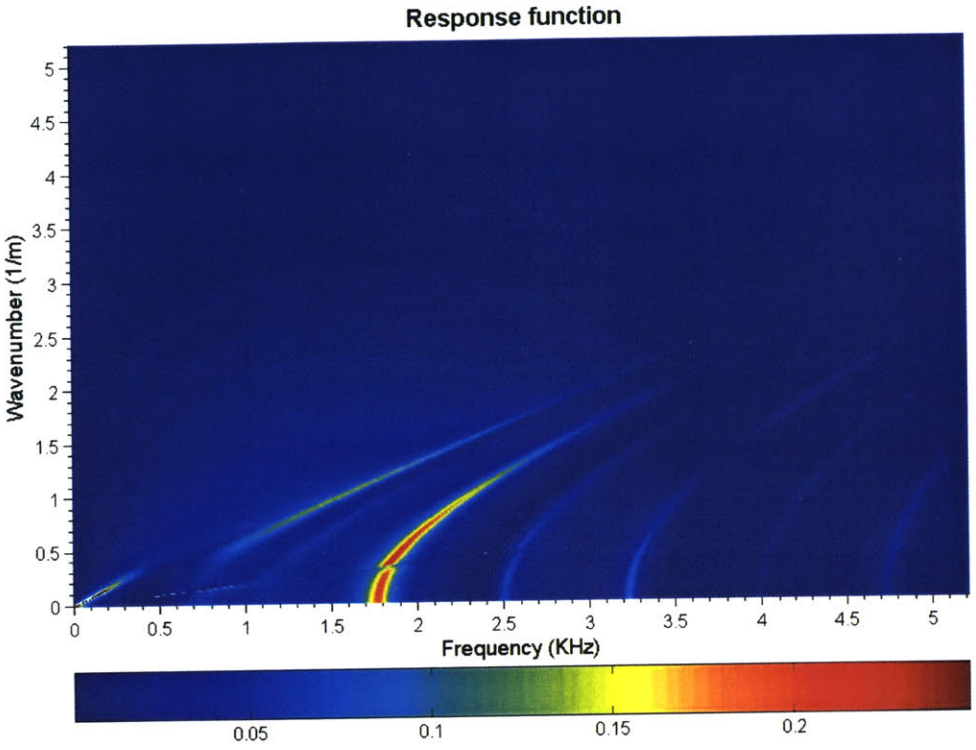

Figure 6.86: Response function for a soil with high damping ratio (0.5ms pulse)

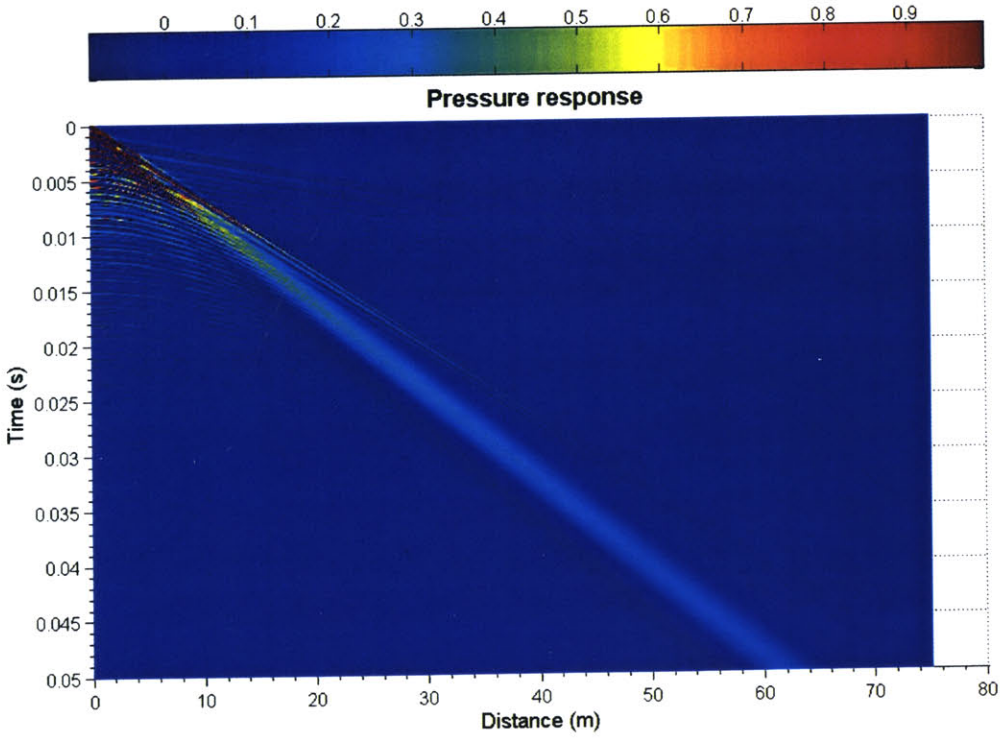

Figure 6.87: Pressure distribution for a soil with high damping ratio (0.5ms pulse)

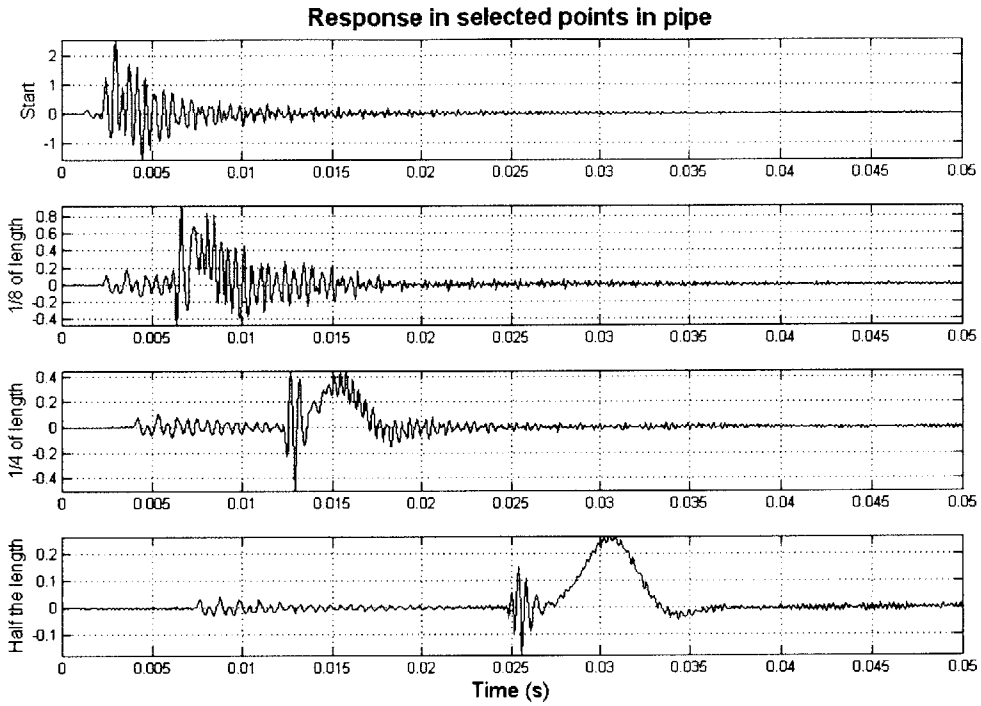

Figure 6.88: Pressures in selected points for a soil with high damping ratio (0.5ms pulse)

As it was expected, the damping ratio of the soil cannot reduce the noise reverberations in the pipe, since the pipe and the water mainly receive the stresses applied by the transmitter. So, the only means of reducing the noise due to higher attenuation levels is the damping of the pipe's material. Higher damping of the steel pipe (5%) leads to some noise reduction, especially from the higher modes and the waves traveling with high speed (higher than 1.5Km/s), as it can be seen in the following diagrams:

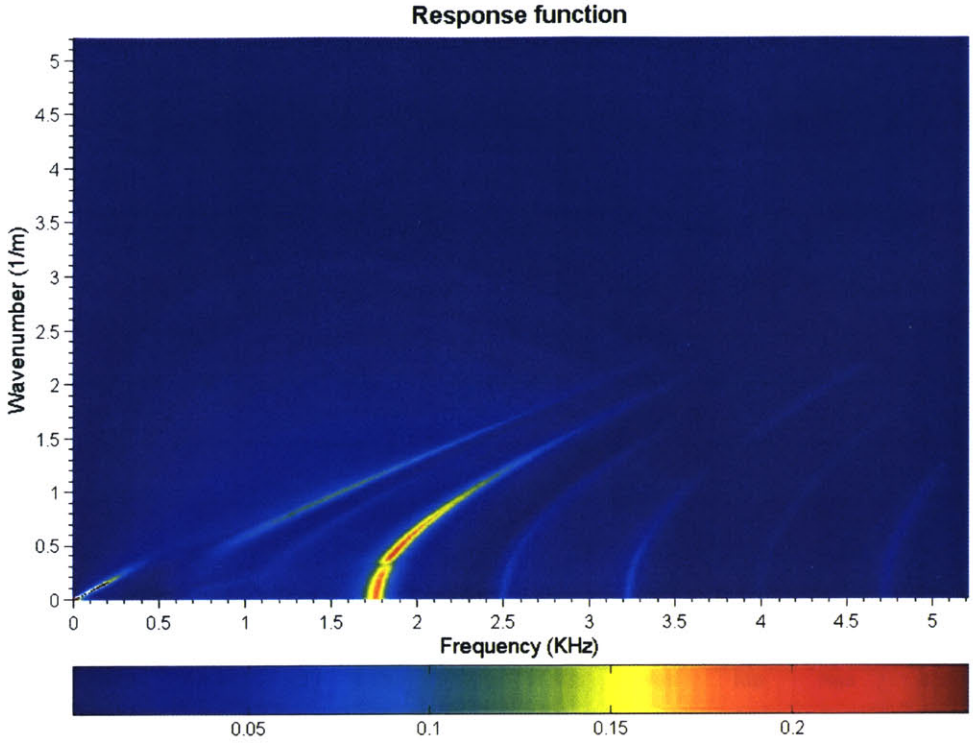

Figure 6.89: Response function for a steel pipe with high damping ratio (0.5ms pulse)

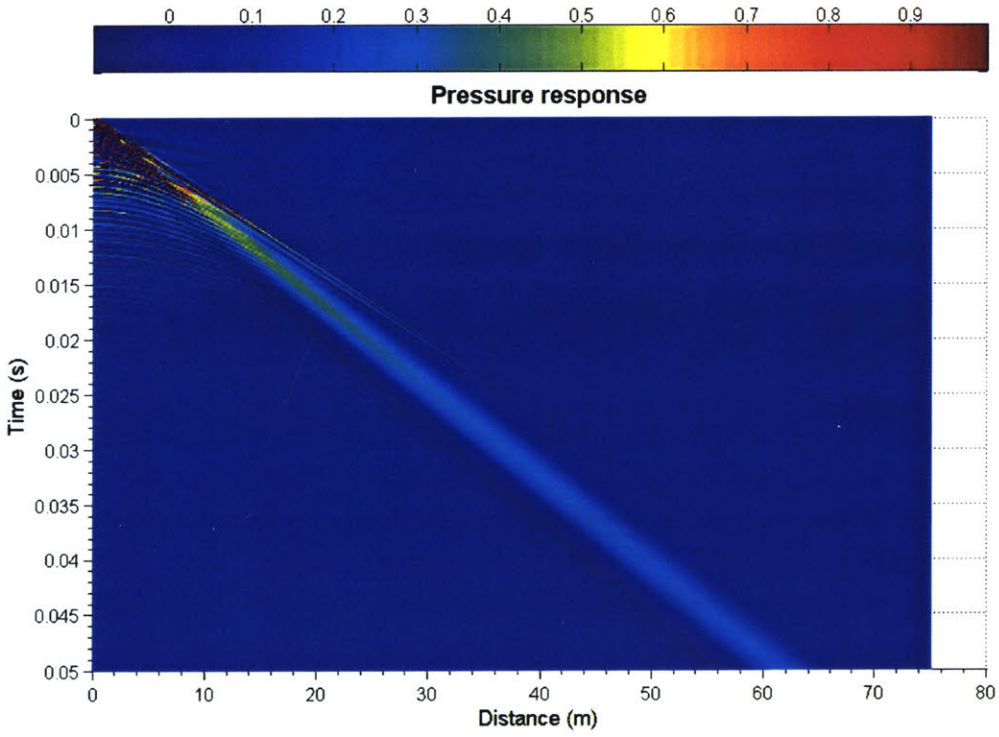

Figure 6.90: Pressure distribution for a steel pipe with high damping ratio (0.5ms pulse)

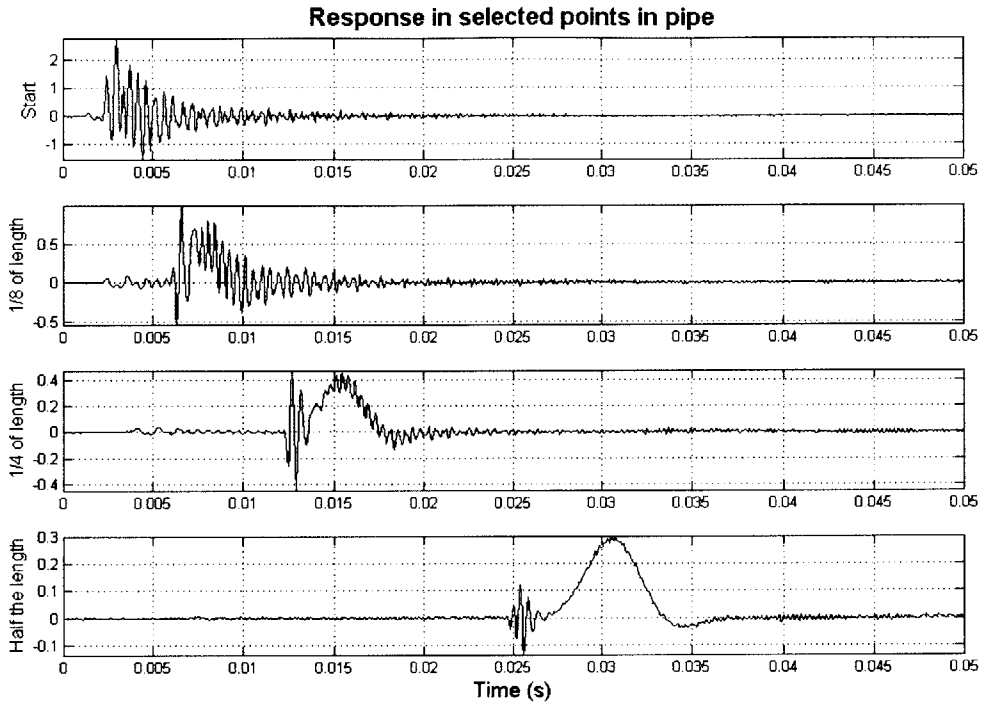

Figure 6.89: Pressures in selected points in a high damping ratio, steel pipe (0.5ms pulse)

6.7 Conclusions

The stiffness matrix approach used to solve the acoustic wave propagation problem in any cylindrically layered system was proven to be accurate in many simplified cases and at the same time very useful in cases where there is no easy analytical solution. The method was used to simulate a variety of real life and extreme system layout cases and many important facts were established.

First, the nature of the excitation is very crucial to the need of a complete analysis versus a simplified one. Using a simple check formula of $\frac{L}{t_0} \leq \frac{\omega_{01}}{2\pi} = \frac{z_{01} c_f}{2\pi R}$ (low frequency excitation), it can be decided if a complete analysis is needed, or if the system can be modeled a stiff pipe/simplified case. At the same time, the stiffness of the pipe was proven to be very important to the overall system stiffness, in contrast to the properties of the soil, which were shown not to play a significant role in a steel pipe case. Consequently, there is

no need for high accuracy in the estimation of the soil parameters, when the pipe stiffness is the one that defines the overall rigidity of the surrounding media. On the other hand, in the case of the concrete pipe of lower rigidity soil played an important role in the final response, even when the tube wave velocity was approximately the same between the various cases. Analogous conclusions were drawn for the damping ratio of the pipe and the soil. A general note would be that, although one can calculate the main signal wave speed in the pipe ("zero" mode) with absolute accuracy, it is very difficult to predict the noise level of the signal, since it is defined by the characteristic frequencies of the system, which are difficult to calculate analytically for an arbitrary layout.

The radius of the pipe was also shown to have a very significant effect on the noise due to higher mode propagation in the pipe. As it was expected from the analytical solution of the simplified case, the radius of the pipe is inversely related to the cut-off frequencies of the higher modes and consequently to the number of modes propagating in the pipe. This fact means that in low radius pipes (lower than 1m) the signal propagates with lower noise and for higher distances.

In general, the main parameters that affect the wave propagation in the pipe were investigated and easy to use criteria for choosing a complete or a simplified method of analysis were established. Given these criteria, a generalized way of dealing with the wave propagation problem in any cylindrically layered media can be established. This decision-making process will be presented in the next chapter, along with the final conclusions. As a final note one can say that a set of realistic values will probably demand a complete analysis in order to give accurate results, as shown in the base case of chapter 6.6.

7. Conclusions

7.1 Simplified analysis versus complete analysis

As it was seen in chapter 6, based on the simplified method of chapter 4, the results of the complete analysis versus the more elaborate, complete one are in absolute match when the pipe is much stiffer than the fluid. Moreover, based on White's approximation of the total stiffness of the system, an equivalent tube speed can be calculated, so that the simplified analysis can be used for low frequency and wavenumber excitations with the same results.

However, it was clearly shown that for average realistic properties of the soil and the pipe's size and material, the approximation of a "stiff boundary" is not accurate. At the same time, the source size and the required frequency of information transmission produce a signal that is not of low frequency or low wavenumber. Given these realistic constraints, one is probably bound to have errors when using the simplified analysis in a real value problem.

The next chapter will present the decision-making tools on where to use the simplified analysis of the wave propagation in the pipe and any cylindrically layered system in general, given the properties of the real life problem.

7.2 Proposed method of analysis

The following chart provides a quick way of deciding on a simplified or complete analysis of the wave propagation problem in the pipe, or any other surrounding medium (or media). Using this diagram, one only has to investigate and decide only on the absolutely required parameters of the problem. The use of this chart is not limited, however, to a three-layered media system. It can be used to decide on the optimal analysis for any kind of system, as the complete analysis is not limited to any number of layers.

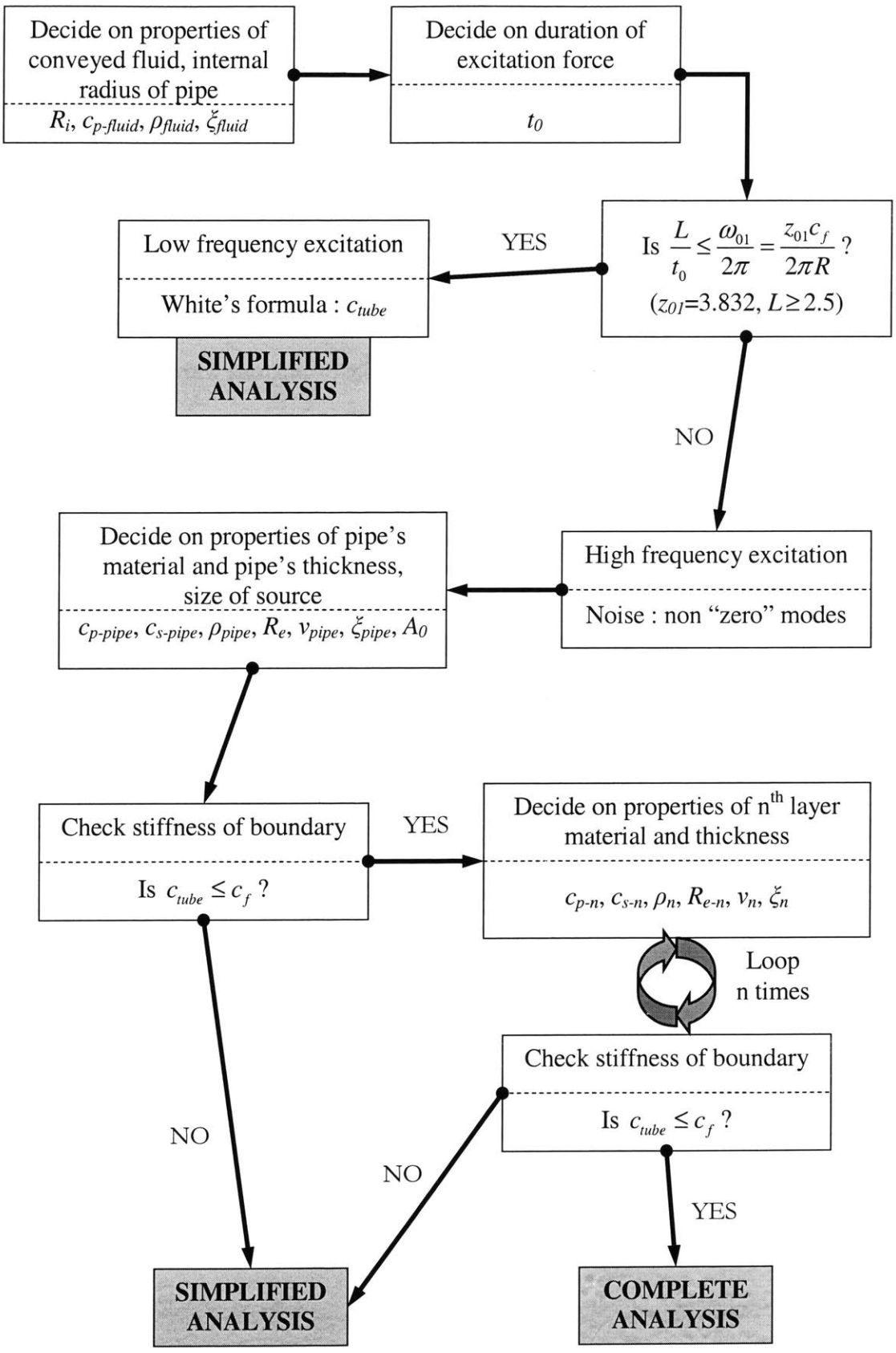

Chart 7.1: Decision-making diagram for analysis method

7.3 Future research

This thesis presented a comprehensive way of dealing with the problem of acoustic wave propagation in cylindrically layered systems for any kind of excitation and layout of the system. However, the properties of the system were considered not varying with the azimuth (θ angle) or the level of deformation. At the same time, only cases with axisymmetric loading were presented, because of the high level of calculations needed in any other case. Consequently, future research can be targeted on solving the problem, without taking into account these approximations, but mainly on how to make the computational level lower, in order to take into account any kind of loading.

Moreover, since the scope of this thesis was to develop a complete and time-efficient method of analysis, the properties of the wave propagation in the pipe under any layout were studied only briefly. Future research can be targeted on evaluating the results if the method with experiments (actual scale or smaller) and dealing with many more cases of cylindrically layered media, as various types of boreholes or pipes that lie under the sea.

At the same time, the beam forming method could be studied more in an analytical and experimental level to develop noise reduction systems for any kind of loading and system layout. Based on that, one could develop systems of constant information feed with constant emitting of sound data uncontaminated by noise, based on the theoretical predictions of the complete model.

Appendix A: Stiffness matrix tables

Table 1: Stiffness matrix for cylindrical layers

$1 \rightarrow$ outer surface , $2 \rightarrow$ inner surface
See Tables 2, 3 for the definition of the element matrices used below

$$\mathbf{K} = \begin{Bmatrix} r_1 \mathbf{F}_1^{(1)} & r_1 \mathbf{F}_1^{(2)} \\ -r_2 \mathbf{F}_2^{(1)} & -r_2 \mathbf{F}_2^{(2)} \end{Bmatrix} \begin{Bmatrix} \mathbf{J}_1 & \mathbf{Y}_1 \\ \mathbf{J}_2 & \mathbf{Y}_2 \end{Bmatrix}^{-1} \quad \text{Single layer}$$

$$\mathbf{K}_{ext} = -r\,\mathbf{F}\,\mathbf{H}^{-1} \quad \text{Unbounded exterior region}$$

$$\mathbf{K}_{core} = r_1 \mathbf{F}_1^{(1)} \mathbf{J}_1^{-1} \quad \text{Solid core of radius } r_1 \ (r_2 = 0)$$

Table 2
Matrices for displacements in cylindrical layers

$$k_P = \omega/\alpha \qquad k_S = \omega/\beta$$

$$k_\alpha = \sqrt{k_P^2 - k_z^2} \qquad k_\beta = \sqrt{k_S^2 - k_z^2}$$

$$\mathbf{J} = \begin{Bmatrix} J'_{\alpha n} & n\dfrac{J_{\beta n}}{k_\beta r} & \dfrac{k_z}{k_\beta} J'_{\beta n} \\ n\dfrac{J_{\alpha n}}{k_\alpha r} & J'_{\beta n} & n\dfrac{k_z}{k_\beta}\dfrac{J_{\beta n}}{k_\beta r} \\ -\dfrac{k_z}{k_\alpha} J_{\alpha n} & 0 & J_{\beta n} \end{Bmatrix} \qquad \mathbf{Y} = \begin{Bmatrix} Y'_{\alpha n} & n\dfrac{Y_{\beta n}}{k_\beta r} & \dfrac{k_z}{k_\beta} Y'_{\beta n} \\ n\dfrac{Y_{\alpha n}}{k_\alpha r} & Y'_{\beta n} & n\dfrac{k_z}{k_\beta}\dfrac{Y_{\beta n}}{k_\beta r} \\ -\dfrac{k_z}{k_\alpha} Y_{\alpha n} & 0 & Y_{\beta n} \end{Bmatrix}$$

$$\mathbf{H} = \begin{Bmatrix} H'_{\alpha n} & n\dfrac{H_{\beta n}}{k_\beta r} & \dfrac{k_z}{k_\beta} H'_{\beta n} \\ n\dfrac{H_{\alpha n}}{k_\alpha r} & H'_{\beta n} & n\dfrac{k_z}{k_\beta}\dfrac{H_{\beta n}}{k_\beta r} \\ -\dfrac{k_z}{k_\alpha} H_{\alpha n} & 0 & H_{\beta n} \end{Bmatrix}$$

$$J_{\alpha n} = J_n(k_\alpha r) \qquad J_{\beta n} = J_n(k_\beta r)$$

$$Y_{\alpha n} = Y_n(k_\alpha r) \qquad Y_{\beta n} = Y_n(k_\beta r)$$

$$H_{\alpha n} = H_n^{(2)}(k_\alpha r) \qquad H_{\beta n} = H_n^{(2)}(k_\beta r)$$

$$H'_{\alpha n} = \frac{dH_{\alpha n}}{d(k_\alpha r)} \qquad H'_{\beta n} = \frac{dH_{\beta n}}{d(k_\beta r)} \quad \text{etc.}$$

$$\mathbf{T}_n = \mathbf{diag}\begin{bmatrix} \cos n\theta & -\sin n\theta & \cos n\theta \end{bmatrix} \text{ or } \mathbf{T}_n = \mathbf{diag}\begin{bmatrix} \sin n\theta & \cos n\theta & \sin n\theta \end{bmatrix}$$

Table 3
Elements of matrices for stresses in cylindrical surfaces

$$\mathbf{F}=\left\{f_{ij}(H_{\alpha n},H_{\beta n})\right\} \qquad \mathbf{F}^{(1)}=\left\{f_{ij}(J_{\alpha n},J_{\beta n})\right\} \qquad \mathbf{F}^{(2)}=\left\{f_{ij}(Y_{\alpha n},Y_{\beta n})\right\}$$

in which $H_{\alpha n}$ etc. are the same as in table 2. We list below only the elements of $\mathbf{F}$. To obtain the elements of $\mathbf{F}^{(1)},\mathbf{F}^{(2)}$, replace the $H_{\alpha n},H_{\beta n}$ functions by $J_{\alpha n},J_{\beta n}$ or $Y_{\alpha n},Y_{\beta n}$, as appropriate.

$$f_{11}=-k_\alpha\left\{\lambda\left[1+\left(\frac{k_z}{k_\alpha}\right)^2\right]H_{\alpha n}+2\mu\left[\frac{H'_{\alpha n}}{k_\alpha r}+\left(1-\left(\frac{n}{k_\alpha r}\right)^2\right)H_{\alpha n}\right]\right\}$$

$$f_{12}=\frac{2n\mu}{r}\left(H'_{\beta n}-\frac{H_{\beta n}}{k_\beta r}\right)$$

$$f_{13}=-2k_z\mu\left\{\frac{H'_{\beta n}}{k_\beta r}+\left[1-\left(\frac{n}{k_\beta r}\right)^2\right]H_{\beta n}\right\}$$

$$f_{21}=\frac{2n\mu}{r}\left[H'_{\alpha n}-\frac{H_{\alpha n}}{k_\alpha r}\right]$$

$$f_{22}=-k_\beta\,\mu\left[2\frac{H'_{\beta n}}{k_\beta r}+\left(1-2\left(\frac{n}{k_\beta r}\right)^2\right)H_{\beta n}\right]$$

$$f_{23}=k_z\frac{2n\,\mu}{k_\beta r}\left[H'_{\beta n}-\frac{H_{\beta n}}{k_\beta r}\right]$$

$$f_{31}=-2k_z\,\mu H'_{\alpha n}$$

$$f_{32}=-k_z n\,\mu\frac{H_{\beta n}}{k_\beta r}$$

$$f_{33}=k_\beta\mu\left[1-\left(\frac{k_z}{k_\beta}\right)^2\right]H'_{\beta n}$$

Appendix B: Symbols Index

ϕ	Velocity Potential
r	Radial distance
t	Time
θ	Azimuth
z	Distance on pipe axis
c	Velocity of sound waves
J	Bessel function of first kind
Y	Bessel function of second kind
H^i	Hankel function of the i kind (i=1,2)
k,k_z	Axial wavenumber
k_a	Bessel function compressional wavenumber
k_0,k_p	Wavenumber of compressional waves
n	Order of wave
j	Order of Bessel function
k_{nj}	Rigid pipe wavenumbers (of j^{th} Bessel function and n^{th} wave order)
S	Strength of source
z_{nj}	Roots of $J_n(x)=0$
z'_{nj}	Roots of $J_n'(x)=0$
ω_{nj}	n^{th} cut-off frequency for j^{th} order Bessel function
η	Artificial damping ratio of the EWM
p	Pressure
Δt_0	Delay of pulse excitation
z_0	Spacing of sources in beam forming
N_l	Number of interfaces in the cylindrically layered system
R,R_c	Pipe internal radius
u	Displacement
u_r	Radial displacement
u_θ	Azimuthial displacement

u_z	Axial displacement
K ,**K**	Stiffness – Stiffness matrix
σ	Stress
σ_{system}	Stresses along the external to the fluid system
K_{system}	Stiffness matrix of the external to the fluid system
u_{system}	Displacements of the external to the fluid system
K_{ext}	Stiffness matrix of external infinite medium
u_{1r}	Axial displacement at radial distance, where pressures need to be calculated
σ_{1r}	Axial stress applied from the external to the fluid system
p^*	Pressure at $r=R_c$ caused by a source in an infinitely extending fluid
u_r^*	Displacement at $r=R_c$ cause by a source in an infinitely extending fluid
K_{ii}	Stiffness components relating stresses and displacements of the same DOF
K_{ij}	Stiffness components relating stresses and displacements of different DOFs
K_{fe}	Infinitely extending fluid region stiffness
K_{fi}	Fluid core stiffness
K_{cons}	Consolidated matrix around u_{1r}
k_s	Wavenumber of compressional waves
k_β	Bessel function shear wavenumber
α, c_p	Compressional wave velocity (P waves)
β, c_s	Shear wave velocity (S waves)
U,D,V	Matrix decomposition components
f_{ij}	Components of the stress matrix
x	Space
t_0	Total duration of impulse in pipe
A_0	Total area of impulse generation in pipe
$f(k,t)$	Fourier transform of the force in the wavenumber domain
$F(\omega,k)$	Fourier transform of the force in the wavenumber and frequency domain
ω	Frequency
N	Discretization points in double Fourier transform
n_f	Total points of discretization in time : $2n_f+1$
n_k	Total points of discretization in space : $2n_k+1$

$n_{kactual}$	Maximum number of rows to be stored in FFT computations: $2n_{kactual}+1$
$n_{factual}$	Maximum number of columns to be stored in FFT computations: $2n_{factual}+1$
$k_{z\max}$	Maximum wavenumber under consideration
$\omega_{\max}$	Maximum frequency under consideration
L	Ratio of $\omega_{\max} - k_{z\max}$ under study to the "frequency" – "wavenumber" of the impulse (inverse period)
a	External radius of pipe
b	Internal radius of pipe
μ,λ	Lame constants
h_{pipe}	Thickness of pipe (or any solid cylindrical layer)
ν_{pipe}	Pipe's material Poisson ratio
E_{pipe}	Pipe's material Young's modulus
μ_{pipe}	Pipe's material shear modulus
M_{pipe}	Cylindrical solid layer "bulk" stiffness
c_{fluid}	(Compressional) Wave velocity in fluid
ρ_{fluid}	Fluid density
$c_{s\,pipe}$	Shear wave velocity in solid
$c_{p\,pipe}$	Compressional wave velocity in solid
c_{tube}	Tube wave velocity

Bibliography (in chronological order)

M. Mersenne, "Harmonie Universelle", Paris (1636)

J. Tyndall, "On Sound", Longmans (1867)

J.W.S. Rayleigh, "The theory of Sound", Volumes I and II, first printed in 1877, Dover Publications 1945

Dr. W. H. Stone, "Elementary lessons on sound", Macmillian & Co. (1879)

H. Lamb, "Dynamical theory of Sound", Arnold Edward & Co. (1910)

J. Broadhouse, "Musical Acoustics or the phenomena of sound as connected to music", Scholarly Press, Inc. (1926)

I.B. Crandall, "Theory of vibrating systems and sound", D. Van Nostrand Company Inc, Princeton (1926)

P.M. Morse, "Vibration and Sound", McGraw-Hill Book Company Inc., NY (1930)

A.B. Wood, "A textbook of Sound", George Bell & Sons, London, (1930)

H.F. Olson, "Music, Physics and Engineering", Dover Publications, NY (1952)

M. A. Biot, 1952. "Propagation of elastic waves in a cylindrical bore containing fluid", J. *Appl. Phys.*, 23, 997-1005.

T.C. Lin, G.W. Morgan, "Wave propagation through fluid contained in a cylindrical elastic shell", *J. of the Acoust. Soc. of Am.* 28 (1956) 1165–1176.

D. C. Gazis, "Three Dimensional Investigation of the Propagation of Waves in Hollow Circular Cylinders: I. Analytical Foundation", *J. Acoust. Soc. of Am.*, Vol 31, No. 5, pp. 568-573, May 1959a.

J. M. Tyler, T. G. Sofrin, "Axial flow compressor noise studies" *1962 SAE Transactions* 70. 309-332

V.N. Merkulov, V.Yu. Prikhodko, V.V. Tytekin, "Excitation and propagation of normal modes in thin .fluid-filled elastic shells", *Akustichesky Zhurnal* 24 (1978) 723–730 (in Russian).

M. Silk, K. Bainton, "The propagation in metal tubing of ultrasonic wave modes equivalent to Lamb waves", *Ultrasonics*, 17 (1), pp. 11-19, 1979

J.H. James, "Computation of acoustic power, vibration response and acoustic pressure of fluid filled pipes", *Admiralty Marine Technology Establishment*, Teddington, May, 1982, AMTE(N) TM82036.

C.R. Fuller, F.J. Fahy, "Characteristics of wave propagation and energy distributions in cylindrical elastic shells filled with fluid", *Journal of Sound and Vibration* 81 (1982) 501–518.

C.R. Fuller, "The input mobility of an infinite circular cylindrical elastic shell filled with fluid", *Journal of Sound and Vibration*, 1983;87: 409–27.

J.E. White, "Underground Sound – Application of Seismic waves", Elsevier, Amsterdam – Oxford – New York, (1983)

D. E. Amos, "A Portable Package for Bessel Functions of a Complex Argument and Nonnegative Order," *Trans. Math. Software*, 1986

M. Möser, M. Heckl, K. H. Ginters, "On sound propagation in fluid-filled straight cylindrical pipes", *Acustica* 60 (1986) 34–44.

E. Kausel, J.M. Roësset, "Frequency domain analysis of undamped systems", *J. Eng. Mech.*, 118 (4) (1992), 721-734

J. Simmons, E. Drescher-Krasicka, H. Wadley, "Leaky axisymmetric modes in infinite clad rods I", *J. Acoust. Soc. Am.* 92(2) (1992) 1061-1090

M. Viens, Y. Tshukahara, C. Jen, J. Cheeke, "Leaky torsional modes in infinite clad rods", *J. Acoust. Soc. Am.* 95 (2) (1994) 701-707

B. Pavlakovic, M.J.S. Lowe, D.N. Alleyne, P. Cawley, "Disperse: a general purpose program for creating dispersion curves" in: D.O. Thompson, D.E. Chimenti (Eds.), *Review of Progress in Quantitative NDE*, vol. 16, Plenum Press, New York, 1997, pp. 185-192.

O. Poncelet, M. Deschamps, "Lamb waves generated by complex harmonic inhomogeneous plane waves", *J. Acoust. Soc. Am.* , 102 (1) (1997), 292-300

M. Frigo, S.G. Johnson, "FFTW: An Adaptive Software Architecture for the FFT", Proceedings of the 1998 ICASSP Conference, vol. 3, pp. 1381-1384

V.N. Rama Rao, J.K. Vandiver, "Acoustics of fluid-filled boreholes with pipe", *J. Acoust. Soc. Am.*, 105 (6) (1999), 3057-3066

Hegeon Kwun, Keith A. Bartels, Christopher Dynes, "Dispersion of longitudinal waves propagating in liquid-filled cylindrical shells", *J. Acoust. Soc. Am.* 105 (5) (1999) 2601-2611

A. Bernard, M. Deschamps, M.J.S. Lowe, "Comparison between the dispersion curves calculated in complex frequency and the minima of the reflection coefficients for an embedded layer", *J. Acoust. Soc. Am.* 107 (2) (2000), 793-800

C. Aristegui, M.J.S. Lowe, P. Cawley, "Guided waves in fluid-filled pipes surrounded by different fluids", *Ultrasonics*, 39 (2001) 367-375

X.M. Zhang, J.R. Liu, K.Y. Lam, "Coupled vibration analysis of fluid-filled cylindrical shells using the wave propagation approach", *Applied Acoustics*, 62 (2001) 229-243

E. Kausel, "Compendium of Fundamental Solutions in Elastodynamics", Cambridge University Press, in print

Bibliography (in alphabetical order)

Amos, D. E., "A Portable Package for Bessel Functions of a Complex Argument and Nonnegative Order," *Trans. Math. Software*, 1986

Aristegui C., Lowe, M.J.S., Cawley, P., "Guided waves in fluid-filled pipes surrounded by different fluids", *Ultrasonics*, 39 (2001) 367-375

Bernard, A., Deschamps, M., Lowe, M.J.S., "Comparison between the dispersion curves calculated in complex frequency and the minima of the reflection coefficients for an embedded layer", *J. Acoust. Soc. Am.* 107 (2) (2000), 793-800

Biot, M. A., 1952. "Propagation of elastic waves in a cylindrical bore containing fluid", J. *Appl. Phys.*, 23, 997-1005.

Broadhouse, J., "Musical Acoustics or the phenomena of sound as connected to music", Scholarly Press, Inc. (1926)

Crandall, I.B., "Theory of vibrating systems and sound", D. Van Nostrand Company Inc, Princeton (1926)

Frigo, M., Johnson, S.G., "FFTW: An Adaptive Software Architecture for the FFT", Proceedings of the 1998 ICASSP Conference, vol. 3, pp. 1381-1384

Fuller, CR., "The input mobility of an infinite circular cylindrical elastic shell filled with fluid", *Journal of Sound and Vibration*, 1983;87: 409–27.

Fuller, C.R., Fahy, F.J., "Characteristics of wave propagation and energy distributions in cylindrical elastic shells filled with fluid", *Journal of Sound and Vibration* 81 (1982) 501–518.

Gazis, D.C., "Three Dimensional Investigation of the Propagation of Waves in Hollow Circular Cylinders: I. Analytical Foundation", *J. Acoust. Soc. of Am.*, Vol 31, No. 5, pp. 568-573, May 1959a.

James, J.H., "Computation of acoustic power, vibration response and acoustic pressure of fluid filled pipes", *Admiralty Marine Technology Establishment*, Teddington, May, 1982, AMTE(N) TM82036.

Kausel, E., "Compendium of Fundamental Solutions in Elastodynamics", Cambridge University Press, in print

Kausel, E., Roësset, J.M., "Frequency domain analysis of undamped systems", *J. Eng. Mech.*, 118 (4) (1992), 721-734

Kwun, H., Bartels, K.A., Dynes,C., "Dispersion of longitudinal waves propagating in liquid-filled cylindrical shells", *J. Acoust. Soc. Am.* 105 (5) (1999) 2601-2611

Lamb, H., "Dynamical theory of Sound", Arnold Edward & Co. (1910)

Lin, T.C., Morgan, G.W., "Wave propagation through fluid contained in a cylindrical elastic shell", *J. of the Acoust. Soc. of Am.* 28 (1956) 1165–1176.

Merkulov, V.N., Prikhodko, V.Yu., Tytekin, V.V., "Excitation and propagation of normal modes in thin fluid-filled elastic shells", *Akustichesky Zhurnal* 24 (1978) 723–730 (in Russian).

Mersenne, M., "Harmonie Universelle", Paris (1636)

Morse, P.M., "Vibration and Sound", McGraw-Hill Book Company Inc., NY (1930)

Möser, M., Heckl, M., Ginters, K.H., "On sound propagation in fluid-filled straight cylindrical pipes", *Acustica* 60 (1986) 34–44.

Olson, H.F., "Music, Physics and Engineering", Dover Publications, NY (1952)

Pavlakovic, B., Lowe, M.J.S., Alleyne, D.N., Cawley, D.N., "Disperse: a general purpose program for creating dispersion curves" in: D.O. Thompson, D.E. Chimenti (Eds.), *Review of Progress in Quantitative NDE*, vol. 16, Plenum Press, New York, 1997, pp. 185-192.

Poncelet, O., Deschamps, M., "Lamb waves generated by complex harmonic inhomogeneous plane waves", *J. Acoust. Soc. Am.* , 102 (1) (1997), 292-300

Rama Rao, V.N., Vandiver, J.K., "Acoustic of fluid-filled boreholes with pipe", *J. Acoust. Soc. Am.*, 105 (6) (1999), 3057-3066

Rayleigh, J.W.S., "The theory of Sound", Volumes I and II, first printed in 1877, Dover Publications 1945

Silk, M., Bainton, K., "The propagation in metal tubing of ultrasonic wave modes equivalent to Lamb waves", *Ultrasonics*, 17 (1), pp. 11-19, 1979

Simmons, J., Drescher-Krasicka, E., Wadley, H., "Leaky axisymmetric modes in infinite clad rods I", *J. Acoust. Soc. Am.* 92(2) (1992) 1061-1090

Dr. Stone, W. H., "Elementary lessons on sound", Macmillian & Co. (1879)

Tyler, J. M., Sofrin, T. G., "Axial flow compressor noise studies" *1962 SAE Transactions* 70. 309-332

Tyndall, J., "On Sound", Longmans (1867)

Viens, M., Tshukahara, Y., Jen, C., Cheeke, J., "Leaky torsional modes in infinite clad rods", *J. Acoust. Soc. Am.* 95 (2) (1994) 701-707

White, J.E., "Underground Sound – Application of Seismic waves", Elsevier, Amsterdam – Oxford – New York, (1983)

Wood, A.B., "A textbook of Sound", George Bell & Sons, London, (1930)
X.M. Zhang, J.R. Liu, K.Y. Lam, "Coupled vibration analysis of fluid-filled cylindrical shells using the wave propagation approach", *Applied Acoustics*, 62 (2001) 229-243